STUDY OF FLOW DYNAMICS OF SOLID PHASE IN FLUIDIZED BED SYSTEM USING RADIOISOTOPE TECHNIQUES

By
Sunil Goswami

CHEM01201404002

Bhabha Atomic Research Centre, Mumbai, India

A thesis submitted to the

Board of Studies in Chemical Sciences

In partial fulfillment of requirements

for the Degree of

DOCTOR OF PHILOSOPHY

of

HOMI BHABHA NATIONAL INSTITUTE

December, 2018

Homi Bhabha National Institute

Recommendations of the Viva Voce Committee

As members of the Viva Voce Committee, we certify that we have read the dissertation prepared by **Mr. Sunil Goswami** entitled **"Study of flow dynamics of solid phase in fluidized bed system using radioisotope techniques"** and recommend that it may be accepted as fulfilling the thesis requirement for the award of Degree of Doctor of Philosophy.

Chairman – Prof. Ashutosh Dash Das **Date:** 10|12|2019

Guide / Convener – Prof. Lalit Varshney Lalit Varshney **Date:** 10|12|2019

Examiner – Prof. C. S. Mathpati **Date:** 10/12/2019

Member 1- Prof. Sharmila Banerjee SBanerjee **Date:** 10|12|2019

Member 2- Prof. A. K. Pandey Pandey **Date:** 10|12|19

Member 3- Prof. Y. K. Bhardwaj **Date:** 10/12/2019

Technical Adviser- Prof. H. J. Pant Pant **Date:** 17.12.2019

Final approval and acceptance of this thesis is contingent upon the candidate's submission of the final copies of the thesis to HBNI.

I/We hereby certify that I/we have read this thesis prepared under my/our direction and recommend that it may be accepted as fulfilling the thesis requirement.

Date: 18|12|2019

Place: Kharghar, Navimumbai

Lalit Varshney

(Signature)
Guide

STATEMENT BY AUTHOR

This dissertation has been submitted in partial fulfillment of requirements for an advanced degree at Homi Bhabha National Institute (HBNI) and is deposited in the Library to be made available to borrowers under rules of the HBNI.

Brief quotations from this dissertation are allowable without special permission, provided that accurate acknowledgement of source is made. Requests for permission for extended quotation from or reproduction of this manuscript in whole or in part may be granted by the Competent Authority of HBNI when in his or her judgment the proposed use of the material is in the interests of scholarship. In all other instances, however, permission must be obtained from the author.

Sunil Goswami
18/12/2019
Sunil Goswami

DECLARATION

I, hereby declare that the investigation presented in the thesis has been carried out by me. The work is original and has not been submitted earlier as a whole or in part for a degree / diploma at this or any other Institution / University.

Sunil Goswami
18/12/2019

Sunil Goswami

List of Publications arising from the thesis

Journal

1. “Measurement of mixing time and holdup of solids in gas–solid fluidized bed using radiotracer technique”, Sunil Goswami, Jayashree Biswal, J. Samantray, D. F. Gupta, H. J. Pant, Journal of Nuclear and Analytical Chemistry, 302 (2014) 845-850.

2. “Residence time distribution study in a pilot-scale gas–solid fluidized bed reactor using radiotracer technique” H. J. Pant, V. K. Sharma, Sunil Goswami, J. S. Samantray, I. N. Mohan, Tirupathi Naidu, Journal Radioanalytical and Nuclear Chemistry, 302(2014) 1283–1288.

3. “Study of adsorption characteristics of Au(III) onto coal particles and their application as radiotracer in a coal gasifier”, Sunil Goswami, Harish Jagat Pant, Rajwardhan Nandram Ambade, Bhasakar Paul, Lalit Varshney, Ashutosh Dash, Applied Radiation and Isotope, 122 (2017) 127-135.

4. “Radiotracer investigations in a pilot-scale fluidized bed gasifier (FBG)” Sunil Goswami, H. J. Pant, V. K. Sharma, Lalit Varshney, Applied Radiation and Isotopes 149 (2019) 22–30.

Conferences/Symposia

1. “Evaluation of Performance of Two Different Air Distributors Used in a Cold Flow Pilot-Scale Fluidized Bed Gasifier Using Radiotracer Technique”, Sunil Goswami, H. J. Pant, V.K.Sharma, J. S. Samantray, Lalit Varshney, K.S.S. Sarma, NAARRI International Conference, National Association for Application of Radioisotopes and Radiation in Industry (NAARRI) Mumbai.

2. “ Study of adsorption characteristics of Au(III) onto grapheme oxide using radiotracer method”, Sunil Goswami, Abhiudaya Kumar, H.J. Pant, A. Dash, National Symposium on Applications of Radioisotopes and radiation Technology in Industry, Healthcare and

Agriculture organized by National Association for Applications of Radioisotopes and radiation in industry (NAARRI) at Amity University, Noida, Uttar Pradesh during August 2016.

3. "Measurement of Mixing Time of Solids in a Gas-Solid Fluidized Bed System Using Radiotracer Technique" Jayashree Biswal, Sunil Goswami, J.S. Samantray, Dev Gupta, H.J. Pant, International Conference on Application of radiotracers in Chemical, Environmental and Biological Sciences (ARCEBS-14), Jan.23-27, 2014, Fort, Kolkata.

4. "Residence Time Distribution Study in a Pilot-Scale Gas-Solid Fluidized Bed System Using Radiotracer Technique", H.J. Pant, V.K. Sharma, Sunil Goswami, J.S. Samantaray, N.I.G.N. Mohan, Tirupathi Naidu, Gursharan Singh, Proceedings of DAE-BRNS Fifth Symposiuon Nuclear Analytical Chemistry (NAC-V) Jan. 20-24, 2014, Page no. 373-374.

Others

1. Sunil Goswami, H. J. Pant, Jayashree Biswal, J. S. Samantray, V. K. Sharma, Ashutosh Dash, Synthesis, characterization and application of Au-198 nanoparticles as radiotracer for industrial applications, Applied Radiation and Isotopes, 111 (2016) 18–25.

2. Investigation of flow dynamics of aqueous phase in a pulsed sieve plate column using radiotracer technique, Sunil Goswami, Nirvik Sen, J. S. Samantray, H. J. Pant, V.K. Sharma, K.T. Sheony, J Radioanal Nucl Chem (2017) 313:669–676.

3. Flow investigation in an industrial-scale soaker using radiotracer technique, H.J. Pant, Sunil Goswami, V.K. Sharma, S.K. Maity, M.O. Garg, Applied Radiation and Isotopes 124 (2017) 119–123.

4. Radiotracer Investigation in a glass production unit, H.J.Pant, Sunil Goswami , Jayashree Biswal, J. S. Samantray, V.K.Sharma, Sorabh Singhal, Applied Radiation and Isotope, 116 (2016) 41-50.

5. Synthesis, Characterization, Neutron Activation, and Application of Scandium Oxide Microsphere in Radioactive Particle Tracking Experiments, Jayashree Biswal, Sunil Goswami, Harish Jagat Pant, Yashwant Ramdas Bamankar, Tadpatri Venkoba Rao Vittal Rao, Rajesh Kumar Upadhay, Ashutosh Dash, I&EC Research, 2016, 55, 3−12

Sunil Goswami
18/12/2019

Sunil Goswami

DEDICATIONS

To

My Parents

Shivji Goswami and Rameshwari Goswami

&

My Children Aaradhya, Daksh and

Wife Priyanka

ACKNOWLEDGEMENTS

First and Foremost, I would like to express my sincere gratitude to my research guide **Dr. Lalit Varshney** for the continuous support to my Ph.D. study and research, for his patience and motivation. His guidance enabled me to develop an understanding of the subject and helped me in the submission of this thesis. He will be a source of inspiration always. I would also like to express my deep sense of gratitude to my technical adviser and my immediate superior in BARC from the day of my joining, **Dr. H. J. Pant** for introducing me the research field of radioisotope applications. He has taught me all the fundamentals of the radioisotope techniques and guided me at every step of my thesis work. His suggestions and guidance at every stage of this work has been very crucial and I am grateful to him for helping me at every stage of thesis from beginning to the end.

I am also thankful to Dr. Ashutosh Dash, Chairman, Dr Sharmila Banerjee, Dr A.K. Pandey and Dr.Y.K. Bhardwaj member of doctorial committee for their valuable suggestions and discussions during course of the study. I am highly tankful to the M/S Thermax Limited, Pune, India and M/S Bharat Heavy Electrical Limited, Hyderabad, India for providing large scale fluidized bed facility, technical, logistic support to carry out the radiotracer experiments.

I would take this opportunity to thank my colleagues from radiotracer application section for their technical suggestions, encouragement and cooperative attitude which have greatly helped in my research work. Special thanks to Shri V. K. Sharma and Dr. Jayashree Biswal for their tremendous help and guidance. Their enthusiastic and scientific approach towards research is a source of inspiration to me.

4. Radiotracer Investigation in a glass production unit, H.J.Pant, Sunil Goswami , Jayashree Biswal, J. S. Samantray, V.K.Sharma, Sorabh Singhal, Applied Radiation and Isotope, 116 (2016) 41-50.

5. Synthesis, Characterization, Neutron Activation, and Application of Scandium Oxide Microsphere in Radioactive Particle Tracking Experiments, Jayashree Biswal, Sunil Goswami, Harish Jagat Pant, Yashwant Ramdas Bamankar, Tadpatri Venkoba Rao Vittal Rao, Rajesh Kumar Upadhay, Ashutosh Dash, I&EC Research, 2016, 55, 3−12

Sunil Goswami
18/12/2019

Sunil Goswami

CONTENTS

Page No.

CHAPTER 5 -- 114

MEASUREMENT OF THE FLOW DYNAMICS OF THE COAL PARTICLES IN COLD AND HOT FLOW FLUIDIZED BED GASIFIER USING RADIOACTIVE PARTICLES -- 114

Nomenclature

Symbol	Description
FBR	Fluidized bed reactor
IGCC	Integrated gasification and combined cycle
PCC	Pulverized coal combustion
HELE	High efficiency and low emission
GRD	Gamma ray densitometry
CHNS	Carbon, hydrogen, nitrogen, sulphur
ATR	Attenuated total reflectance
BET	Brunauer-Emmett-Teller
RTD	Residence time distribution
FBG	Fluidized bed gasifier
SC	Super critical
USC	Ultra super critical
μ	Attenuation coefficient
k	Linear attenuation coefficient
A	Activity
Z	Atomic number
n	Neutron
p	Proton
γ	Gamma energy
GM	Gieger Muller
NaI(Tl)	Sodium iodide doped thallium detector
ρ	Density
eV	Electron Volt
DAS	Data acquisition system
SCA	Single channel analyzer
MCA	Multi-channel analyzer
PM	Photomultiplier tube
t	Time
$t_{1/2}$	Half -life
λ	Decay constant
C(t)	Tracer concentration at time t
E(t)	Normalized tracer concentration at time t
t_{mix}	Mixing time
MRT	Mean residence time
M_n	n^{th} moment around the origin
τ	Theoretical mean residence time
V	Volume
Q	Flow rate of the reactor
$\delta(t)$	Dirac delta function
ADM	Axial dispersion model
CSTR	Continuously stirred tank reactor
U	Linear velocity
D	Dispersion coefficient

Pe	Peclet number
N	Tank number
α	Back mixing ration
$\bar{t}$	Experimentally measured mean residence time
σ^2	Variance
σ	Standard deviation
r	Recycle ratio
$E_{exp}(t)$	Experimental normalized tracer concentration
$E_m(t)$	Model simulated normalized tracer concentration
Ads.%	percentage of adsorption
K_d	Distribution coefficient
C_0	Initial concentration of Au(III) solution
C_t	Concentration of Au(III) solution at any time t
C_e	Equilibrium concentration of Au(III)
Q_t	Adsorption capacity of Au(III) on coal at any time t
Q_e	Adsorption capacity of Au(III) on coal at equilibrium time
IR	Infra-red
SEM	Scanning electron microscope
EDS	Energy dispersive spectra
pH	Concentration of $[H^+]$ ion in the solution
ΔG^o	Changes in Gibbs free energy
ΔH^o	Changes in enthalpy
ΔS^o	Changes in entropy
K_c	Equilibrium constant
T	Temperature
R_L	Separation factor
b	Langmuir adsorption constant
Q_s	Maximum adsorption capacity
β	Activity coefficient
ε	Polanyi Potential
E	Mean adsorption energy
K_2	Second order rate constant
h	Initial adsorption rate
A	Arrhenius constant
R	Universal gas constant
E_a	Activation energy
V_a	Superficial gas velocity
BH	Bed height
U_{mf}	Minimum fluidization velocity
I_a	Counts measured on empty bed
I_s	Counts measured on packed bed
I_f	Counts measured in fluidized bed
ε_a	Gas holdup
P	Pressure
D	Inner diameter of the fluidizer section
τ_p	Time of plug flow component

τ_B	Time spent in the bed
N_B	Number of tanks in bed section
α_B	Back mixing ratio of bed material
f_R	Recycle fraction of flow
$\boldsymbol{\tau_R}$	Time of recycle
N_R	Number of tank in recycle stream
τ_T	Total time spent in the system
f_{BP}	Fraction of bypass
$\bar{t}_b$	MRT coal exiting from bottom of the reactor
$\bar{t}_f$	MRT coal exiting from top of the reactor

Chapter 1

Introduction

1.1. Background:

Electricity is one of the greatest scientific achievements of 20th Century, ahead of automobiles, telecommunications, computers and even healthcare in terms of its positive impacts on quality of life (IPG, 2003). It is an essential part of modern life and one cannot think of a world without it. Electricity is defined as the flow of electrical charges. It is a basic part of nature as well as one of the most widely used forms of energy. The electricity that we use is a secondary energy source because it is produced by converting primary sources of energy such as coal, natural gas, nuclear energy, solar energy and wind energy into electrical power. It also referred to as an energy carrier, which means it can be converted into other forms of energy such as mechanical energy or heat. Worldwide different sources are used to produce electricity.

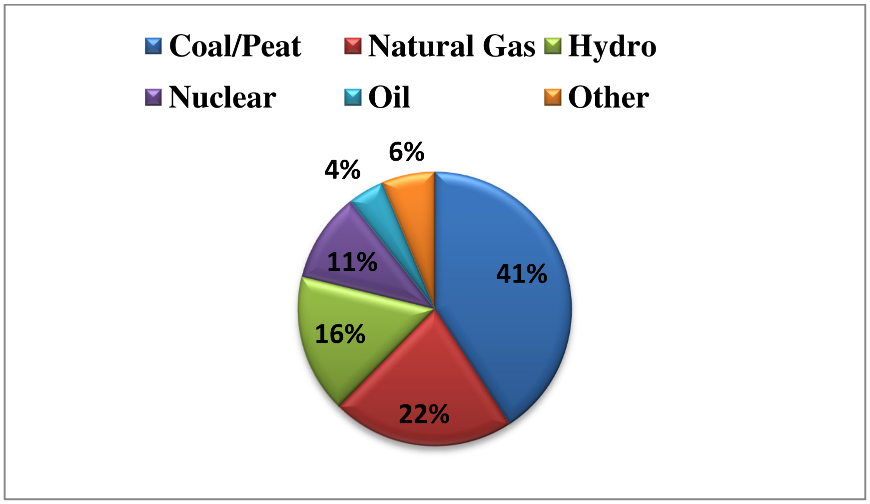

Fig.1.1. World electricity generation by source (IEA, 2017)

A chart representing different sources used for the electricity production worldwide is shown in the Fig.1.1 (IEA, 2016). This chart indicates that worldwide electricity generation using was coal at 40.8%, natural gas at 21.6%, nuclear at 10.6%, hydro at 16.4%, other sources (solar, wind, geothermal, biomass, etc.) at 6.3% and oil at 4.3%. This clearly indicates that coal plays a major role in the production of the electricity worldwide. The amount of electricity production in different countries as per the IEA reports using coal is shown in the Fig. 1.2.

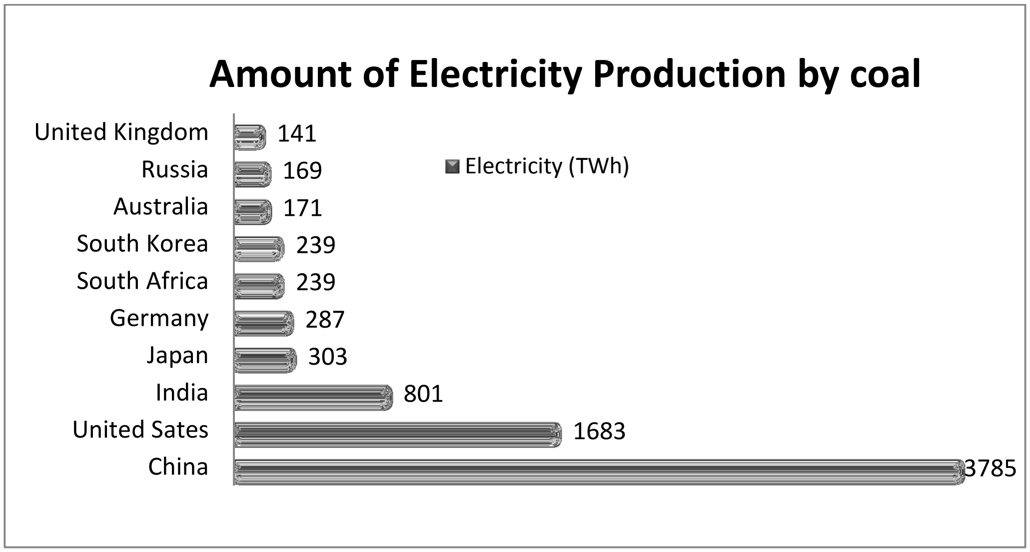

Fig.1.2. Electricity produced by the different countries using coal (IEA, 2017)

It is clearly evident that both developed countries (United Nations, United Kingdom, Germany, Russia, Japan and Australia) and developing countries (China, Indian, South Africa, South Korea) are heavily dependent upon the electricity production using the coal. India is second largest producer of coal behind China and above USA and in world India is second largest importer to coal (PS, 2018). The various source of electricity generation in India is presented in the Fig. 1.3. India is currently undergoing profound transformation from developing to developed country. Therefore, the demand of electric energy is increasing as a result of economic and population growth as well as the various structural changes from growing urbanization and industrialization (IIE, 2018). This growing demand of the electricity is heavily dependent on coal in India as in the other developing and developed nations.

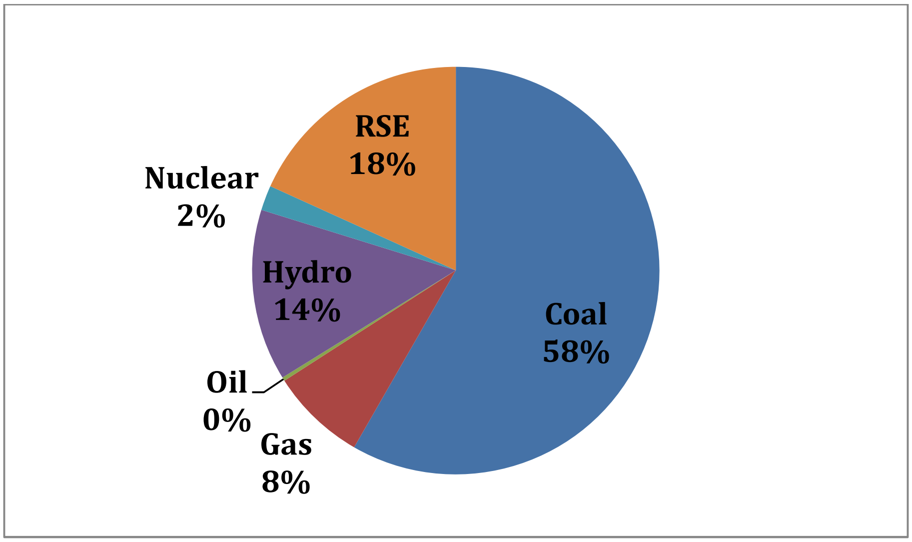

Fig.1.3. India electricity generation by source (Ministry of power,2)(RSE: Renewable Energy Sources) include small hydro project, biomass gasifier, biomass power, urban & industrial waste power, solar and wind energy)

Coal is the most abundant fossil fuel in India. India is having vast coal reserves (125 billion tonnes). It accounts for ~60% of electricity production (MoC-GOI, 2018). The dominance of coal in India's energy programme can be attributed to two key factors: affordability and access. Even though, competitiveness of renewables sources of electricity production is rapidly improving with time. The dependency of coal is expected to remain. It is the most affordable option for coming 30 to 40 years, driven by low domestic coal prices and ease of availability.

As, in the present scenario, the generation of electricity from coal is done by their combustion in thermal power plants. The function of the coal fired thermal power plant is to convert the chemical energy available in the coal to electricity. This conversion of coal to electrical energy is done in three steps. In the first step coal is combusted in the boiler and its chemical energy converted into thermal energy. In the second step this thermal energy is used to convert water into the steam. In the final step, this steam is used to rotate the turbine blades and finally electricity is produced based on Faraday's Principle of electromagnetic induction. Conventional coal-fired power plants, which used to boils water to generate steam that activates a turbine, have efficiency of about 32% for the electricity production. Supercritical (SC) and ultra-supercritical (USC) power plants that operates at temperatures and pressures above the critical point of water, i.e. above the temperature and pressure at which the liquid and gas phases of water coexist in equilibrium, at this point there is no difference between water gas and liquid water. This results in higher efficiencies – above 45%. Supercritical (SC) and ultra-supercritical (USC) power plants require less coal per megawatt-hour, leading to lower emissions of hazardous gaseous in the environment, higher efficiency and lower fuel costs per megawatt (Ma and Turchi, 2011). Now days, many of the conventional coal fired power plants are changing to SC and USC.

The oxidation of carbon present in coal produces, energy as well as the chemical compounds harmful for the environment and public health. Thermal power plants used for the production of electricity also produces CO_2, SO_x, NO_x, particulate matter, volatile hydrocarbons as by-products (Munawer M.H., 2018). Theses chemicals are harmful for the environment and public health. The thermal power plants are the major contributor to these gases in the environment worldwide (Barreira et al., 2017). However, there is regular growing demand of electricity in India and worldwide. Therefore, there is always concern for developing energy efficient process for the electricity production from coal in thermal power plants. Other available sources of electricity production are not able to provide low cost sustainable electricity. Hence, the dependency of the electricity production on coal is much higher. At the same time, the release of environmental hazardous gaseous needs to decreased due to the stringent environment regulatory policies for the betterment of the environment and public health. Therefore, government has designed the clean coal technology initiative.

1.2. Clean coal technologies:

It can be divided in four directions i.e. pre combustion, advanced combustion, post combustion and conversion (Machowska H. and Knapik E., 2011). The pre-combustion is purifying the coal prior to combustion, thus it helps in maintaining pollution limits during combustion of coal particles. The aim of advanced combustion is to improve the effectiveness of energy transformation and it helps in reducing the amount of coal burnt and pollution. Advanced post combustion is to purify the exhaust fumes to decreases the release of hazardous gases in the environment. In recent years, it has been the fourth direction that attracts most attention; it is related to new coal conversions technology, i.e. coal gasification technology. Coal gasification is steadily becoming the basis of advanced coal utilization technologies (Hayashi et al., 2006; Henderson, 2003). It enables not only high efficiency in electric power production, But also eliminates environmentally harmful gaseous efficiently. In addition to this, it also provides raw material for valuable chemical products, such as liquid fuels, methanol and hydrogen. A typical example of coal gasification technique proposed to be used in industry is the integration of gasification with electric power generation known as integrated gasification and combined cycle (IGCC) (Jay et al., 2002; Minchener, 2005; Emun et al., 2010). The IGCC is a technology that suits to us as it promotes high efficiency and low emission technology to produce electricity from coal.

1.3. Integrated Gasification Combined Cycle (IGCC)

It is a combination of two leading technologies. The first technology is called coal gasification, which uses the partial oxidation of the coal to create a clean-burning gas (syngas). The second technology is called combined-cycle, which is the most efficient method of producing electricity commercially available today. Both the technologies briefly discussed below:

1.3.1. Coal Gasification: The gasification portion of the IGCC plant produces a clean coal gas (syngas), which acts as the fuels for the combustion turbine. Coal is combined with oxygen in the gasifier to produce the gaseous fuel, mainly hydrogen and carbon monoxide. The gas is then cleaned by a gas cleanup process. After cleaning, the coal gas is used in the combustion turbine to produce electricity.

1.3.2. Combined-cycle: This design consists of a gas combustion turbine generator, a heat recovery steam generator and a steam turbine/generator. In the first step, heated gas in combustion turbine is used to run the gas turbine and production of the electricity. Subsequently, the exhaust heat from the combustion turbine is recovered in the heat recovery steam generator to produce steam. This steam then passes through a steam turbine to power another generator, which produces more electricity. Thus, combined cycle is more efficient than conventional power generating systems because it re-uses waste heat to produce more electricity. The integration of these technologies provide the high efficiency of the combined-cycle design with the low cost coal fuel.

1.3.3. Advantages of IGCC: The various advantages of the IGCC over the conventional electricity generation plant are discussed below (Huber et al, 1984) :

1. High thermal efficiency:The existing commercial IGCC power plant in the international market boosts a net efficiency of 43%, 5% higher than the traditional coal fired units .

2.Low pollution: It enjoys a desulfuration rate of 99% with sulfur recovery function, and low NO_x emission rate which equals to 1/20 of the traditional coal fired units. Moreover, the dust emission is close to zero.

3. Low water consumption:It accounts for 1/2 - 2/3 of the consumption of water in comparison to traditional coal fired units.

4. Flexibility to use different grades of coal: IGCC can use coal with low ash melting points, which is difficult to use in conventional pulverized coal-fired power plants. As a result, IGCC broadens the variety of coal grades that can be used in coal-fired power plants.

5. Multifunctional: With the poly-generation technology, it could supply electricity, heat, gasified coal and chemical material at the same time.

1.4. Motivation Behind the study

The development of IGCC technology depends upon the type of coal available and reactor selected for the gasification (Mondel et al., 2011; Goel M., 2010; Phillips, 2003). The selection of coal is the least flexible factor due to economical and geo-political reasons. Hence, it is necessary to select a suitable, efficient and easy to operate and maintain gasification technology which suits best to the properties of the coal to be processed. In India huge source of lignite coal is available and they have very high ash content. The average ash content in the in lignite’s is about 42% (Mondel et al., 2011). In order to gasify high ash Indian coal three suitable gasifer are moving bed, entrained bed and fluidized bed gasifier (Minchener, 2005). Moving bed gasifier are used to handle high ash content coals, but the major drawback of this technology is the generation of huge tar in the process and difficulties in handling in the fines (Mondel et al., 2010). Entrained flow gasifiers are usually recommended for coals with low ash content. In this gasifier, high ash lignite coal will lead to a decrease in gasification efficiency and an increase in slag production and disposal. Therefore, it is necessary to remove ash from the solid waste for efficient operation. The huge heat loss occurs in handling high ash coal and efficiency of the plant decreases tremendously. Therefore, entrained flow gasifier is not suitable for handling high ash Indian coals (Phillips, 2003).

In order to gasify high ash Indian coal, the suitable gasifer is fluidized bed gasification (Grootjes et al., 2015; Phillips 2003). It has a number of advantages over the other gasification systems such as rapid and uniform mixing, high degree of contact between the phases, high heat and mass transfer between gas and solid phases, almost negligible tar formation, absence of moving parts in the hot region (Kunni and Levenspiel, 2013). The fluidized bed gasifier offers a simpler and robust method for gasification of coal particulates. Hence, fluidized bed gasifier will be most suitable for high ash Indian coals. Although, there had been extensive literature and correlations are available for the designing the fluidized bed rector (FBR) (Knowlton et al., 2005). The principle of the fluidization technique is simple, in practice there have been many disastrous failures because of the change in behaviour between different matters and different scales of units was insufficiently appreciated. The radioisotope techniques are the only particle way to measure the hydrodynamics of solid phase accurately at large and pilot-scale plant (Roy, 2017). Hence, in the present thesis, the solid phase hydrodynamics of the solid phase is studied using different radioisotope techniques.

1.5. Objective of the study:

The board objectives of the study is to measure the solid phase hydrodynamics of fluidized bed rector using radioisotope technique in batch mode and continuous mode fluidized bed rector. The specific objectives of the study as follows:

1. Measurement of gas phase or solid phase hold up in batch type fluidized bed rector using radioisotope techniques
2. Preparation of the solid phase radiolabelled particles for the hydrodynamics measurements in the FBR
3. Study of the mixing time of the solid phase in the batch type FBR
4. Study of the residence time distribution of solid phase col particles in cold flow and hot flow fluidized bed rector.
5. Development of the suitable mathematical model describing the flow dynamics of the solid phase in FBR.

Chapter 2

Theoretical and experimental methods applied in the radiotracer techniques

---

2.1.Introduction of Radioisotope techniques

The radioisotope based techniques have been in use to solve the problems of industry for years. However, research and development of this technology continues in undiminished manner. There are two main reasons for the long lasting interest in the technology is as follows:

- Radioisotope based techniques are industry driven. Because of their distinctive properties, radioactive isotopes can be used to extract information about industrial plant processes that cannot be obtained by any other conventional techniques. Generally, the information obtained using radioisotope technique is online without disrupting the plant operation. This can lead to substantial economic benefits from reduction in the shutdown time.
- The radioisotope techniques use knowledge of the many fields of science and technology including radioisotope production, radiation detection, data acquisition, treatment and analysis, and mathematical modeling (Fig. 2.1). Development in any of these areas acts as additional urge for the advancement of radiotracer methodology. This presents a constant challenge to the radioisotope expert, who must have a comprehensive knowledge of these disciplines to make the outcome of the technology more and more accurate with time.

The radioisotope techniques applied in the industry using sealed sources and radiotracer technique. These techniques are applied for trouble shooting, monitoring, control, inspection, optimization purposes in the industry. The application of the radioisotope based techniques extensively requires research for obtaining reliable information from given system. The details of theses methodology is discussed in detail as follows:

2.1.1. Sealed source techniques

A large number of studies in the industrial process system are carried out using sealed sources techniques. In these applications, the radioactive sealed source remains encapsulated and acts as radiation source. The change in the intensity of the sealed source radiation is recorded, as it transverses the process material. This change in the intensity of the radiation is related of the process system parameters. In most of the applications, the sealed sources are employed in two ways: in ‘short term’ process studies which investigate specific features of plant operation and as instruments for analysis, measurement and control. The short term studies include measurement of liquid levels (storage vessel, catalyst bed reactor, packing in absorber tower), thickness and corrosion monitoring, defects in welds and casting, misconstruction in the industry. In addition to this, gamma scanning is used as indispensible tool for online problems in industrial process columns. As an instrument, sealed source and gamma radiation source assembly is used for level gauge, level alarm, proportional level indicator, dust and humidity monitor and smoke detector (Charlton and Husk, 1992). In the present study, sealed source technique has been used for the estimation of the void fraction or fraction of the solid present in the fluidized bed reactor which is discussed in the next section.

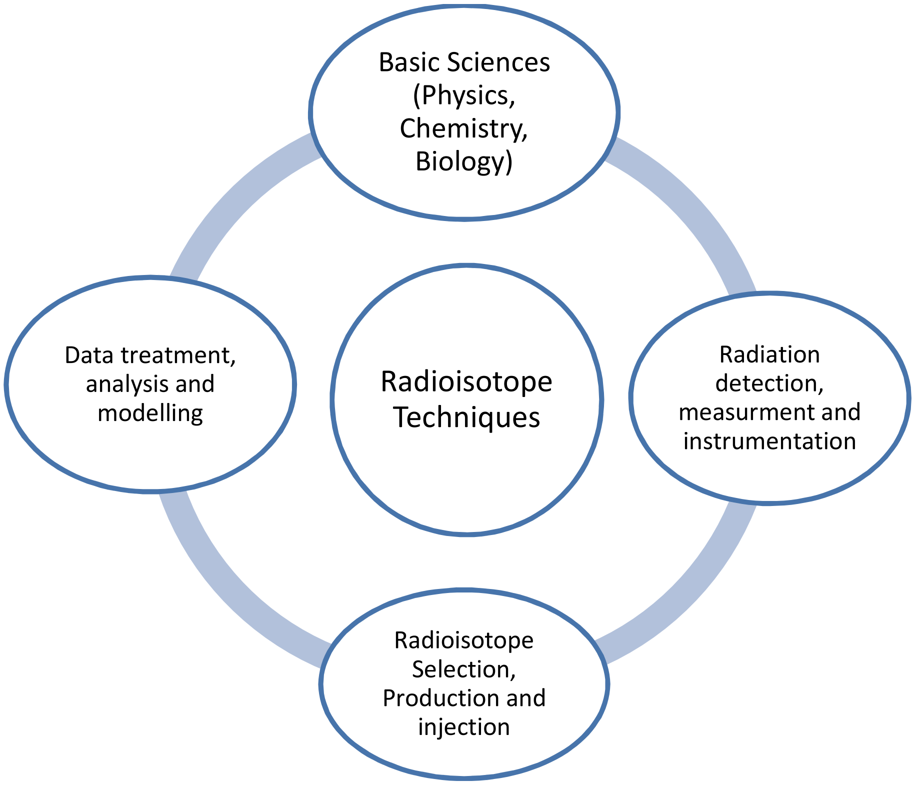

Fig. 2.1: Radioisotope technology and interconnected fields (Taken from IAEA, 2004B and redrawn)

2.1.1.1.Methods for the measurement of phases fraction of in FBR

Fraction of the different phase's present in multiphase flow system (MPFS) or fluidized bed reactor (FBR) is one of the crucial parameters that need to be known accurately for predicting the performance of systems. Various techniques used for void fraction measurements based on the different principles are listed in the Table 2.1.Most of the conventional methods are intrusive i.e. we need to install sensor in contact with the process fluid (Sthal and Rohr, 2004). The installation of this sensor itself disturbs the flow of the system and results are not accurate as expected. The other classes of techniques are non-intrusive techniques, in these techniques, the measurement assemblies are installed outside the process system such that there is not direct physical contact between process material and measurement system. The void fraction measurement using these techniques is much more accurate than the intrusive techniques. As listed in the Table 2.1, electrical charge, ultrasonic and x and γ ray based techniques are non-intrusive. The electrical charge and ultrasonic techniques are suitable for void age measurement in the laboratory scale systems. However, these cannot be applied in the pilot scale and full scale industrial system. Therefore, the radiation techniques (gamma and X-ray) appear to be attractive in many such applications, because they are non-intrusive, quite reliable and widely used in difficult experimental circumstances. X-rays were used in earlier experiments because high beam intensities were easily available (Grodstein, 1957). A corresponding gamma source to the same intensity of the X-ray would require an activity in range of thousands of curies, which will be extremely difficult to handle.

The major shortcomings of X-ray based densitometer are: (i) Instability of the beam (ii) short penetration across metallic walls. To resolve the first problem, reference beams are used. These results in a rather complex system, which is not portable in industrial complex process systems (Chan and Banerjee, 1981). To solve the second problem, windows of low density materials are fabricated in the metallic test sections at the time of installation of plant. However, this is not possible in each and every plant, especially in high pressure systems where thick metal walls are essential. Hence, in many practical situations, the X-ray technique is not applicable and γ-ray technique can be applied with the ease.

Table 2.1: Different techniques used to measure void fraction in multiphase flow systems

Measurement Method	Fundamental principle of the technique	Type of method	Reference
Pitot Tube	Mechanical method based on determination of momentum by means of differential pressure measurements.	Intrusive	Al-Hasan et al., 2007; Wang and Han, 1999
Electrical capacitance	This technique is used to measure the local dielectric constant of the gas-solid suspension, which is linked to the local volume fraction of solids.	Intrusive	Collin et al., 2009; Demori et al. 2010
Electrical impedance	The principle of the impedance method is to measure the conductance of the two-phase mixture between electrodes which are placed around or within the flow.	Intrusive	Davidson et. al., 2004; Dickin and Wang, 1995
Optical	A beam of light is projecting through a medium from one boundary point and detecting the level of light received at another boundary point. It is designed by using a group of emitter-receiver pairs such as LED and photo detector	Intrusive	Fischer at al., 2011; Link et al. 2009; Meggitt, 2010, Wang et al. 2009
Electrical charge	Pneumatically conveyed particulate matter such as solids acquires charge during the transportation by several processes such as symmetrical charge separation and frictional charging. **Limitation:** Charge varies with size, material and humidity	Non-intrusive	Green et al., 1997; Bidin, et al., 1995; Rahmat, 1996
Ultrasonic	Ultrasound wave is generated with typically Piezoelectric ultrasound transducers, transmitted in direction of the measurement object and received with other or the same ultrasound transducers. **Limitation:** Lower sensitivity	Non-intrusive	Hoyle, 1996; Daniels, 1996, Abdul et al., 2004; Kevin et al., 2002
X-Ray / γ-ray	The attenuation of the high energy electromagnetic radiation passes through the system of interest gets attenuated. **Advantage:** There is no physical disturbance of the flow field occurs.	Non-intrusive	Kumar et al., 1995; Tan et al. 2007; Thatte et al. 2004; Veluswamy et al. 2011
Intrusive technique: Measurement probes are in contact with process fluid. Non-Intrusive: Measurement probe installed outside the system			

2.1.1.2.Gamma ray densitometry

Gamma radiation is an electromagnetic radiation similar to X-rays. While X-rays are mostly produced in X-ray tubes, gamma radiation is a consequence of the alpha and beta decay of radionuclides. The gamma source of having wide range of energy from approximately 10 keV to 10 MeV is available. Gamma radiation has high energy that can even penetrate high metallic materials used to design industrial process systems that are impossible to penetrate by the X-rays. Gamma densitometry is based on the fundamental principle that electromagnetic radiation is attenuated as it passes through matter due to interaction of photons with the matter. There are more than ten types of elementary processes of interaction of gamma rays with matter (Fano, 1953). The two main interactions concerning gamma densitometry attenuation are photoelectric and Compton scattering interactions (Sprowll and Phillips, 1980). The photoelectric effect generally predominates at lower radiation energies and higher atomic number of the absorber, whereas the Compton Effect is more predominant at higher radiation energies (Schlieper et al., 1987). The capability of material to absorb gamma radiation is characterized by its mass absorption coefficient (μ). The attenuation of mono energetic gamma-radiation in homogeneous material and its resulting exponential loss of intensity are governed by the Beer–Lambert's law, which can be expressed as (Chaouki et al., 1997A; 1997B):

$$I = I_0 e^{-\mu\rho x} = I_0 e^{-k x} \tag{2.1}$$

Where I_0 is the initial radiation intensity, I is the intensity of radiation detected after the beam has travelled a distance x through the absorbing material, ρ represents the density of the absorption material. The linear attenuation coefficient (k) is defined as the product of mass absorption coefficient and the density of absorbing material. The value of the mass absorption coefficient depends on the absorbing material and on the radiation energy.

This principle is very straightforward to calculate the void fraction of the system. However, as pointed out earlier, this technique is to be customized as per the system under the investigation. The different design parameters are to be looked critically before the design of the experiment as discussed in the next section.

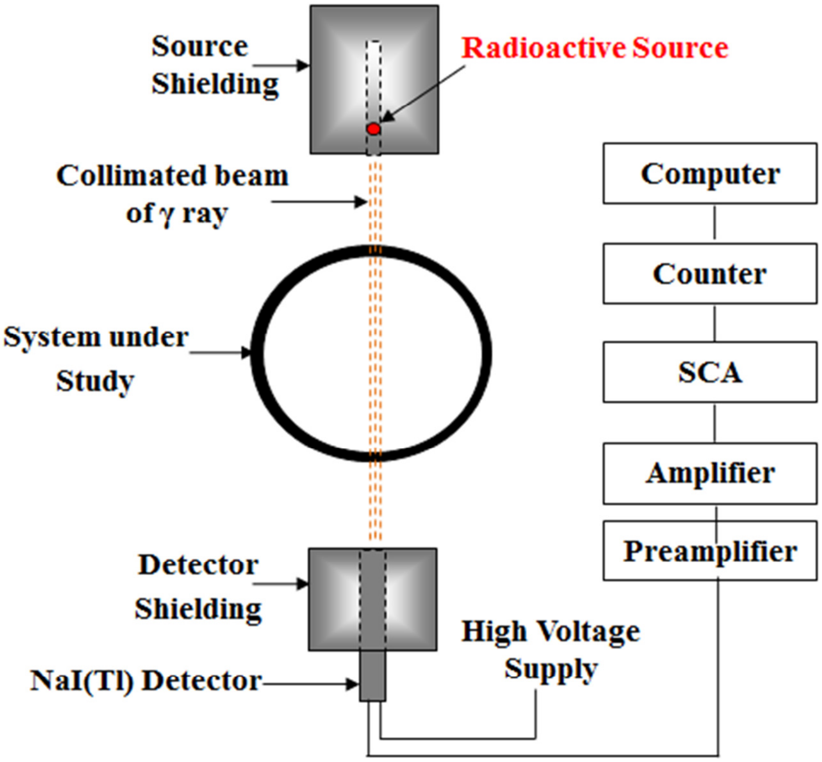

Fig 2.2. Schematic diagram illustrating the gamma ray densitometer (Tjugum et al., 2002)

The various constituents of the gamma ray densitometer are shown in the Fig. 2.2. The gamma ray densitometer consist of a sealed source, shielding material, a radiation detector, a signal processing unit and a system under the study. The selections of the each of these components will depend upon the geometry and material over which the void fraction is to be measured (Chan and Banerjee, 1981; Scoot, 1988; Park and Chung, 2007). A step by step design procedure can be summarized as follows:

1) **To specify the test section geometry and material**: For the suitable design of a gamma densitometer, the dimensions of test section under study and process material must be stated. This is required for the determination of required photon energy and source strength.
2) **Gamma source (with reference to above point):** It is important to choose the appropriate source for use in a given test system. The transmission through the pipe walls and sensitivity to change in material content are the major concerns. Other important points are (1) half-lives of the gamma sources, (2) gamma emission ratio. Some of the commercially available gamma sources are given in Table 2.2. Most of the sources emit gammas photons of different energies. The ideal source for the gamma ray densitometry should be mono-energetic gamma photons with energies having penetration depth enough to transverse the walls of the test section with a measurable attenuation.
3) **To calculate the required source strength:** Once the suitable source is selected, its required strength can be calculated. The required source strength depends in general

on: beam size, losses through window, pipe walls, collimation distance, scintillator efficiency, emission ratio of selected gamma radiation and the counting period. In order to calculate the source strength, it is needed to specify the maximum acceptable measurement error. For a single-beam densitometer the errors involved are: (1) flow regime and geometric associated errors of system (2) statistical error.

Table 2.2: List of the commercially available gamma ray sources

Isotope	Half-Life	Photon energy (KeV) Emission (%)
Am-241	433 y	60(36%), 18 (18%), 14(11%)
Ba-133	10.8 y	384(8.9%), 356(62%), 303(18.3%), 276(7.3%), 81(2.6%), 53(2.14%)
Cs-137	30.2 y	662(85%)
Co-60	5.3y	1333(100%), 1173(100%)
Mn-54	312.7d	835(100%), 5(23%)
Tm-170	128.6d	84.2(3%), 59.4(5%), 52.4(5%), 51.2(5%)
Ir-192	73.8d	468(30%), 316(100%), 308(37%), 296(38%), 206(7.5%)

Since the first type of error is independent of source strength, therefore, the statistical error decides the necessary source strength. It is well known that in radiation counting experiments, the statistical error (ε) involved is given by

$$\varepsilon = \frac{\sqrt{N}}{N} = \frac{1}{\sqrt{N}} \tag{2.2}$$

Where N: counts for arbitrary time period t. The mathematical relation between sensitivity (S) and error is given below

$$\varepsilon_{\alpha} \approx \frac{1}{S.\sqrt{I}} \tag{2.3}$$

That is, the statistical error is inversely proportional to sensitivity. For a given count rate (I), the higher the sensitivity, the smaller will be the error. This is one of the key reasons why the use of lower energy gamma is desirable.

The activity required for the measurement can be calculated using following equation:

$$A_{(dps)} = I_{(cps)}.\epsilon_{g}.\epsilon_{I}.\gamma_{EI} \tag{2.4}$$

Where $A_{(dps)}$: Activity required, $I_{(cps)}$: count required for a given accuracy, ϵ_g: geometric efficiency in the densitometry setup, ϵ_I: intrinsic efficiency of the detector selected, γ_{EI}: gamma emission ratio of the selected source.

(4) To estimate the shielding requirements: Normally, a shielding cask made up of the lead is used to house the source. The details of the cask design are not important as long as it provides adequate shielding and the gamma beam can be turned on and off using an appropriate shutter system. More accurate calculation of the radiation dose coming out from the radiation shielded container can be performed theoretically using Monte Carlo simulations for the radiation transport. After performing all the calculations, it is ensured that total dose received by both the researcher and the public are well below the maximum permissible annual dose rates.

(5) Selection the scintillator and counting system: The choice of scintillators is another important step in the gamma densitometer design. The most significant parameters are detection efficiency and decay constant of the scintillator. High detection efficiency is desirable in order to reduce the required source strength and shielding. A short decay constant is necessary for high count rates to avoid pulse pileup or saturation. The properties of a number of scintillation crystals are given in Table 2.3. Among the many scintillators, NaI(T1) is the most commonly used because of its high detection efficiency. However, its relatively long decay time limits its applications to low count rate experiments (<10^5cps).

Table 2.3: Properties of different type of scintillator crystal

Scintillator	Decay Constant (µs)	Density (g/cm^3)	Conversion Efficiency
NaI (Tl)	0.23	3.67	100
CsI(Na)	0.63	4.51	85
CsI(Tl)	1.0	4.51	45
CsF	0.005	4.11	3
LiI(Eu)	1.4	4.08	35
CaF_2(Eu)	0.9	3.19	50
NE102A	0.002	1.05	<5

For count rate exceeding 10^5 counts, it is highly prone for the fluctuation and thus requires use of other crystals with shorter decay constants. For example, CsF is used because of its shorter decay constant in comparison to NaI, (Guerrero, 1978). However, its very low detection efficiency (~3%) makes it unattractive. Another possible alternative is to use plastic scintillator with typical decay times of 1 to 3 ns. Its detection efficiency is poor. The associated electronics component required is depicted in the Fig. 2.2. The details of the each component will be discussed in the later section.

2.1.2. Radiotracer techniques

The fundamental of radiotracer technique is to label the flowing phase in the system with suitable radioisotope and track its passage at different locations of the system. From the measured radiotracer concentration curve, evaluation of the flow dynamics parameters of the system is done (Fig.2.3) (IAEA, 1990). The radiotracers studies in these industries are done for the purpose of optimize processes, solve problems, investigation and validation of fluid dynamic modeling, improve product quality, save energy and reduce pollution (IAEA, 2001; 2008A). In the various, newly developed process flow systems in the industry, two or more phases such as gas, liquids and solid interact with each other for the production of number of products. Due to the presence of the different moving phases in these systems, it becomes highly complex to understand these systems using the conventional available techniques (Chaouki et al., 1997B). The conventional techniques are used to get system parameters at small scale system (Christophe et al., 2002; Ramírez and Eugenia, 2004). Nevertheless, the radiotracer technique offers a practical means to measure the flow dynamic parameters of these systems with ease (IAEA, 2008B; Pant et al., 2001). The different type of the radiotracer, design of the radiotracer experiment, production of the radiotracer, methods for labeling of different phases, tracer injection and detection and general nalysis of the data is discussed in upcoming different sections:

2.1.2.1.Categories and type of the radiotracer

Any substance provides way to observe, analyses and study the flow behaviors of any system (physical, chemical or biological process) by measuring change in its property such nuclear, atomic, molecular, physical, chemical or biological can act as tracer (IAEA, 2001; 2004A; 2004B; 2013). The brief classification of the radiotracer as follows:

2.1.2.1.1. Active and passive radiotracer

Passive radiotracer: The prerequisite is that the tracer should passively track the phase (gas, liquid, solid) in which it is injected. The chemical and physical behaviour of the tracer should identical to the tracing phase during course of tracing. Moreover, neither the tracer should alter behavior of the traced phase nor fluid phase alters the tracer behavior (IAEA, 2008B).

Active radiotracers: The tracer is taking dynamic part in the process in a qualitatively way. As tracing phase is undergoing change, the tracer correspondingly also changes with it. The degree of the active part-taking is a quantitative measure of the property to be determined. In most of the large scale industrial radiotracer experiments, tracer studies are done using passive tracer (IAEA, 2004A).

2.1.2.1.2. Intrinsic and extrinsic tracer

If any atom present in the tracing phase molecule is replaced by radioactive or stable atom and provides means for tracing the phase of interest in process system known as intrinsic tracer (IAEA, 2008A; 2014). For example, in the case of water, there are three such labels; Oxygen-18 ($^{1}H_2{}^{18}O$) and Deuterium ($^{1}H^{2}H^{16}O$) measured as isotopic ratios

($^{18}O/^{16}O$ and $^{2}H/^{1}H$) with mass-spectrometric techniques and Tritium ($^{1}H\ ^{3}H^{16}O$) measured by nuclear techniques (using liquid scintillation counting).

Any substance having same flow behavior as bulk phase to traced in the process system known as extrinsic tracer (IAEA, 2004B). For example, in case of water, ^{131}I as sodium iodide &^{51}Cr-EDTA are examples of extrinsic tracers

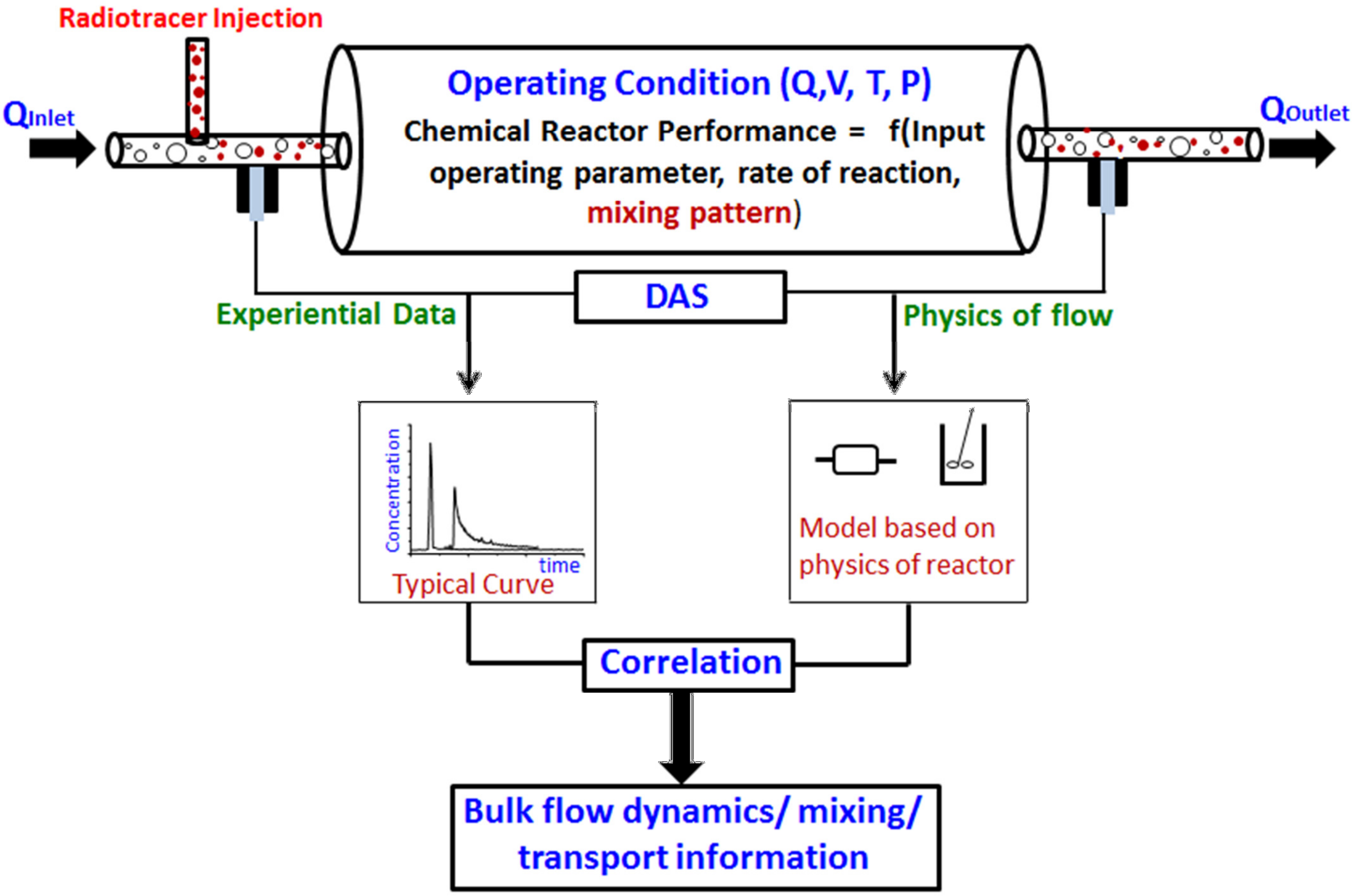

Fig.2.3. General principle of radiotracer technique (Taken from IAEA, 1990 and redrawn)

2.1.2.1.3. Advantages of the radiotracer over the conventional tracers (Charlton,1986; IAEA, 1990; 1991; 2001; 2004A; 2008A; 2015; Pant et al., 2001)

- They have high detection sensitivity for very small concentrations. Some of the radiotracer can be detected in extremely small quantities up to 10^{-17} grams.
- The mass of the tracer used in tracing is negligible as compared with bulk tracing phase. For instance 1 Ci (37 GBq) of $^{82}Br^{-}$ as NH_4Br weighs only 0.9μg. Therefore, they don't interfere in the dynamics of the system under investigation, when injected in the system to study flow dynamics.
- They provide in-situ measurements, providing information in the shortest possible time.
- As the radiation produced by the tracer can penetrate pipe or vessel under study. The measurement can be done online. This is of special importance for many industrial process systems.
- The radiotracer offers the possibility of low memory effect. The radioactive traces are short lived. Hence they disappear and radioactivity level declines to a minimum level in short period. This allows doing of experiments on the same location with the same tracer multiple times.
- Radioactive tracers can be made selective. As different isotopes have different characteristic gamma energy radiation. Therefore, multiple tracers can be injected simultaneously into the system and with the use of nuclear spectrometer all of them can track different phases of the system.

- Radioactive tracer responses are specific in nature i.e. emission of radiation from the radionuclide or tracer is not affected by process parameters such as temperature and pressure.
- The decay of the radionuclide or radiotracer follows simple statistics. It allows the experimenter to compute maximum precision in measurement at any given experiment.
- The radiotracer experiments have extremely high benefit to cost ratio.

2.1.2.2. Design of the radiotracer experiment

2.1.2.2.1. Feasibility assessment

Before carrying out a radiotracer experiment in a process system, the radiotracer experimentalist should access the feasibility of doing the experiment and discussions with the process engineers. All the information such as type of fluid/solid flowing in the reactor and its physical and chemical properties, its operating parameters such as fluid flow rate, temperature, pressure, dimension of the reactor/volume, hydrodynamic parameters such as designed mean residence time and flow patterns, final fate and flow of the material should be collected. The suitable radiotracer injection and monitoring locations should be recognized. Based on the discussion, decision of carrying out the study is to be made. Subsequently, if experiment can be carried out, the next important step is to selection of radiotracer (IAEA, 2001).

2.1.2.2.2. Selection of the radiotracer

The selection of a suitable radiotracer is very important for the study. The physical-chemical behavior, half-life, specific activity, type and energy of radiation and radio-toxicity are main characteristics considered for the selection of a radiotracer (IAEA, 2008C, 2004C).

2.1.2.2.2.1. Physico-chemical form

The physico-chemical behavior of the tracer should be same as the material under the study. In an experiment, if we are aiming to study the dynamic chemical reaction. The suitable tracer for this study is to have identical physical and chemical properties as the tracing phase material (IAEA, 2008A). This tracer is referred to as chemical radioactive tracer. For example, H^3HO for water, $^{24}NaOH$ or $Na^{18}OH$ or NaO^3H for NaOH. In most of the industrial process systems flow behavior of the process material is to be studied. In these cases, the tracers having similar physical properties as the tracing phase is suitable (IAEA, 2014). For example, Br-82 as dibromobiphenyl or I-131 as Iodobenzene is used as tracer to follow the organic path in the petroleum and petrochemical industry. A list of the most extensively used radiotracers to study industrial process systems in industry are presented in Table 2.5.

2.1.2.2.2.2. Half-Life

The half-life of a radiotracer is a crucial factor to be considered while planning for a radiotracer study. It has to be adequately long to allow time to transport the tracer from the nuclear reactor to radiotracer processing laboratory and then to the experimental site and complete the measurement. At the same time, to reduce the level of residual tracer in the exit streams, a short half-life tracer is desirable. In addition to radiological safety considerations, a short half-life is also useful if a series of similar experiments is to be repeated, particularly in a closed system.

2.1.2.2.2.3. Type of radiation and energy

As the gamma emmiting radiation have highest penetration power as compared to other nuclear radiation such as beta and alpha particles and allows online measurment. Hence, in most of industrial applications gamma emmiting radiatrcer are used. However, the penetration of gamma radiation is also dependent on the energy of the radiation. The energy of the gamma radiation should be sufficiently high to penetrate through the walls of the system for '*in situ'* detection and at the same time should not be high enough, so that only modest shielding requires for transportation.

2.1.2.2.2.4. Specific activity

The radioactivity per unit mass of the radiotracer (specific activity) is an important factor to be considered from the radiological safety point of view. Usually, in the radiotracer experiment, we transport minute amount of tracer to the experimental site as they are easy to shield and handle. But the injection of high specific activity at all times have a risk that tracer will get adsorbed to the wall of system and never reach to tracing bulk flow of the system. The possibility of loss of tracer by adsorption is reduced by adding sufficient amount of carrier to tracer solution. The carrier is the non-radioactive counterpart of the tracer. For example inactive ammonium bromide (NH_4Br) could be used as a carrier for radioactive bromine-82 (as $NH_4{}^{82}Br$) and NaI for the I-131 as $Na^{131}I$.

2.1.2.2.2.5. Radiochemical toxicity

The health hazards associated with the radiotracer or radioisotope known as radiochemical toxicity. The harmful effects of the radiation to the humans are well established. Hence, the radiotracer experimentalist is exposed to radiation during radiotracer handling, potential spillage leading to air contamination and inhalation or suspected intake by ingestion mode. The radiotoxicity of a radioisotope or radiotracer depends upon following (ICRP, 1991):

- half-life of radio-nuclide,
- type of emitted radiation and its energy,
- degree of selective localization in the body and
- rate of elimination from the body
- chemical toxic nature

Based on the above properties, grading for radiochemical toxicity for various radioisotopes has been done in four category i) very high toxicity ii) High toxicity iii) moderate toxicty iv) low tocity. The more details about radiotoxicity classification is given in ICRP, 1991. The ideal radiotracer to used in the industry should be low toxicity. Most of the radioisotope used as radiotracers are belong of moderate and low level of the radiotoxocity. The generally used radioisope as tracer in the industry are listed in the Table 2.4, the I-131 and Sc-46 have moderate level of the toxicity and rest of the radiotracer have low radiotoxicity as desired.

2.1.2.2.3. Estimation of the amount of the radiotracer

The second most important step for the planning of the radiotracer is assessment of the amount of tracer required for the radiotracer experiment. The lowest limit of the amount of tracer is assessed, according to measurement sensitivity of detector in desired geometry, accuracy levels required, expected dilution/dispersion from injection to detectionpoints, background radiation present in system and probableloss of the tracer (IAEA, 2004B; Pant et al. 2001). The upper limit is set by radiological safety concerns.

At many times, it may happen that the amount of activity to be injected is less than the upper limit but higher than an optimum amount. This may result in saturation in the response of the inlet detector and subsequently, result in loss of counts and hence it may not be possible to account for tracer quantitatively. This could lead to errors in obtaining the required information. Hence, it is essential to estimate the optimum amount of radioactivity for the radiotracer experiment. The detail mathematics is discussed in IAEA, 2004B document.

2.1.2.2.4. Production of the radiotracer

Nuclear Stability is a concept that helps to identify the stability of an isotope. The two main factors that determine nuclear stability are the neutron/proton ratio and the total number of nucleons in the nucleus. The principal factor that determines the stability nucleus is neutron to proton ratio. Elements with ($Z<20$) are lighter and these elements nuclei and have a ratio of 1:1 to have the same number of protons and neutrons. Elements that have atomic numbers from 20 to 83 are heavy elements, therefore the ratio is different. The ratio is 1.5:1. The reason for this difference is because of the repulsive force between protons: the stronger the repulsion force, the more neutrons are needed to stabilize the nuclei. However, if the ratio of the neutron and proton is changed by any means, the isotope becomes radioactive. Thus, radioisotope production involves introduction of neutrons or protons in the nuclei of stable elements. This is accomplished by bombarding specially prepared targets by neutrons or charged particles. When the bombarding particles impinge on the target nuclei, one or more of several possible nuclear reactions take place leading to the radio activation of the target. These include the (n,γ), (n,p), (n,2n), (n,α), (p,xn), (p,d), (p,α) and other reactions (IAEA, 1991; 2003; 2004C). In each bracket the first letter refers to the bombarding particle and the second letter refers to the particle spontaneously emitted from the nucleus during the reaction (n=neutron; p=proton; d=deuterons, α=alpha particle; γ=gamma photon).

2.1.2.2.4.1. Neutron activation

Neutron activation in nuclear reactors is the most common method of radionuclide production. Nuclear reactors provide intense fluxes of thermal and epithermal neutrons (10^{13} to 10^{14} $n.cm^{-2}.s^{-1}$) (IAEA, 2003). Depending on the energetics of the reaction, the target nucleus first absorbs a neutron and then spontaneously emits either a γ-photon or a charged particle (proton or α particle). The most abundant reaction type is the (n,γ)-reaction.

Table 2.4: Most commonly used radiotracers in industry

Radionuclide	Chemical form	Phase tracing	Half-life	Energies (MeV) (%yield)
^{24}Na	Sodium carbonate, Na_2CO_3 (Na^+) Sodium nitrate, $NaNO_3$ (Na^+) Sodium acetate, CH_3COONa Sodium naphtenate,$C_{10}H_7COONa$	Aqueous Aqueous Organic phase Organic phase Organic phase	15 h	1.369 (100%), 2.754(100%) 3.86 (0.08%)
^{41}Ar	Argon gas	Gas	1.833 h	1.294 (99%)
^{46}Sc	Scandium chloride, $ScCl_3$ (Sc^{3+})	Aqueous	84 d	0.889 (100%), 1.12 (100%)
^{51}Cr	Cr-EDTA, $CrCl_3$, Na_2CrO_4	Aqueous	28 d	0.320 (9.8%)
^{56}Mn	Manganese naphtenate, $(C_{10}H_7COO)_2Mn$	Organic	2.58 h	0.85(100%), 1.8(30%), 2.1 (20%)
^{59}Fe	Iron metal	Solid	45 d	1.099 (55%), 1.292 (44%)
^{79}Kr	Krypton gas	Gas	35	0.51(15%)
^{82}Br	Ammonium bromide, $NH_4Br(Br^-)$ Para-dibromobenzene, $C_6H_4Br_2$ Bromonaphthol, $BrC_{10}H_6OH$ Bromododecane, $C_{12}H_{25}Br$	Aqueous Organic Organic Organic	35.7 h	0.554 (70%), 0.619(39%), 0.698 (25%), 0.776 (85%), 0.828 (24%), 1.044 (34%), 1.317 (24%), 1.475 (15%)
^{99}Mo	Sodium Molybdate (MoO_4^{2-})	Aqueous	66 h	0.14 (88%); 0.74 (14%)
^{99m}Tc	Sodium Pertechnetate (TcO_4^-)	Aqueous	6 h	0.14 (88%)
^{131}I	Sodium iodide, NaI (I^-) Iodo-benzene	Aqueous Organic	8.04 d	0.364 (80%), 0.64 (9%)
^{140}La	Lanthanumnitrate, $La(NO_3)_3$ (La^{3+}) Lanthanum naphthanate, $(C_{10}H_7COO)_3La$	Aqueous Organic	40.2 h	0.33 (19.5%), 0.487 (41%, 0.537 (30%), 0.867 (20%), 0.925 (10%), 1.595 (95.5%), 2.547 (3.5%)
^{198}Au	Choroauric Acid $HAuCl_4$/ Colloidal gold	Solids Aqueous	64.8 h	0.412 (99%)

2.1.2.2.4.2. Charged particle activation

Linear accelerators and cyclotrons are comman sources of charged particles for radionuclide production. In these system, the charged particles are accelerated to high energies of the order of tens of mega volts under the effect of a magnetic field. The accelerated particles are then forced to impinge on specially prepared targets to induce nuclear reactions leading to radionuclide production. To produce a specific radionuclide, one can play with type and energy of projectile and with target nuclide. The most comman radionuclide used for industrial tracing ^{68}Ge [^{69}Ga(p,2n)^{68}Ge] is produced by charge particle activation (Palige, 2011).

2.1.2.2.4.3. Fission product

The fission of ^{235}U or ^{239}Pu in nuclear reactor operation provides a wide variety of radioactive nuclides known as fission products. Some of the long-lived fission products of industrial importance are: ^{85}Kr, ^{90}Sr, ^{99}Mo, ^{131}I, ^{137}Cs and ^{147}Pm. These are recovered during chemical processing of the irradiated fissionable target material.

2.1.2.2.4.4. Radiotracer generators

It is the most practical way to obtiain short lived radioisotope in places situted far from nucler reactor and cyclotron. A radionucidic genertor is based upon principle of mother-dughter nucler genetic reltionship. It is also known as mechnical-physical-chemical devise based on above principle (IAEA, 2013). In the first step of prepartion of the genertor a long lived parent produced by irradiation of suitble targent in the nucler reactor or cyclotron. In the second step, radioctive target is chemiclly fixed in a packed column. In the final step, suitble solvent is used to elute the daughter product. After each elution, system is ready for the next elution after about three to four half-lives of the daughter product (Dash et al., 2017). The most comman generators used for the process material tracing are Ge/Ga and Mo/Tc used in the industry (Palige et al., 2017). A comman list of radionuclidic generator is lised in the Table 2.5.

2.1.2.2.5. Methods for the labeling of the tracing phase

For the radioactive labeling of the different phases different methods are used. The details of the methods follow (IAEA, 2004C):

2.1.2.2.5.1. Solid phase tracing

The three different methods used for the labelling of the solid phase such as internal labelling, surface labelling and mechanical tagging are discussed below:

2.1.2.2.5.1.1. Internal Labeling

In this method small portion of the tracing phase is analysed for the identifiction of the activable element. If the tracing phase is having the activable element. Subsequently, sufficient amount of the trcing phase is irradited in the rector to produce tracer. Table 2.6, provides list of tracers used to labelsolids phse by direct activation of. ^{198}Au, ^{147}Nd, ^{51}Cr, ^{192}Ir, ^{182}Ta, and ^{46}Sc are the radioactive nuclides often induced (IAEA, 2008A).

Table: 2.5. Most common radionuclide generators

		Radiation (MeV)				Radiation (MeV)	
Daughter nuclide	Half-life	β	γ	Parent nuclide	Half-life	β	γ
^{68}Ga	68 min	1.90[a]	0.51, 1.08	^{68}Ge	275 day	EC	-
^{44}Sc	3.92 hr	1.47[a]	0.51-1.16	^{44}Ti	48 yr	EC	0.08
^{99m}Tc	6.0 hr	IT	0.14	^{99}Mo	66.7 hr	1.23	0.18, 0.74
^{140}La	40.2 hr	1.34	0.48-1.60	^{140}Ba	12.8 day	1.02	0.03, 0.54

[a] = Positron emitter; EC=Electron Capture; IT=Internal Transition.

2.1.2.2.5.1.2. Solid surface labeling

(i) The adsorption of a radiotracer (or radionuclide) on the surface of a solid has been used as a labeling method for sand particles and many different materials. The particles are first soaked in stannous chloride ($SnCl_2$) and then placed in an aqueous solution of gold chloride containing radioactive ^{198}Au. The gold exchanges with tin, through a reduction-oxidation process, to produce labeled particles. The labeled sand can be used in aqueous systems with no appreciable loss of tracer. Some materials like cement, carbon black, aluminum powder or any material having affinity for the adsorption can also be labeled with ^{198}Au.

(ii) Sometimes ion exchange properties of the material are used for surface labeling. For example, clay may be labeled with cations such as $^{51}Cr^{3+}$ and catalyst particles with ^{143}Cs, ^{60}Co, ^{144}Ce as polyvalent ions with valencies from 1 to 4. Other surface labelling methods for sand and silt using ^{198}Au, ^{51}Cr, ^{46}Sc have been widely used for sediment transport studies.

Table 2.6: A list of the mateials activated directly in the reactor

Irradiated material	Induced radionucldes
Coal	^{46}Sc, ^{59}Fe
Clinker, cement	^{24}Na, ^{140}La
Cracking catalyst	^{140}La
Gold ore	^{198}Au, ^{59}Fe, ^{42}K, ^{140}La, ^{56}Mn, ^{24}Na, ^{46}Sc,^{51}Cr
Copper ore	^{64}Cu, ^{42}K, ^{140}La, ^{24}Na, ^{59}Fe

(iii) In the last method, if the solid phase is having adequate affinity for adsorption/ absorption. Then, a selected radionuclide solution is adsorbed/ absorbed for the preparation of radiotracer.

2.1.2.2.5.2. Liquid phase tracing

In general both the aqueous and organic phase are labeled for the radio-tracing studies in the industries the methods of the labeling are discussed below:

2.1.2.2.5.2.1. Organic phase tracing

The only intrinsic radiotracers for organic materials are ^{3}H, ^{14}C, ^{32}P and ^{35}S labelled compounds. Being beta-emitters, these are measured through sampling followed by liquid scintillation counting. Therefore these are rarely used for industrial investigations. However they are extensively used in laboratory investigations and in oilfield tracer tests (inter-well tracing). Extrinsic tracers are more widely used for tracing organic phase in the industry are listed in the Table 2.7:

Table 2.7. Common industrial radiotracer used for the organic phase tracing

Tracer	Chemical form	Boiling Point (°C)	Decomposition (°C)	Melting point (°C)
p-dibromobenzen	$C_6H_6{}^{82}Br_2$	219	---	87
dibromobiphenyl	$C_6H_6{}^{82}Br_2$	355		164
Bromo-dodecane	$C_{12}H_{25}{}^{82}Br$	240	160	---
Bromonapthol	$^{82}BrC_{10}H_6OH$	130	150	84
Iodo-benzene	$C_6H_5{}^{131}I$	188	---	-31

2.1.2.2.5.2.2. Aqueous phase tracing

The only choice of intrinsic radiotrcer for aqueous phase is Tritiated water (HTO). Which is mostly used in the laboratory measurment and interwell tracer technology in reservoir engineering for the enhanced recovery of oil from depletd oil wells. Externsic tracers most commonly used in aqueous solutions in industrial application are listed in Table 2.8.

2.1.2.2.5.3. Gas phase tracing

Most comnnly used gas phase tracer (^{41}Ar and ^{79}Kr) produced by direct neutron activtion in the nuclear reactor. Wheres, radioactive methy bromide ($CH_3{}^{82}Br$) gas is produce by chemical reaction between $K^{82}Br$ and $(CH_3)_2SO_4$. Apart from these three other tracers used are listed in IAEA, 2015.

2.1.2.2.6. Injection of the radiotracer

The radiotracer tracer should be injected in a manner so that it does not disturb the steady flow in the system. A radiotracer could be injected into the system using any of the following types of injections i.e. impulse, pulse, step input, periodic input and random input (Levenspiel, 1999; Foglar, 2005). An impulse injection (Dirac Delta function) is most comman type of injection in industrial radiotracer applications as it is easier to interpret and requires of relatively lesser amount of radiotracer (activity) for study. It also reduces radiation the hazards and unnecessary radiation exposures to the radiation workers. An injection system or device is usually used to inject the radiotracer into the system as an impulse.

Table 2.8: Commonly used radiotracer for the aqueous phase

Radionuclide	Half-life	γ-energy (MeV)	Chemical form
^{24}Na	15h	1.37(100%), 2.75(100%)	Na_2CO_3, $NaHCO_3$
^{82}Br	36h	0.55(70%), 1.32(27%)	NH_4Br
^{140}La	40h	0.33-2.54	La-EDTA, $La(CH_3COO)_3$
^{198}Au	2.7d	0.411(100%)	$HAuCl_4$
^{131}I	8.04d	0.36(80%), 0.64(9%)	NaI, KI
^{46}Sc	84d	0.89(100%), 1.48(100%)	Sc-EDTA, $ScCl_3$
^{51}Cr	27.8d	0.325(9%)	Cr-EDTA

From simple needle syringe or peristaltic pump to complex remote injection system are designed to inject the rdiotrcer in the process system. With liquid systems operating at atmospheric pressure, a satisfactory injection may be performed by emptying a small vessel containing the tracer solution directly into the stream of interest. For pressures up to range 10 x 10^5-20 x10^5 Pa, a simple pneumatic injector consisting of a pressure vessel connected to a valve on the test pipe is used (IAEA, 2004B; Pant et al., 2001; IAEA, 2008C). The tracer solution or particles filled in a vessel is pressurized by compressed air cylinder connected to this system, to push the tracer into the line (Fig.2.4).

2.1.2.2.7. Detection of the radiotracer

The type of detector to be used depends on the radiation emitted and its energy, as well as the measuring environment, the precision required and the nature of the phase being traced. Gamma radiations can be detected by ionization chambers, scintillation detectors and semi-conductor detectors (Knoll, 2000). The convenient and easy to maintain detector is Geiger- Müller (GM) counter (a aype of gas filled detector). it is simple, rugged and low-cost, one more reason for this being useful is that it produces pulses that donot require electronic amplification. But due to its shorter and less flat counting plateau, it is not very accurate. The GM is not able to discriminate either the type or the energy of the radiation (IAEA, 2008A).

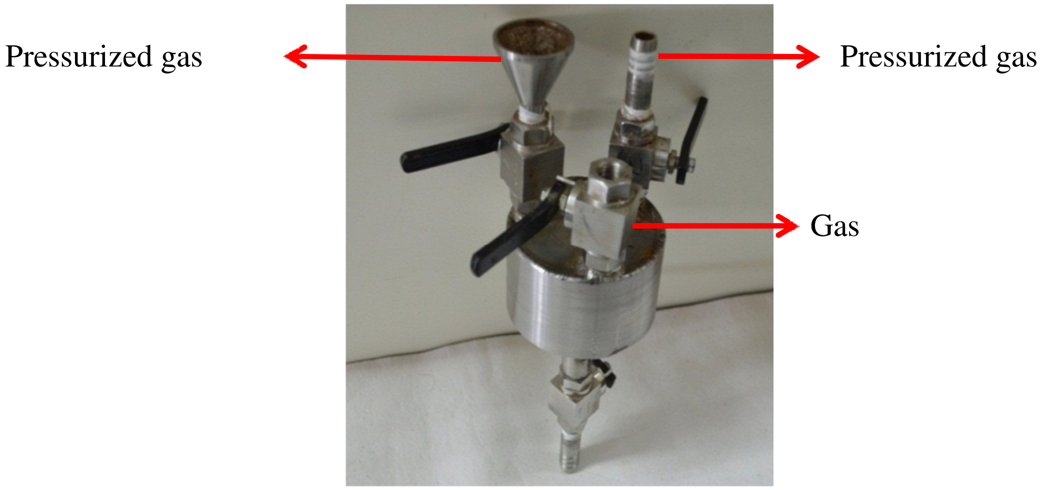

Fig. 2.4. A typical radiotracer injection system for an impulse injection of radiotracer

In oveall we can conclude that Gas-filled detectors use in radiotracer application is less used due to its inherent small efficiency of detection and stopping power for γ rays. Next alternative of the detectors is semiconductor detectors. They are the solid state equivalents of gas-filled ionization chambers. The density of the solid is much higher than the gas. The efficiency of semiconductor detector for the gamma radiation is about 2000 to 5000 times ionization chambers. Semiconductors have a small band gap between their conduction and valance band. This fundmental property of semiconductor is utilized to detect radiation. As, the gamma radiation falls on the semiconductor detector, creation of the electron and hole pair occurs. The charge created in this process is collected by the externally applied electrical field to the semiconductor detector. Using this basic principle, detection of the radiation is possible with semiconductor detector. The most widely used semiconductor detectors are made up of silicon (Si) and germanium (Ge). To create single electron-hole pair in the Si and Ge detector minimum energy required is 3 to 5 eV respectively. Hence, signal with high strength is produced as the energy required per transition is much lower. Besides this, the magnitude of the signal is proportional to the energy of the radiation. Therefore, they are widely used for isotope energy identification. The limitation of the semiconductor detector is that even at room temperature thermal energy is enough for creation of electron-hole pair. It acts as background for the signal produced by the radiation. To reduce the high background signal, semiconductor detector are always cooled using liquid nitrogen to reduce the backgound. The another problem associated with them is impurities present in the semiconductor (Si nd Ge) materials. These impurities decreases the magnitude of the signal produced by the intraction of the radiation with the semiconductor significantly. Because of this, the semiconductor detector crystals cannot be grown above 1cm thickness. The last factor that limts efficiency of semiconductor detector for gamma ray detection is their low atomic number. Although, the semiconductor detectors have high efficiency than gas filled detector, they are not popular choice of detector in the radiotracer application in the industry (IAEA, 2008 A; 2008B).

In most of the radiotracer application in the industry application of the radiotracer, scintillation detectors are used. Whenever, a gamma radiation falls on the any detector. It causes ionization and excitation of the atom or molecule present in the detector. These ionized and exited atom or molecules are not stable. They go through recombination and deexcitation. In this process, they release energy. In most of the materials, this energy is dissipated. On the other hand, in scintillator material the energy is dissipated by emission of visible light. The radiation detectors are made up of organic molecules and inorganic substances. However, the organic scintillators are made up of the carbon, nitrogen, hydrogen and oxygen. All these, elements are low Z elements having less efficiency for the gamma radiation. Thus, they are not preferred for the industrial radiotracer applications (Wilkinson III, 2004).

Transparent inorganic scintillator crystals made up of the higher Z elements, having high density can be produced within a large range of sizes. These type of scinatillators are able to absorb different γ energies with good efficency. The scintilation property of inorganic scintillators is due their crystal arrangement. The few scintillating crystals that can be used in the industry for densitometry measurement are listed in the Table 2.9.

The widely used detectors in radiotracer applications is scintillating NaI(Tl) detector. The sodium iodide (NaI) crystals donot scintillte visible ligth at room temperture due to their high band gap. The pure NaI emmits the radiation in UV range of energy spectrum by intraction of the gamma radiation. Hence, using the pure NaI, gamma radiation detection is not possible. To overcome this limitation NaI detectors are dopped with small amount of the thallium(Tl). Hence the detector is called NaI(Tl) detectors. Due addition of the Tl in the NaI crystal, the band gap decreases and now they emmit radiation in the visible region. The visible light emmited by the NaI(Tl) can be efficiently multiplied in photomultiplier (PM) tubes to detect gamma radiation. The Fig. 2.5 shows the construction of a typical scintillation detector consisting of a NaI(Tl) crystal and PM tube assembly.

Reasons for the wide popularity of NaI(Tl) scintillation detectors in industrial radiotracer applications as follows (Choppin et al., 2017, Cherry et al, 2012):

1.The higher density ($\rho = 3.67$ g/cm^3) and comparatively large atomic number ($Z = 53$) of the NaI(Tl) detectors. They act as efficient detector for gamma radition.

2. They are efficient detector than the gas filled detectors. They require ~30 eV to produce one visible light photon per gamma radiation absorbed.

3. They transprent to the visible light emiited by interaction of gamma radiation. As result, the loss of detector efficecy due to self absorption is minimum.

4. They can be grown in different sizes and shapes as per requirement (Fig. 2.6).

5. The light emitted by their scintillation scintilatiuon process is matched with response of the PM tube. The spectrum of the light emitted by scintillation process is shown in Fig. 2.7.

The semiconductor detector have better resolution and gas filled detector are cheper than NaI(Tl) detectors. However, semdicondutor are always require constant cooling by the liquid nitrogen. At the same time efficiency of the gas filled detector is much lower. The NaI(Tl) requires no colling and having efficiency higher than gas filled detector. It makes them an obivous choice for all the radiotrcer experimets carried out in different process systems.

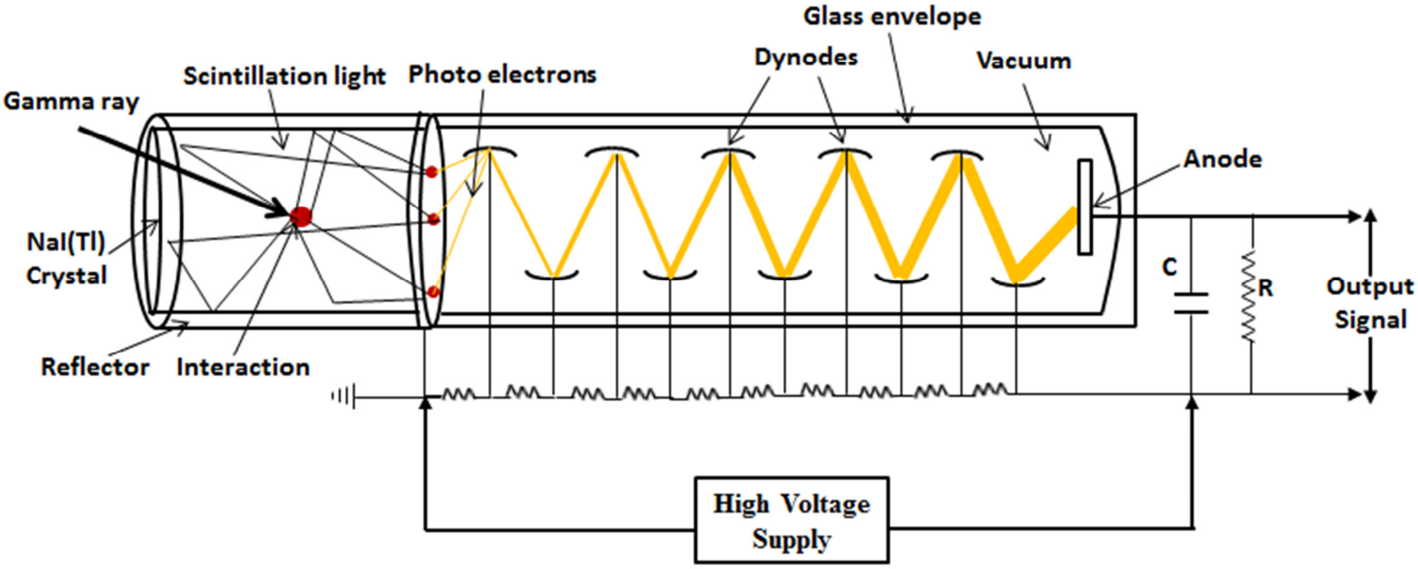

Fig. 2.5: Arrangement of NaI(Tl) craystal and PM tube in a typical scintillation detection assembly.

2.1.2.2.8. Data acquisition system for radiotracer experiment

Most of the radiation counting carried out in the radiotracer experiments is done using dedicated computer data acquisition systems (DAS) shown in the Fig 2.12. In these DAS different electronic components such as preamplifier, amplifiers, single channel analyzer (SCA) and counter and timer are embedded in electronic board in individual box. They are known as channels. There no possibility of change of the electronic components between the channels. This acts a specifically designed instrument for the radiotracer experiments.

Fig. 2.6:Various NaI(Tl) Crystal and photomultiplier tube assemblies (Cherry et al, 2012)

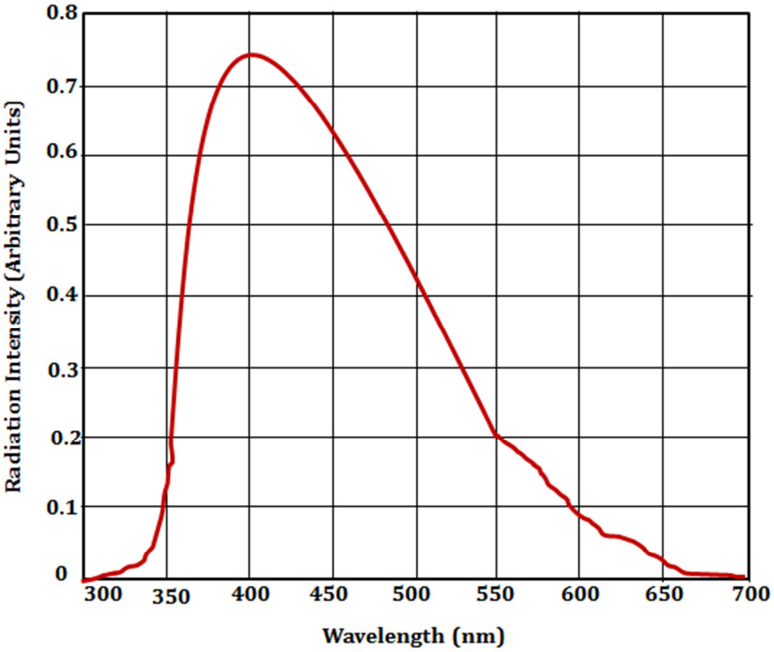

Fig.2.7. Emission spectrum of NaI(Tl) scintillator at room temperature assemblies (Knoll, 2000)

Table:2.9. Properties of the comman scintillator materials can be used in the radiotracer application in the industry

Property	NaI(Tl)	BGO	LSO(Ge)	GSO(Ce)	CsI(Tl)	CeF_3	LuAP(Ce)	$LaBr_3$(Ce)	Plastic
Density (g/cm^3)	3.67	7.13	7.40	6.71	4.51	6.16	8.34	5.3	1.03
Effective atomic no.	50	73	66	59	54	51	65	46	12
Pluse decay time (ns)	230	300	40	60	1000	27	18	35	2
Photon yield (per KeV)	38	8	20-30	12-15	52	4.4	12	61	10
Index of refraction	1.85	2.15	1.82	1.85	1.80	1.68	1.97	1.9	1.58
Hygroscopic	Yes	No	No	No	Slightly	No	No	Yes	No
Peak emmision (nm)	415	480	480	420	540	340	365	358	Various
BGO: $Bi_3Ge_4O_{12}$, GSO: Gd_2SiO_5, LSO: $Lu_2(SiO_4)O$, $LuAlO_3$, Plastic: NE102A									

They can channels from 5 to 32 in single unit. Hence these DAS used to carry out small scale laboratory to industrial scale RTD studies. Different detectors can be connected to the different channels using cables. The selection of the DAS is depends upon scale of the process system.

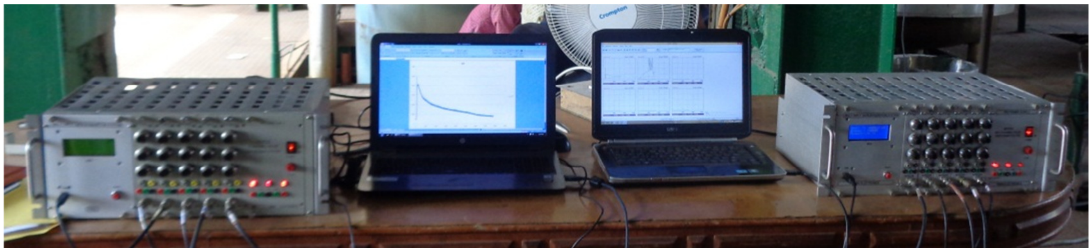

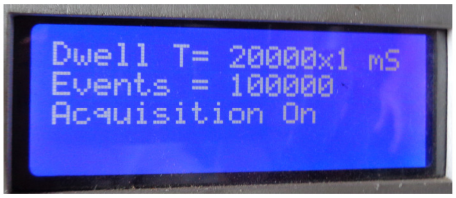

Dwell T= 20000x1 mS
Events = 100000
Acquisition On

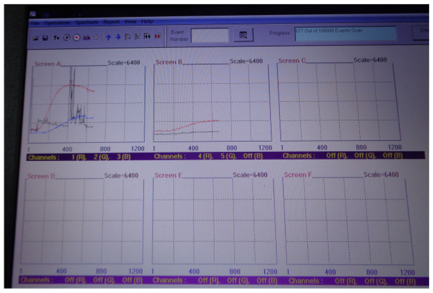

Fig.2.8. Two 5 channel unit, one 24 channel unit, the settings display on DAS and its computer controlled display.

Prior to the each experiment depending upon the radiotracer used, the response of the all the detectors is made identical. This is done in two steps, in the first step the SCA output of voltage each detector is seen in the oscilloscope. The output voltage each detector is adjusted to equal in magnitude and fairly above the background electronic signal. In the second step the response of the each detector is observed in specified geometry. It is always made sure all the the detector give identical response.

2.1.2.2.9. Data treatment and analysis

Even, in a precisely planned and wisely executed radiotracer experiment, it is always necessary to apply some corrections to experimental radiotracer data to obtain meaningful and desired information. The reasons for the correction are i) The first reason for treatment is that no signal is ever noise free ii) the detection of the radiation is statistical in nature: if the number of counts (N) recorded by detector is small (due to small amount of injected activity or counting time period is small), the statistical noise will hide the valuable desired signal iii) The undesirable gamma ray radiation sensed by the radiation detector placed at the vicinity of the injecting device or of the storage of spent fluid iv) due to large RTD of the system and human error, complete data could not be recorded.

A suitable treatment of radioactive tracer data can require up to nine successive stages, as illustrated in the flow chart (Fig.2.13) (IAEA, 2004B). This is general procedure for the data treatment in many cases some of the steps can be skipped according to the nature of the radiotracer data. The details of the each step are discussed below:

2.1.2.2.9.1. Conversion of non –equidistant points to equidistant points

Generally counting time interval or dwell time of measurement in a radiotracer experiment is constant. The end result of above measurement is that we get an equidistant concentration time data. However, in some cases it may be required to change time interval during the course of the measurement. In order to estimate the moments and mathematical modelling of data (IAEA, 1996).It is convenient to have equidistant data. Therefore, it is required to convert non-equidistant data into equidistant data by linear interpolation technique (Stegowski, 1993). This step of treatment is not so common in the radiotracer data treatment. However, It may require in the special cases.

2.1.2.2.9.2. Dead time correction

In all the detector systems, there will be a minimum amount of time that must separate two events in order that they will be recorded as two separate pulses. In some cases the limiting time set by processes in the detector itself and in other cases the limit may arise in associated electronics. This minimum time of the separation is usually called the dead time of the counting system. Because of the random nature of radioactive decay, there is always some probability that a true event will be lost because it occurs too quickly following the preceding event. These dead time losses can be overcome rather severe when high count rate are encountered in an experiment, the accurate counting measurement made under these condition must include some correction for these losses. The practical methods for measuring dead time and methods to apply the corrections are discussed in details in Knoll, 2000.

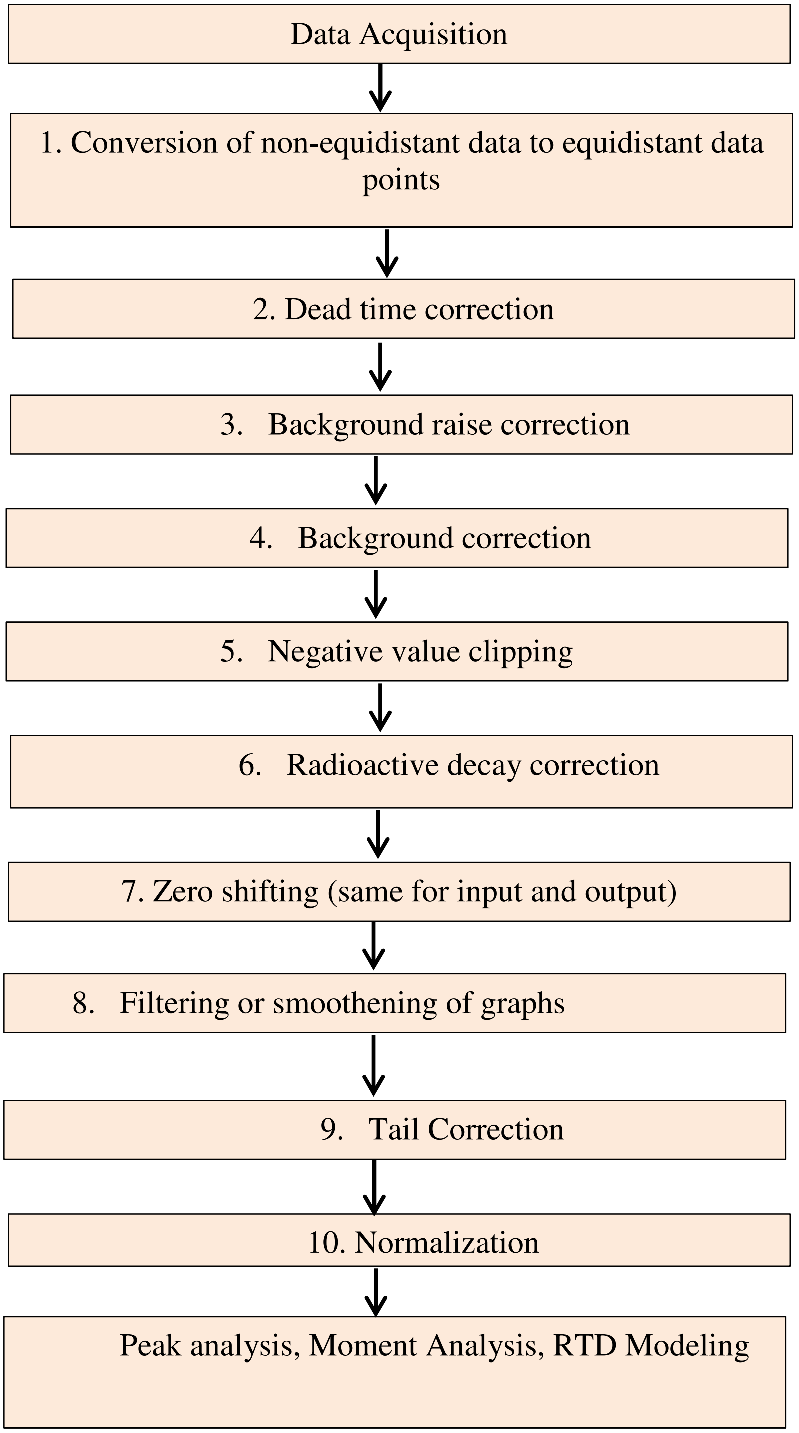

Fig.2.9. Steps involved in the data treatment of a radiotracer experiment (Taken from IAEA, 2004 and redrawn)

2.1.2.2.9.3. Background correction

The background radiation level is always present in any measurement due to the naturally occurring radioisotopes present in the environment and system under the investigation. To apply the background radiation level corrections in a radiotracer experiment generally prior to the radiotracer injection in a experiment 30 – 40 readings were recorded and subsequently 30-40 readings were recorded. After the experiment average of the background count is taken and subtracted from each radiotracer data to get background corrected counts.

2.1.2.2.9.4. Negative value clipping

Being statistical nature of the radiation, there is a fluctuation in the radiotracer concentration occurs and some of the values observed are lower than the average background level radiations. These values are generally observed at the beginning and end of the radiotracer curve. In the actual system counts cannot go lower than the average background radiation level. These negative values are corrected by replacing the negative values to zero.

2.1.2.2.9.5. Radioactive decay correction

As the radioactive decay follow exponential decrease with time. Hence, it is essential correct experimental data for decay correction. The decay corrected count rate is given as:

$$n = m\,e^{\lambda t} = m\,e^{0.693t/t_{1/2}} \qquad (2.5)$$

where λ is decay constant, t and $t_{1/2}$ are arbitrary time and half-life of the radioisotope respectively.

2.1.2.2.9.6. Background raise correction

In some of the experimental situations, the outlet tracer concentration distribution curves may be distorted due to increased background radiation levels during the experiment. One of the possible and common reasons for increase in background level is accumulation of tracer in a storage tank near the outlet detector. The situation is usually encountered when high energy gamma emitting tracers are used and the outlet detector is not shielded adequately. Such situations should be carefully examined before carrying out the experiment and thus outlet detector shielded adequately. However, If adequate shielding is not done, the Thyn et al., 2000 and 2004 have suggested the methodology for the raise in the background in the detail.

2.1.2.2.9.7. Zero shifting

To observe the background level radiation in a radiotracer experiment mostly 30 to 40 readings are observed to have an average value of background radiation level. However, this shifts the radiotracer concentration observation time in the recorded curve. It results in the evaluation of the higher residence time of the system than the actual. To correct the time bias, the time of the injection of the radiotracer is regarded as zero and shifting of the time is done.

2.1.2.2.9.8. Filtering/ smoothing

The aim of filtering / smoothing step is to minimize the fluctuations due to counting statistics or electronic noise. Any selected filtering method selected, it must be ensured that in process of smoothing and filtering essential features of the experimental data are not lost. Several methods are available for the filtering and smoothening of the experimental observed data (Thyn et al., 2000). The widely used method for the smoothing and filtering of the data is Fourier transform. It can be used to compute the signal frequency spectrum and undesired (usually high frequency) components can be eliminated (IAEA, 2004B).

2.1.2.2.9.9. Tail correction

Tail correction is one of the very important steps in preliminary processing of radiotracer data. In some cases end portion of the curve is not recorded due to long residence time of the system, extensive tail of the curve and data acquisition system problems. Data acquisition in tracer is complete, if the background radiation level in the start and end of experiment is same. However, due to the above mentioned reasons the radiotracer concentration curve does not go to the zero. The objective of tail correction is to extend the radiotracer curve in a manner, so that the residence time of the system does not become too large due to the extrapolation of the tail. Generally, a suitably selected exponential decay function is used to fit the tail portion of the curve and extended as function of the time till count rate becomes zero or negligibly small (Thyn et al., 2000).

2.1.2.2.9.10. Normalization

After all the corrections are made, the tracer concentration curves are normalized.It is done by division every point of curve by area of the experimentally observed count time curve.The resulted new curves are called normalized residence time distribution curve. The area under the normalized radiotracer concentration curve is unity. After normalization, the data can be presented in different forms. Since the most of the radiotracer experiment are planned to inject radiotracer as an impulse, the normalized response of tracer concentration cure represents transfer function of the system and is defined as (Levenspiel, 1999; Foglar, 2005; Stegowaski and Nowak, 2007).

$$E(t) = \frac{C(t)}{\int_0^{\infty} C(t)dt} \tag{2.6}$$

Since the tracer distribution is measured in discrete time interval, the above equation can be written as:

$$E(t) = \frac{C(t)}{\sum_i C(t)dt} \tag{2.7}$$

The area under the normalized transfer function (E(t)) is equal to unity. Thus,

$$\int_0^{\infty} E(t)dt = 1 \tag{2.8}$$

2.1.3. Application of the radiotracer technique

The radiotracers are applied in the various industries to obtain the different process parameters of the complex systems. The valuable information obtained from these experiments has high cost to benefit ratio. The leak detection, sediment transport, effluent dispersion, mixing time measurement study, residence time distribution measurement, flow rate measurement, wear rate measurement and radioactive particle tracking technique are applied in the industry (Godfroy et al., 1997; IAEA, 2009, Samantray et al. 2014; IAEA, 2014; Sharma et al., 2006; Goswami et al., 2014; Muthukumar,et al., 2010; Pant et al., 2016; Biswal et al., 2018; Upadhyay, 2010). The mixing time measurement and residence time distribution are discussed in detail in the following section:

2.1.3.1.Mixing time measurement

Mixing plays a fundamental role in many industrial applications, but due to its complexity in fluidized bed reactors or multiphase flow systems, theoretical approaches are very limited. Monitoring or measuring the mixing properly is of great importance from the practical point of view and for the validation of theoretical models as well (Harnby et al., 1997).

Mixing time is defined as the time required for achieving a certain degree of homogeneity of injected tracer in a process vessel. As per the general definition time corresponding to fluctuations in counts is lower than ±5% of the final equilibrium value know as mixing (Fig. 2.14) (Thyn et al., 1996). Generally, mixing time is determined by the measurement of the dynamic distribution of a small amount of material (tracer) added in the vessel and its measurement at different locations. From an experimental standpoint, several techniques have been developed for measuring the mixing time. Based on the disturbances produced in the measured flow, they can be classified into two groups: non-intrusive and intrusive. However, depending on the type of data generated, they can be also classified into direct measurements and indirect measurements. From a macro mixing standpoint, the bulk mixing time is the time required to get all points in the vessel uniformly distributed, while the local mixing time is the measure of how fast a material is distributed in a particular region of the vessel, which depends on the local turbulence. Therefore, local measurements are time and space dependent, while bulk mixing time is based on time dependent measurements (temporal measurements) (Patterson et al., 2004). The various physical and chemical technique can be used for the determination of mixing time are listed in Table 2.10. Depending upon the different situations any technique can be used.

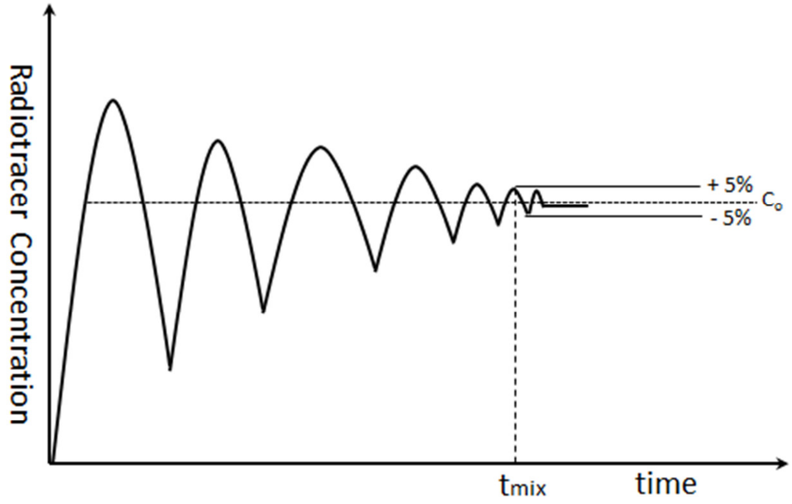

Fig 2.10. Typical curves generally observed in the mixing time measurement studies

Table 2.10: Different methods used for the measurement of the mixing time

Physical Property	Basic Methodology	Reference
Temperature (Intrusive, direct, Bulk)	This can be done by adding a liquid of different temperature into the bulk solution. Hereby, the temperature at different locations in the tank is monitored over time by sensors. In this case, mixing has been defined as the minimum residual fluctuation of temperature. **Disadvantage:** This physical technique is not suitable for highly viscous solution, since the viscosity of a fluid is a function of temperature.	Mayr et al., 1992; Karcz and Szoplik, 2008
Electrolytic conductivity (Intrusive, direct, Bulk)	Measuring conductivity is also commonly applied for determining the effectiveness of mixing. With this technique, an electrolyte solution is added to the tank, and the conductivity of the bulk solution is detected as a function of time. **Disadvantage:** This method is not suitable for nonconductive solutions.	Biggs, 1963; Kramers et al., 1953; Rielly and Britter, 1985; Karcz and Szoplik, 2008
Refractive Index (Non-intrusive, Indirect, Local)	Optimal mixing time can also be determined by measuring the scattering of light, when two liquids with different refraction indices are mixed. **Disadvantage:** Not for industrial system	Vusse, 1955; Zlokarnik, 1967; 1968
Colorimetric Method (Non-intrusive, Indirect, Local)	This technique is the simplest and the easiest method which is mostly used to ascertain the optimal mixing time. This technique is based on either neutralizing or redox reactions. With the former, acid or base is added to the bulk. The latter reflects the redox reaction between sodium thiosulfate and iodine with starch as indicator. **Disadvantage:** visual techniques require transparent reactors and clean media and are inappropriate for stainless steel vessels.	Himmler and Schierholz, 2004; Rousseaux et al., 2001
Planar laser induced	This method is applied by adding a fluorescence indicator to the bulk solution. Excited by a	Kling, 2003; Reungoat et

fluorescence (Non-intrusive, Indirect, Local)	laser, the fluorescence indicator emits light of a particular color (usually yellow-green). Fluorescence is detected here by sensors or observed by cameras. **Disadvantage**: It cannot be used in opaque systems.	al., 2007
Radioactive tracer technique (Non-intrusive, Direct, Local)	The principle of this method is that a radioactive liquid tracer is added to the bulk solution and its moment is measured by using scintillation detector. The main advantage of this technique is that the concentration of the tracer can be measured at high temperature. Where most other methods are not suitable. This technique is non-invasive and accurate. **Disadvantage**: Exposure to radioactivity.	Pant et al., 2001; Thyn, 1996
Liquid crystal thermography (Non-intrusive, Direct, Local)	The thermochromic liquid crystal presents different colors at different temperatures. By considering this property, the color changes in a solution can be visually analyzed. Similar to the colorimetric method, an advantage of this technique is that it is easy to identify dead zones. However, it is still subjective due to the visual observation by researchers and is unsuitable on an industrial scale. Any light disturbance from the surroundings could result in deviations of the mixing time. **Disadvantage:** Not for industrial system	Lee and Yianneskis, 1997

2.1.3.2.Residence time distribution measurements

For the production of various products required for the day to day life are manufactured in the different process systems. Each process requires a different type of reactor based on nature of the process involved. Therefore, the design of the reactor is very important to produce a product of desired quality with minimum cost and produces highest possible yield (Levenspiel, 1999; 2012; IAEA, 2008A). Two most common type of the reactors used in the industry are i) Batch type reactors ii) continuous type reactor as per the mode of the operation.

i) **Batch type process:** A process in which all the reactants are added together at the beginning of the process and products removed at the termination of the reaction is called a batch process. Mixing of the reactants and mixing time in batch type reactors is very critical and governs the performance of such reactors

ii) **Continues type process**: A process in which the reactants are fed to the reactor continuously and the products or byproducts are withdrawn in between while the reaction is still progressing. Continuous production will normally give lower production costs as compared to batch production, but it faces the limitation of lacking the flexibility of batch production. Continuous reactors are usually preferred for large scale production. The product distribution and conversion in such processes strongly depends on mixing behavior and residence time of species in this reactor.

2.1.3.2.1. Measurement methodology of RTD

All the continuously operating industrial systems are designed to have either plug flow (no axial mixing) or well mixed flow patterns (instantaneous complete mixing). But real systems never follow completely these ideal flow patterns. In major of the cases, the deviation from ideal flow patterns is considerable and has a direct bearing on product quality and process efficiency. The deviations may be either due to occurrence of malfunctions in the system or poor design of the system. The problem of non-ideality is well related to scale-up of a process. Often the uncontrolled parameter in scale-up is the magnitude of the non-ideality and unfortunately differs widely between large and small units. Therefore, overlooking this parameter may lead to gross error in design of the system and scale-up of the process. Experimentation in pilot scale system helps to optimize the design and operating conditions. In addition to this, malfunctions such as fouling, bypassing, channeling etc. occur during the course of operation of the system can also be encountered.

A group of process material entering in a flow system at a particular time may take different paths through the system and consequently take different times to exit the system. The distribution of these times is called the residence time distribution (RTD) (Danckwerts, 1953). RTD is an important characteristic of continuous flow systems and provides vital information about hydrodynamic behavior of the system. RTD is defined as area normalized response of process system to an impulse injection of stimulant (tracer) (IAEA, 2008B).

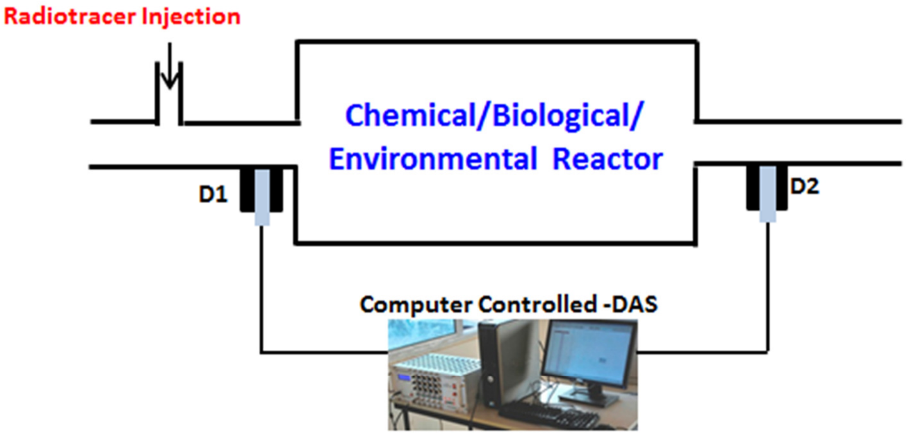

Fig.2.15. A typical experimental setup for measurement of residence time distribution

The most common approach for the measurement of the RTD is stimulus-response method as shown in Fig.2.15. It is used to measure RTD experimentally by injecting a suitable stimulus i.e. tracer at the inlet of the reactor at some time t=0 and then measuring the tracer concentration (C) at the outlet of the reactor as a function of time (Foldiak, 1993; Foglar, 2005; Idakiev et al., 2013). In the most of the residence time distribution measurement passive radioactive tracer is used. The success of a radiotracer experiment depends on injection of radiotracer into the reactor. There are many methods of injection of a tracer into a reactor, but impulse and pulse injection methods are most commonly used methods of tracer injection into a reactor. In an impulse injection, a plug of concentrated tracer is instantaneously injected into the system at inlet in shortest possible time. Tracer injection time is with in the 3 to 5% of system MRT. Then tracer injection is approximated to impulse or Dirac delta function.The measured experiment curve at the outlet of the curve will directly give RTD of the process system. From the measured RTD curve, the information about flow anomalies is obtained by analyzing the shape of the curves (By passing, stagnancy, Channeling, parallel flow path) and mean residence time (MRT) is estimated. The measured RTD curve is modeled using suitable models to estimate the degree of mixing in the system (IAEA, 2004B; 2008A; Fogler, 2005).

2.1.3.2.2. Data treatment of RTD

The concentration versus time data obtained at the end of the radiotracer experiment needs to be treated and analyzed to draw the meaningful and desired information. The basic steps involved in the treatment are discussed in the previous section 2.1.2.2.9.

2.1.3.2.3. Calculation of the moments

Moments are used to characterize the residence time distribution functions in terms of statistical parameters such as mean residence time, variance, skewness etc. (IAEA, 2004B). The moments around the origin are defined as:

$$M_n = \int_0^\infty t^n E(t)dt \tag{2.9}$$

where, n = 0, 1, 2, 3... The zeroth moment (M_0) of the normalized residence time distribution gives the area under the distribution which is equals unity.

The mahtemtical relation for the calculation of the mean residence time (MRT) is given as:

$$M_1 = \bar{t} = \int_0^\infty t\, E(t)dt \tag{2.10}$$

Normally, $\bar{t}$ is equal to τ.

The mathemtical relation to measure to spread of the RTD is given below:

$$M_2 - M_1^2 = \sigma^2(t) = \int_0^\infty (t - \bar{t})^2\, E(t)dt \tag{2.11}$$

where, $M_2 = \int_0^\infty t^2 E(t)dt$ is second moment about the origin. The skewness, peakedness are third and fourth of RTD curve are often used.

For close-close boundry process system having volume (V) and process fluid (constant density) flowing through the system at rate Q. The theoretical mean residence time (τ) (theoritical mean residence time) of the fluid is defined as:

$$\tau = {}^{V}\!/_{Q} \tag{2.12}$$

For the process system operating efficently, the values of experiemtal and theoritical MRT are equal. However, if the experiemtal MRT of the system is higher or lower than thoeritical MRT. There exixts malfunction in the system. The higher experimental MRT value corresponds to exchange between dead and active zone of the process system. Wheres, lower experimental MRT of the system corresponds to dead volume present in the system. The residence time distribution functions are often expressed in terms of independent to time dimensions ($\theta = t/\tau$) (IAEA, 2008A). Thus

$$E(\theta) = \tau . E(t) \tag{2.13}$$

2.1.3.2.4. RTD models

The residence time distribution (RTD) is methodology used to evaluate design parameters of the any process system. This technique is easy to implement in any scale process of system. The RTD curve itself provides vital hydrodynamic parameters of the process system. However, to have quantitative information about the hydrodynamic parameters, the experimental RTD curve must be simulated using a model representing the flow of the reactor (Danckwerts, 1953).

An approach used to simulate the experimental RTD curves known as systematic or semantic modelling. In this approach, fundamental fluid flow theory is utilized to derive mathematical equations gives response close to experimentally measured curve. However, the only understanding of the numerical or mathematical models is not enough to describe the process flow completely. The radiotracer analyst requires knowledge of process flow conditions of system, operating parameters and sufficient experience in the radiotracer field. It provides basic understanding of process flow and change in flow pattern at higher scales (Lecrec, 1995; Martin, 2001; IAEA, 2008B; Levenspiel, 2012; Potier et al., 2015; Claudel et al., 2003).

2.1.3.2.4.1. Models for the ideal flow

In an ideal plug-flow reactor there is no mixing and the fluid elements leave in the same order they arrived. In other words this flow is pure convection (Todreas and Kazimi, 2012). Therefore, fluid entering the reactor at time t will exit the reactor at time t + τ, where τ is the residence time of the reactor. The residence time distribution function is therefore a Dirac delta function (δ) at τ (Fig.2.16) if the pulse is a Dirac delta function. The variance of an ideal plug-flow reactor is zero.

$$E(t) = \delta(t - \tau) \tag{2.14}$$

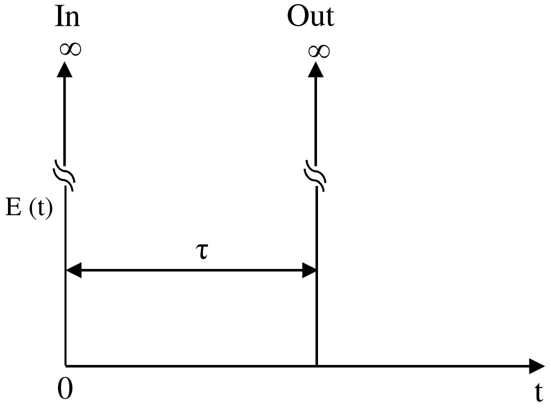

Fig.2.11. RTD of a plug flow reactor (Taken from IAEA, 2004B and redrawn)

An ideal continuous stirred-tank reactor (CSTR) is based on the assumption that the flow at the inlet is completely and instantly mixed into the bulk of the reactor (IAEA, 2004B; Foglar, 2005). The reactor and the outlet fluid have identical, homogeneous compositions at all times. An ideal CSTR has an exponential residence time distribution as shown:

$$E(t) = \frac{1}{\tau}\exp\left(-{}^{t}/_{\tau}\right) \tag{2.15}$$

An ideal continuous stirred-tank reactor (CSTR) is based on the assumption that the flow at the inlet is completely and instantly mixed into the bulk of the reactor. The reactor and the outlet fluid have identical, homogeneous compositions at all times. An ideal CSTR has an exponential residence time distribution as shown in Fig.2.17. The Variance of an ideal reactor equals to τ^2.

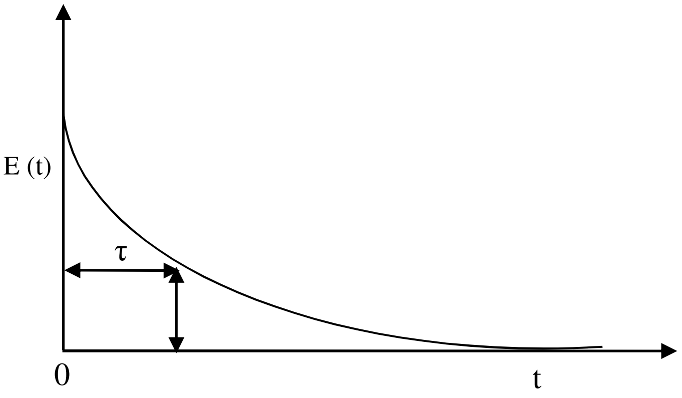

Fig.2.12. RTD of a ideal CSTR (Taken from IAEA, 2004B and redrawn)

2.1.3.2.4.2. Models for the non-ideal flow

Real process system flows are never close to either plug flow model or perfect mixer. The non-ideality present in the real process systems, the ideal process flow systems needs to be modified suitably to simulate the experimentally measured RTD data. The selection of a model to simulate RTD data depends upon the shape of the RTD curve and process flow information available about the system. The most widely used and accepted models used for the quantification of the non-ideality in process system are axial dispersion and tank-in-series models. The other extension of the tank in series model such as gamma distribution model and Tank in series with back mixing model are also discussed below:

2.1.3.3.4.2.1. Axial dispersion model

The axial dispersion model (ADM) is commonly used model to quantify axial mixing in flow systems. The model postulates the majority flow in process system as a plug, into the plug small amount of axial dispersion is overlaid. Small amount of radiotracer is injected as impulse at the inlet and measured at outlet of system. The degree of dispersion observed in the outlet curve is expressed by Fick's law. The mathematical equation representing radiotracer balance equation in one axis is given below (IAEA, 2004A; 2008A; Levenspiel, 1999):

$$\frac{\partial \mathrm{C}}{\partial \mathrm{t}} + \mathrm{U}\frac{\partial \mathrm{C}}{\partial \mathrm{x}} = \mathrm{D}\frac{\partial^2 \mathrm{C}}{\partial \mathrm{x}^2} \tag{2.16}$$

Where C: tracer concentration, U: linear velocity, D: axial dispersion coefficient, t: time and x: axial coordinate. For the measurement of tracer at two axial locations along the system with open-open boundary conditions, the normalized solution of the above tracer balance equation is given as (Levenspiel and Smith, 1957; Tsamatsoulis and Papayannakos, 1994).

$$\mathrm{E(t)} = \frac{1}{2}\sqrt{\left(\frac{\mathrm{Pe}}{\pi\tau\mathrm{t}}\right)}\,\exp\left(-\frac{\mathrm{Pe}\,(\tau-\mathrm{t})^2}{4\tau\mathrm{t}}\right) \tag{2.17}$$

Where E(t): normalized tracer concentration, Pe: Peclet number (UL/D), L: distance between two measuring locations, τ: mean residence time of system. The peclet number (Pe) and MRT (τ) are two model parameters. The fraction of the convective to dispersive effects is Pe. The low and insignificant value of Pe suggests dispersion is dominant in the process system. Whereas, at high value of Pe convection dominants in the process system. It clearly indicates that Pe→∞ represents plug flow and Pe→0 represents well-mixed flow conditions inside the system (Kreft and Zuber, 1978; Kumar et al., 2012).The effect of varying Pe is shown in Fig.2.18.

2.1.3.3.4.2.2. Tank in series model

A representative physical picture of the tanks-in-series model (TISM) is presented in Fig.2.19. According to the model, a system is represented by a series of N-perfectly mixed tanks (CSTRs) of equal volume and mean residence time. The analytical solution of the model for an impulse injection (Dirac's delta function) of tracer at the inlet of the reactor is given by (Foglar, 2005; Levenspiel, 2012):

$$E(t) = \left(\frac{N}{\tau}\right)^N \frac{t^{N-1}\exp\left(-{}^{Nt}/{}_{\tau}\right)}{(N-1)!} \tag{2.18}$$

Where, τ: total mean residence time (V/Q), V is system total volume, Q is process flow rate in system. Two ends of ideal flow pattern depicted by, N = 1 for perfect mixing and N →∞ for plug flow (Pant and Yelgoankar, 2002).

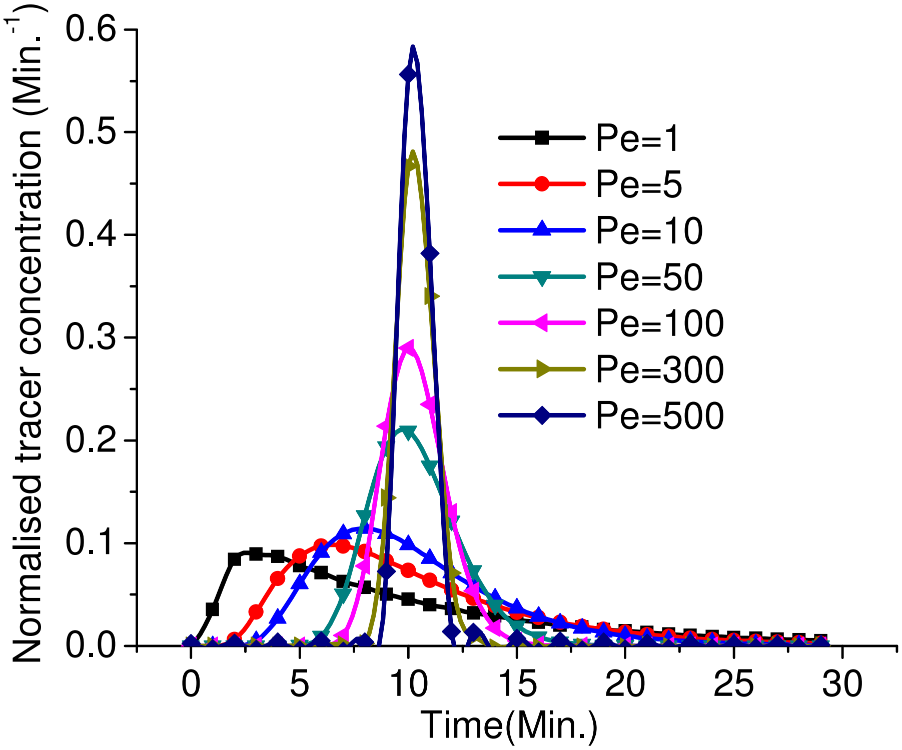

Fig.2.14. Axial dispersion model as a function of the Péclet number.

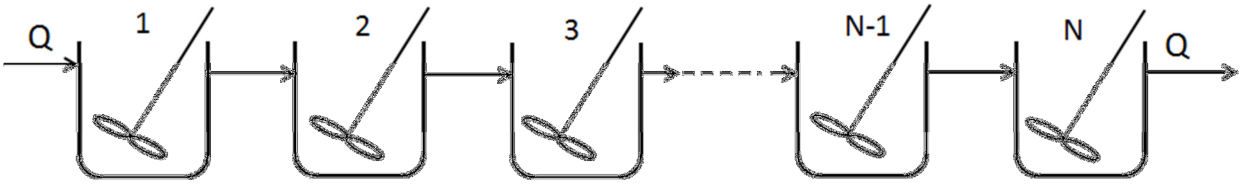

Fig.2.15. Physical representation of CSTRs in series model

The parameter N plays same in the TISM as the Pe in the ADM. The change in the response of the TISM at different values of N is shown in Fig.2.20. The relation between the TISM and ADM is given below:

$$\mathrm{Pe} = 2.\mathrm{N} \tag{2.19}$$

First and second moments of the perfect mixers in series model are given as:

First moment:

$$\bar{t} = \tau \tag{2.20}$$

Second moment

$$\sigma^2(t) = {\tau^2}/{N} \tag{2.21}$$

The axial dispersed plug flow model is mostly used in continuous flow systems such as pipe or a packed column. While, tank in series model is used for the systems having instant high degree of mixing.

2.1.3.2.4.2.3. Modified tank in series model (Gamma distribution model)

Buffham and Gibilaro 1968, have proposed, extension of tank in series model i.e. Gamma distribution model. The solution of the Gamma distribution model to an impulse injection of tracer as given in equation 2.22, was used for modeling of the RTD data (IAEA, 1990; Nauman and Buffham, 1983).

The value of N is 1 for a continuous stirred tank reactor (CSTR) and tends to infinity for a plug flow system (PFR). The model can provide reasonably good representation of a wide range of mixing phenomena. The model parameter, N is restricted to positive, integral values and there is no problem in representing distributions with modest degree of mixing (large N) and small adjustments may be achieved by changing N. When it comes to using the tanks-in-series model for small values of N, the fact that N takes integral values is a serious handicap. In order to overcome this problem, the tanks-in-series model is modified with the adjustable index of mixing in which case N need not be an integral.

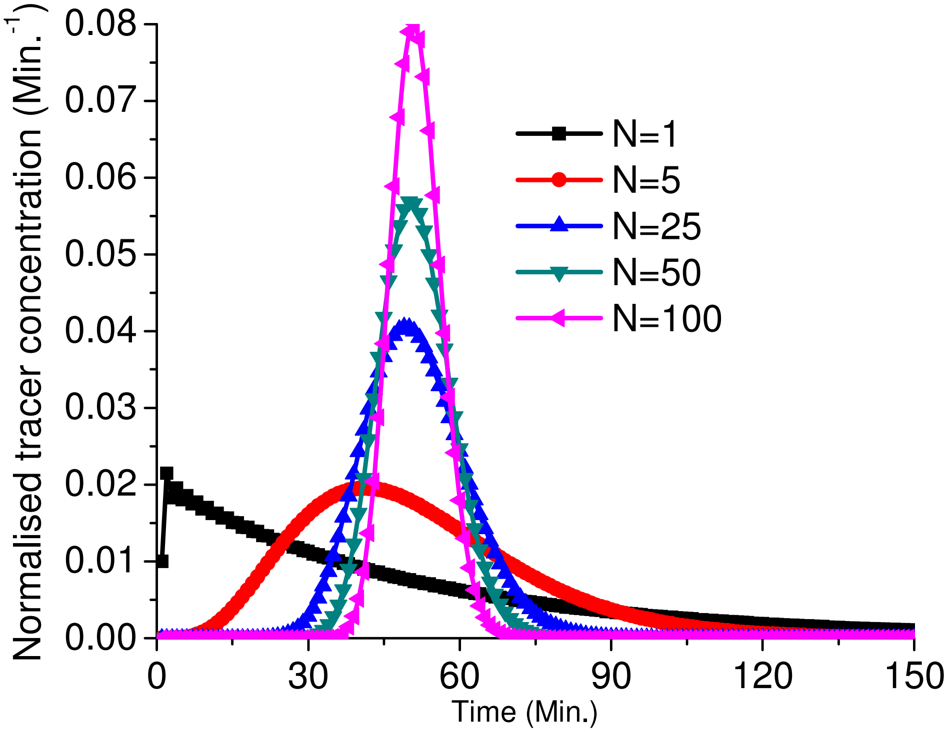

Fig.2.20. The response of tank in series model at different values of N

Thus, the modified tanks-in-series model, known as Gamma function model is given as (Nauman and Buffham, 1983).

$$\mathrm{E(t)} = \left((\mathrm{N^N t^{N-1} e^{(-Nt/\tau_m)}})\ /(\tau_\mathrm{m}^\mathrm{N}.\Gamma(\mathrm{N})\right) \tag{2.22}$$

Where, Γ(N) is called gamma function.

$$\Gamma(\mathrm{N}) = \int_0^\infty e^{-x} x^{N-1} dx \tag{2.23}$$

The gamma function can be thought of as a generalized factorial function because Γ(N) = (N-1)! when N is a positive integer.

The main use of the gamma function model is to simulate slight deviations from the perfect mixer. Two different types of deviations are possible for the experimental data. If the model gives N>1, the RTD curve rises somewhat more slowly than would be expected for a single stirred tank. When the model gives N<1, the RTD curve rises sharply more than expected in case of a exponential distribution. Physically, this condition corresponds to bypassing or short-circuiting of some of the entering fluid.

2.1.3.2.4.2.4. Tank in series with back mixing model

Tanks-in-series with back mixing mode (TISBM) was found suitable for simulating RTD data of the systems having counter current flow and high degree of back mixing in the system. The block diagram of the model is shown in Fig.2.21. The tracer balance equations for the model are given as (Pant et al., 2015; Roemer and Durbin, 1987; Shoren et al., 2016):

For the first tank

$$\tau_1 \frac{dC_1}{dt} = \delta(t) + f\,C_2 - (1+f)C_1 \tag{2.24}$$

For n^th tank

$$\tau_1 \frac{dC_i}{dt} = (1+f)\,C_{i-1} + fC_{i+1} - (1+2f)C_I \tag{2.25}$$

For I = 2, 3, 4, ……, N-1

For N^th tank

$$\tau_1 \frac{dC_N}{dt} = (1+f)\,(C_{N-1} - C_N) \tag{2.26}$$

Where, $\tau_{n:}$ mean residence time in each tank (V/NQ), V: total volume, α: back flowrate ratio (q/Q) q: exchange flow rate between the tanks, Q: flow rate through the system, c_1, c_n and c_N concentration of tracer at the outlet of fist tank, n^th tank and N^th tank, respectively. The above system of equations is transformed and solved in the Laplace domain. Subsequently, the obtained solution is transformed back in to the time domain and compared with the experimentally obtained RTD curve to obtain model parameters. The impulse responses of the model for different backflow rate ration are given in Fig. 2.22.

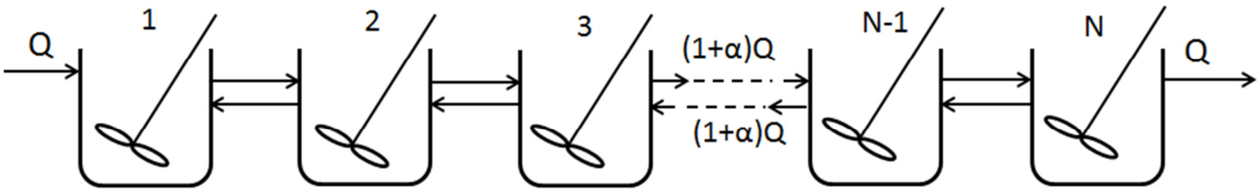

Fig.2.17. Block diagram of tanks-in-series with backmixing model

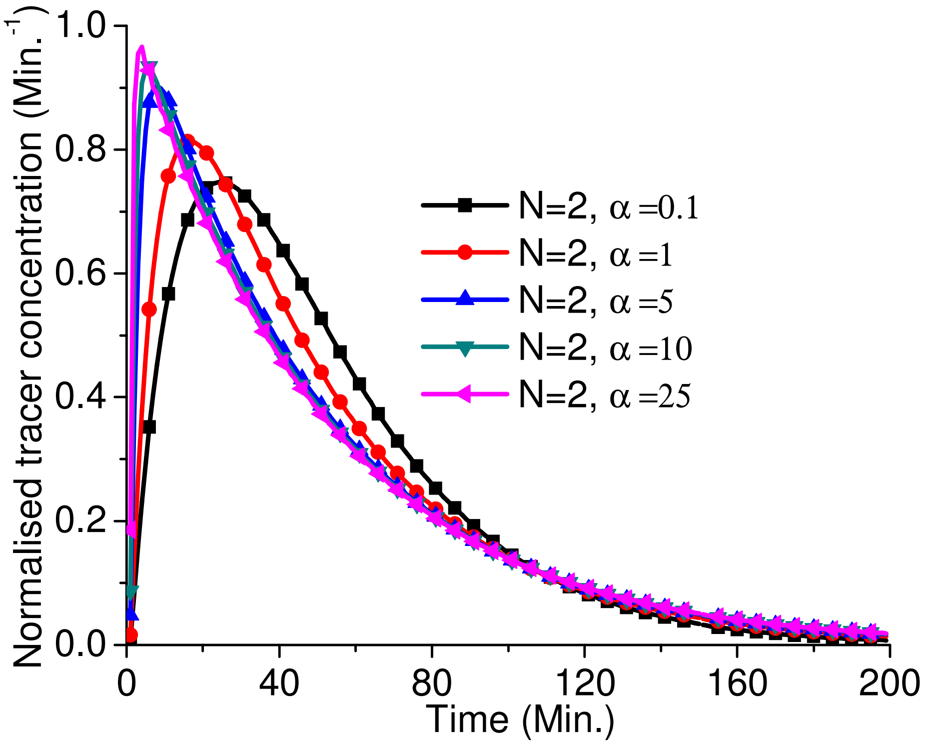

Fig.2.18: Variation of RTD curves for same tank number at different back mixing ratio

2.1.3.2.5. The combination rules to describe complex flow using basic models:

The models described above are used to describe the flow pattern of the various process systems. However, there exists a certain possibility that these models cannot able describe flow behavior of all the experimental cures. For example none of the model describes the multiple peaks present in a recycling process system. Similarly, they don't describe bypassing and parallel flow in a system. Hence, it is essential to have certain set of well-defined rules to combine basic models to simulate any shape of the experimental RTD curve. In general practice, basic models are combined in parallel, series and recycling modes (Nauman and Bauffam, 1983; IAEA, 2004B; IAEA, 2008A; Levenspiel, 2012; Pant and Sharma, 2015; Shoren et al., 2018). The rules re briefly described below:

2.1.3.2.5.1. Models in parallel

The schematic diagram of two model system in parallel is shown in Fig. 2.23:

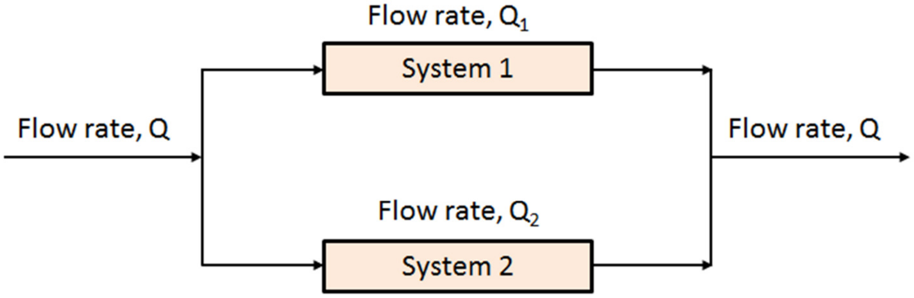

Fig.2.19. Models in parallel.

System has RTD $E_i(t)$, MRT $\bar{t}_i$ and variance σ_i^2. The mathematical relation defining overallRTD $E(t)$ of system is given below (IAEA, 2004B; IAEA, 2008A) :

$$E(t) = \frac{Q_1}{Q} E_1(t) + \frac{Q_2}{Q} E_2(t) \tag{2.27}$$

Mathematical reltions for the calculation of MRT and varience for models in parallel are given below:

MRT of system

$$\bar{t} = \frac{Q_1}{Q}\bar{t}_1 + \frac{Q_2}{Q}\bar{t}_2 \tag{2.28}$$

Vrience of the system

$$\sigma^2 = \frac{Q_1}{Q}\int_0^\infty \left(\bar{t} - \bar{t}_s\right)^2 f_1(t)\,dt + \frac{Q_2}{Q}\int_0^\infty \left(\bar{t} - \bar{t}_s\right)^2 f_2(t)\,dt \tag{2.29}$$

2.1.3.2.5.2. Models in series

The schematic of two model system in series is shown in Fig.2.24.

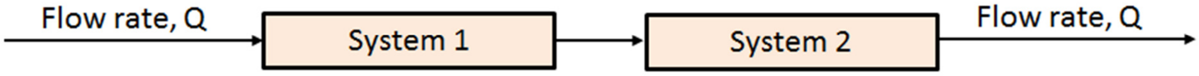

Fig.2.20. Models in series

The overll RTD E(t) of the two system in series is determined by convolution of the RTD function of the subsystems (IAEA, 2004B; IAEA, 2008A)

$$E(t) = E_1(t) * E_2(t) \tag{2.30}$$

Equations used for the calculation of MRT and varience of system in series is given below:

MRT of system

$$\bar{t} = \bar{t}_1 + \bar{t}_2 \tag{2.31}$$

Varience of system

$$\sigma^2 = \sigma_1^2 + \sigma_2^2 \tag{2.32}$$

2.1.3.2.5.3. Models with recycle

The schematic of two model system in recirculation is shown in Fig. 2.25.

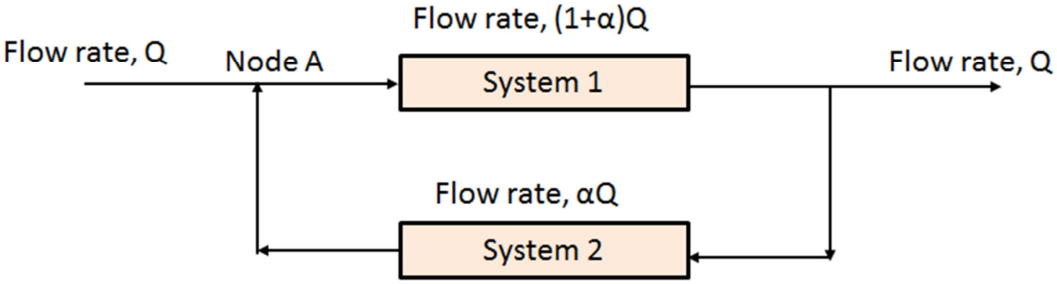

Fig.2.21. Models with recycling

The rule of mathematical equation in time domain is not simple and in most of the cases it is solved in the lapalace domain (IAEA, 2008A; Nauman, 2008). However, the mass balance equation at node A is given by:

$$E_1(t) * [\delta(t) + \alpha E_2(t) * E_1(t)] = (1 + \alpha)E(t) \tag{2.33}$$

Equations used for the calculation of MRT and varienceof systems inrecycle are as follows:

MRT of system

$$\bar{t} = (1+\alpha)\bar{t}_1 + \alpha\bar{t}_2 \tag{2.34}$$

Varience of system

$$\sigma^2 = (1+\alpha)\sigma_1^2 + \alpha\sigma_2^2 + \frac{\alpha}{(1+\alpha)}(\bar{t}_1 + \bar{t}_2)^2 \tag{2.35}$$

2.1.4. Techniques for the parameter estimation

A mathematical model used to simulate the experimental RTD cure has unfixed model parameters and variable time. Generally the time variable is fixed by the end time experimental RTD curve and time difference between the two data points. The model parameters are varied and the corresponding concentration to the each experimental time is calculated. The radiotracer concentration corresponding to the experimental RTD for a time‘t’ is defined as $E_{exp}(t)$. Similarly, model concentration corresponding to the same time‘t’, is defined as $E_m(Pi, t)$. Where, Pi is the different model parameters depending upon the selected model for a study. To get the most appropriate valueof model parameter representing the experimental curve is selected by calculating the error in the values between $E_{exp}(t)$ and $E_m(Pi, t)$. The widely used method is for this is the least square curve fitting method (Michelsen, 1972; PROGEPI/SYSMATEC, 2000; Pant, 2001; IAEA, 2004B; IAEA, 2008A). The best model parameter corresponding to minimum sum of squares of the difference between $E_{exp}(t)$ and $E_m(Pi, t)$. A mathematical relation for the calculation of the sum of square of error is given below

$$\varepsilon = \int_0^\infty [E_{exp.}(t) - E_m(t, Pi)] = \text{minimum} \tag{2.36}$$

Chapter 3

Study of adsorption characteristics of Au(III) onto coal particles and their application as radiotracer in a coal gasifier

---

3.1. Introduction

Radiotracer techniques are widely used for various applications in industry and environment because of their many advantages over conventional tracers and often do not have suitable alternatives for most of the industrial situations (IAEA, 1990, 2008B; Charlton, 1986; Pant et al., 2001; Jung et al., 2010). There are numerous radiotracers available for tracing liquid phases in industry that can be easily produced by irradiating suitable targets in a nuclear reactor followed by chemical processing in laboratory. In case of tracing gas phase, the enriched gaseous targets of Krypton-78 and Argon-40 are irradiated and used as radiotracers. However, for tracing solid phases in industrial systems, the radiotracers are mainly prepared using three methods i.e. direct activation, surface or volumetric labeling and artificial preparation (IAEA, 1990; 2008C).None of the above-mentioned methods can be used for preparation of a radiotracer of solid phase tracing applications in all the industrial situations. Different methods are used for different situations. In direct preparation method, neutron activation analysis of the process material is performed to identify the activable elements prior to the preparation of the radiotracer for the actual radiotracer test. If the process material contains suitable activable elements that can produce radioisotopes of desired nuclear characteristics, then a suitably estimated amount of the process material is irradiated in the reactor to produce desired amount of radioactivity for use as radiotracer (Pant et al., 2001). This method is commonly used for preparation of radiotracer for tracing catalyst in Fluid Catalyst Cracking Units (FCCU) in refineries (Pant et al., 2009A), clinker in rotary klin in cement industry and minerals (gold, copper, iron etc.) in mineral processing industry. In surface/volumetric labeling, a suitably selected radioisotope is labeled on the process material to prepare the radiotracer (Pant et al., 2009B,). Generally Gold-198 (^{198}Au), Scandium-46 (^{46}Sc), Chromium (^{51}Cr), Hafnium-170/181 ($^{170/181}$Hf) radioisotopes are used to label solid matrices such as sand, silt, mud, coal, catalysts, refractory materials etc. to prepare radiotracers for tracing solid phases (IAEA, 2004). Another variant of the method is to prepare solid phase radiotracer by adsorbing or soaking a desired radioisotope on the solid process material. In artificial tracer method for preparation of solid phase radiotracer, a solid material mixed with a suitable quantity of the activable element having the identical physical properties as that of the process material is prepared and used as radiotracer. Artificially prepared scandium or iridium glass particles are commonly used for preparing solid phase radiotracer in sediment transport studies (IAEA, 2014).

The adsorption approach is often used for preparation of radiotracer for tracing coal phase in gasifiers, fluidized beds, combustors and boilers etc. in energy industry. The approach usually involves soaking or suspending coal particles in suitably selected radioactive solution (^{198}Au,^{46}Sc)for a pre-decided time period followed by decanting and drying of the coal particles (Pant et al, 2009A; 2009B). Subsequently, the activity adsorbed on coal particles was estimated on the basis of comparison of initial and final concentration of radioactivity in the radioactive and decanted solution. However, the approach provides an approximate estimation of amount of activity to be used for the tracing experiment. For estimation of an appropriate amount of activity required for tracing coal or solid phases in industrial systems, the adsorption characteristics and percentage of adsorption of the selected radioisotope is required to be known to avoid under or over estimation of activity. The use of overestimated activity will lead to saturation of the detectors and unnecessary radiation health hazards to the operators and environment. However, at the same time, the use of underestimated activity may not be sufficient for measurements. Therefore, for estimation of an appropriate amount of activity required for a radiotracer experiment, the characteristics of Au(III) should be studied and optimized conditions needs to be obtained for efficient labeling. The adsorption of any specific radioisotope on coal particles will depend on factors such as pH of the solution, concentration of the solution, temperature, soaking or stirring time, coal amount etc. To the best of authors knowledge, there is no study reported in literature on adsorption characteristics of Au(III) on coal particles using radiotracer method.

A systematic study was carried out for the adsorption of $^{198}Au$from an aqueous solution onto the surface of coal particles with an objective to prepare radiotracer for tracing coal in gasifiers and estimate amount of activity to be used. The effect of experimental factors that influence the adsorption of *Au(III) in form* $AuCl_4^-$ *of* onto the coal particles, such as pH, adsorbent dose, initial gold concentration, temperature and contact time of adsorbate and adsorbent, have been assessed and a careful control has been exercised to ensure optimum adsorption using $^{198}AuCl_4^-$ as radiotracer.Furthermore, kinetics of the adsorption and applicability of various isotherm models was analyzed.

3.2. Experimental

The experimental procedure involved characterization of coal particles, production and preparation of radioactive solution of ^{198}Au, performing the batch experiments for adsorption of coal particles and conducting a few test runs for RTD measurements. These steps are described below in details.

3.2.1. Characterization of coal particles

The coal particles obtained from Bharat Heavy Electricals Limited (BHEL), Hyderabad India were characterized and subsequently used for adsorption studies. Bulk and true densities were determined by using specific gravity bottle and pycnometer (Thermo scientific, Mumbai, India). A sieve analysis was done using a set of IS sieves to assess the particle size distribution. Sieve analysis tests were conducted with hand shaking. Elemental analysis of coal particle was performed using a Euro Vector CHNS element analyzer (Euro EA 3000, Milan, Italy). For CHNS (Carbon, Hydrogen, Nitrogen and Sulphur) determination, samples are weighed in tin capsules and introduced into the combustion reactor where with the proper amount of oxygen and combustion catalysts, the sample is combusted. After combustion the resulted gases are carried by a helium flow, swept through a GC column to separate combustion gases and finally detected by a thermal conductivity detector (TCD). The*infrared (IR) spectra were recorded using* an attenuated total reflectance (ATR)*FTIR spectrophotometer*(*Shimadzu IR affinity 1*).The ATR accessory is equipped with a single-reflection diamond ATR hemisphere and a spring-loaded mechanical press for compacting solid samples at the ATR waveguide surface with uniform and reproducible pressure. *Surface areas* of coal particle samples were *determined* by nitrogen adsorption (BET method based on N_2 adsorption-desorption isotherms) *using a Quantasorb*adsorption unit (Quantachrome GmbH & Co.KG, Odelzhausen, Germany). The nitrogen adsorption-desorption data were recorded at liquid nitrogen temperature (77 K) and surface area was calculated using the BET (Brunauer, Emmett, and Teller) equation from selected N_2 adsorption data. The *scanning electron microscopeCamScan*-4DV (*CamScan*, Cambridge,*UK*) was used to investigate surface morphology. For SEM measurements, the samples were coated with a thin layer of gold and mounted on a copper stab using a double stick carbon tape. The chemical analysis for the trace level of metal ions was carried out using

Inductively Coupled Plasma-Atomic Emission Spectroscopy (*Activa* S*ICP-OES Spectrometer*, Horiba Group, UK). A high resolution γ-ray spectrometer consisting of a HPGe detector coupled to a PC-based 4 K channel analyzer (MCA) obtained from Eurysis Measures, France and analyzing software was used for γ-ray spectroscopic measurement of ^{198}Au sample to ascertain its radionuclide purity.

3.2.2. Production of ^{198}Au and preparation of stock solution

Gold wire weighing 25 mg was accurately weighed, encapsulated in a quartz ampoule**,** kept in a cold-pressure-weld type cylindrical 1S aluminum container [22 mm(ϕ) × 44 mm (l)], sealed by cold press welding and irradiated in DHRUVA research reactor at Trombay, Mumbaiin a neutron flux of ~ 7.5×10^{13} n.cm^{-2}.s^{-1}for one week. At the end of irradiation, the irradiated targets were cooled for 24 h, loaded in a lead shielded flask and transported from reactor toa radiochemical processing laboratory.

Table 3.1: Characterization of the coal particles

Parameter	Value
Particle size(mm)	1-3
Bulk Density of coal (g/cm^3)	0.8
Particle Density of coal (g/cm^3)	1.6
Surface area (m^2/g)	3
Proximate analysis	
Moisture(wt %)	4.19
Ash(wt %)	38.2
Volatile matter(wt %)	31.9
Fixed carbon(wt %)	25.69
Ultimate analysis	
Carbon(wt %)	37.4
Hydrogen(w t%)	2.86

Nitrogen(wt %)	0.72
Sulphur(wt %)	0.8
Oxygen(wt %)	10.42
Elemental analysis	
Mg(wt%)	0.15
Al(wt%)	3.81
Si(wt%)	8.24
Ca(wt%)	1.0
Fe(wt%)	0.7

The irradiation container containing neutron irradiated gold wire was taken in a lead shielded container to radioisotope processing facility, the seal of the irradiation container was cut opened with the help of an opening unit and irradiated target was transferred to a 150 mL three necked round bottom flask. About 10 mL aqua regia solution (*3:1*molar ratio of *HCl* to HNO_3) was added slowly through the funnel and heated gently at100ºC to dissolve the gold wire till a yellowish solution was obtained. The solution was heated till near dryness to expel nitric acid.

The residue was then reconstituted in 10 mL of 0.1 N HCl and heated to near dryness; this step was repeated three times. Finally, $H^{198}AuCl_4$ as solution was filtered through a G2 filter assembly and collected in a vial connected serially. After appropriate dilution and sampling, the radionuclide purity of the samples was assessed using a pre-calibrated high resolution *HPGe detector* system*coupled to a multi-channel analyzer (MCA).*A pre-calibrated ionization chamber *(Beta-Gamma standard type 1383A, General Radiological Ltd,* England) was used for the measurement of radioactivity content of ^{198}Au. *Activity content of* the ^{198}Au solution used for adsorption studies were *determined* by a 3" x 3"*well type NaI(Tl)* scintillation *counter (Para Electronics* India Pvt. Ltd*, Mumbai,* India).

A stock solution of $HAuCl_{4(aq)}$ of concentration 1000 mg/L was prepared by adding a weighed amount of the $HAuCl_4$ (1g) to 1000 mL of de-ionized water. The stock solution was spiked with 37 MBq (1 mCi) of ^{198}Au as $H^{198}AuCl_4$.This stock solution was subsequently diluted by water of appropriate volume to prepare $HAuCl_4$ solution of different concentrations as per experimental requirement.

3.2.3. Batch adsorption study

Various methods such as such as graphite furnace atomic adsorption (GFAAS), inductively coupled mass spectrometer (ICP-MS), Atomic emission spectroscopy (AES), X-ray spectroscopy and neutron activation analysis can be used to study adsorption of Au(III) on coal particles. But estimation of concentration Au(III) ions in the supernant solution requires extensive sample preparation and make the measurement gold concentration cumbersome. Therefore, in the present study ^{198}Au in form of $^{198}AuCl_4^-$ was used as an intrinsic radiotracer tracer for adsorption study. In the present study batch adsorption experiments were carried out by suspending coal particles in $HAuCl_4^-$ solutions (concentration range 2–30 g L^{-1}) in different initial concentrations (100–500 mg L^{-1}). In each experiment, a known amount of coal particles were suspended in 50 mL solution of known initial concentrationcontaining ^{198}Au in form of $^{198}AuCl_4^-$ in a 250 mL narrow mouth *Erlenmeyer flasks* with heavy duty rim at different pH(1–12) and temperature (303–333 K). The suspensions were agitated mechanically at a constant speed of 150 rpm using a water bath shaker. However, to study adsorption parameters, a small portion of the aqueous phase (1 mL) was separated for the solution at predetermined time intervals. Then, the aliquot was centrifuged at 5000 rpm for 10 minutes. The activity measurement of the supernant solution directly can be used to measure gold concentration in the solution. Therefore, the activity content of 0.5 mL of supernant of centrifuged aliquot was measured in a well-type NaI(Tl) detector, directly related gold concentration in the aqueous solution. Hence, the collected samples were analyzed radiometrically to detect the changes of $AuCl_4^-$ ions concentration.The percentage of adsorption (Ads. %), distribution coefficients (K_d), the concentrations of C_t and C_e and the adsorption capacity of q_t and q_e were calculated using following relationships (Ozeroglu and Keceli, 2009; Czerwinski et al., 1984).

$$\text{Ads.\%} = \frac{A_i - A_t}{A_i}.100 \tag{3.1}$$

$$K_d = \frac{A_i - A_t}{A_i}.\frac{V}{m} \tag{3.2}$$

$$Q_t = (C_0 - C_t).\frac{V}{m} \tag{3.3}$$

$$Q_e = (C_0 - C_e).\frac{V}{m} \tag{3.4}$$

$$C_t = (1 - \frac{Ads.\%}{100}).C_0 \qquad (3.5)$$

where A_i and A_f are the initial and counts of solution (mL), C_0 is the initial Au(III) concentration (mg/L), K_d is the batch distribution coefficient, C_t and C_e are the Au(III) concentrations (mg/L) in solution at time t and at the equilibrium at t = 60 min, respectively. Q_t and Q_e are the amounts of adsorbed Au(III) in terms of mg/g on the coal particles at time t and at equilibrium (t=60 min), respectively. V is the volume of Au(III) solution (L) in the experiment, and m is the amount the adsorbent(g).

3.3. Results and discussion

3.3.1. Characterization of coal particles

Result of the sieve analysis test revealed that the particle are within the ranges of 1-3mm. Bulk density and particle density of the coal as determined by *pycnometer* method were found to 0.8 g/cm^3 and1.6 g/cm^3 respectively. The surface area of the powders as determined by BET method was found to be 3 m^2/g.*CHNS* analysis of the coal particle reveal 37.4,2.86,0.72, 0.8, 10.42 weight percentage of carbon, hydrogen, nitrogen, sulfur, and oxygen respectively. It is obvious from the results of the *CHNS* analysis that the major element in the coal particle is carbon, followed by oxygen, hydrogen, sulfur, and nitrogen respectively. Elemental analysis of the coal particle showed the presence of Mg, Al, Si, Ca and Fe in weight percentage of 0.15, 3.81, 8.24, 1.0 and 0.7, respectively. The physicochemical properties of coal particles are summarized in Table 3.1. It is apparent that coal particles are mainly comprised of oxides of silicon, aluminum and calcium, while oxides of magnesium and iron are present in trace quantity.

The IR spectra of the coal particles before and after Au adsorption spectra reveals that O-H stretching in the wave number range 3600 to 3200 cm^{-1}. The weak bands at 2924.35 and 2849.12 cm^{-1} are indicative of the existence of alkyl chains C-H stretching vibration. The peak at 1602 cm^{-1} is the result of Si-O-Si or Si-O-Al stretching vibrations and at 1459 cm^{-1} is the characteristic peak of C=C stretching vibrations. The IR spectra did not show substantial variation before and after gold adsorption which indicates that the surface moieties remained unchanged.

The Scanning electron microscope (SEM) image of coal particles are shown in Fig.3.1a. The SEM image reveals a coarse and irregular surface and somewhat corrugated. These irregularities help to increase the adsorption on the surface. The surface of coal particle after adsorption showed shiny points due to the adsorption of the gold as shown in Fig.3.1b.

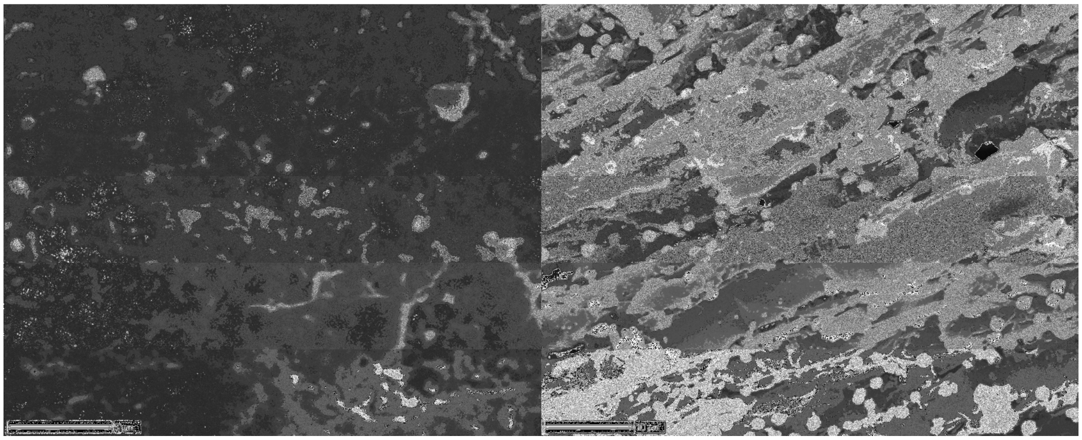

Fig.3.1. SEM-EDX images of coal particles (a) Before adsorption (b) After adsorption

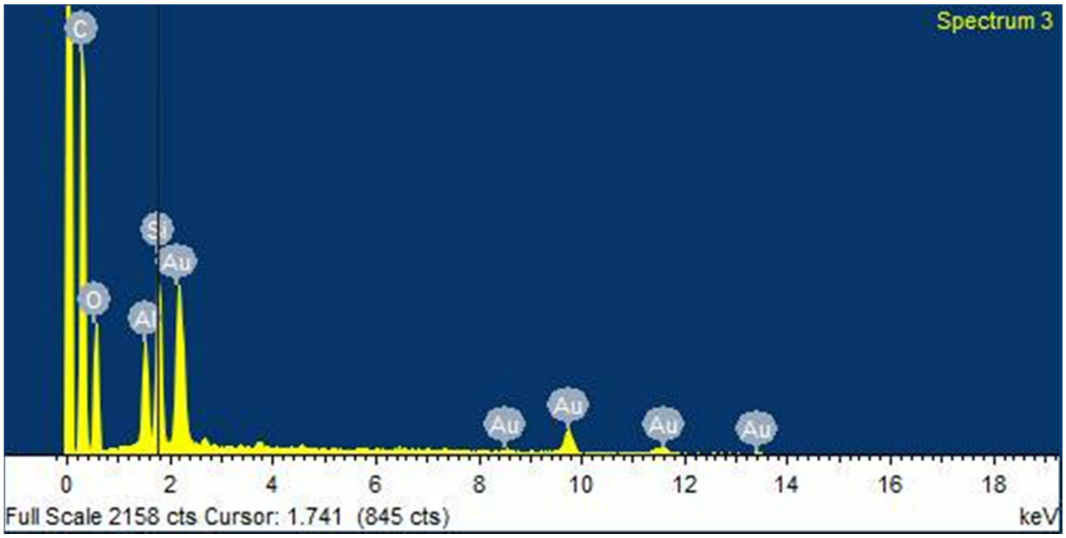

Fig.3.2. EDS spectra of Au(III) adsorbed on coal particles

The EDS spectra (Fig. 3.2) shows peaks pertaining to C, O, Al, Si and Au only which indicates that Au is retained by the coal on its surface. The textural and morphological characteristic of the coal particles used in this study are similar to those of typical carbonaceous materials.

3.3.2. Effect of parameters on adsorption

3.3.2.1. Effect of pH

The pH of the adsorbent solution is one of the most important variables in the adsorption process. Solution pH plays an *important role* in controlling the surface charge of the adsorbent and ionic character of the adsorbate. In the present work the effect of the initial pH of solution on the adsorption of Au(III) on the coal particles at room temperature was studied in the pH range of 1-11. The initial pH value of the gold solution was adjusted by adding 1N HCl and 1N NaOH solutions. The dependence of the adsorption capacity and % of adsorption of Au(III) on the pH is presented in Fig. 3.3. It can be seen that the adsorption capacity of Au(III) increases with pH, reached a maximum at pH 2.5 and thereafter further increase of pH results in gradual decrease of the adsorption capacity. The change in the adsorption capacity of an adsorbent at different pH can be due to the chemistry of both gold and the adsorbent, precisely to the ionic state of the functional group present on the surface of coal particles, their degree of ionization in aqueous solution as well as dissociation of various functional groups on the active sites of the adsorbent and ionic form of the gold at the prevailing pH. The results of the study showed that adsorption of gold on coal particles was favored at lower pH of solution and optimum pH was found to be 2.5. The percentage of adsorption follows similar trend as adsorption capacity. The present findings were supported by earlier workers who have reported that the adsorption of gold as $HAuCl_4^-$over activated rice husk and commercial resin Lewatit TP 214 (Marcali and Aktas, 2011; Aktas et al., 2015).

3.3.2.2. Effect of adsorbate concentration

The rate of adsorption is a function of the initial concentration of the adsorbate and hence considered worthwhile investigating. The initial concentration of the Au solution is very important owing to the fact that a given amount of coal particles has a predetermined capacity to adsorb only a fixed quantity of Au species.The effect of initial concentration of Au(III) ions in the solution on the adsorption of the coal particles at constant coal mass and volume is depicted in Fig. 3.4. From the plot it can be observed that the adsorption capacity of Au(III) ions increased from 15mg/g to 148mg/g as the initial Au(III) ion concentration increased from 100mg/l to 500mg/l and after equilibrium. This is due to the increased driving force of the concentration gradient as the initial Au concentration increases. However, the percentage of adosprtion shows opposite trend and decreases from 91% to 72% as gold concentration increases from 100mg/l to 500mg/l. The reason behind this is that as gold concentration increases the availability of active binding site decreases, which leads to lower percentage of adsorption. Similar, patterns of adsorption of Fe(III) on chitin were reported by Karthikeyan et al. 2005.

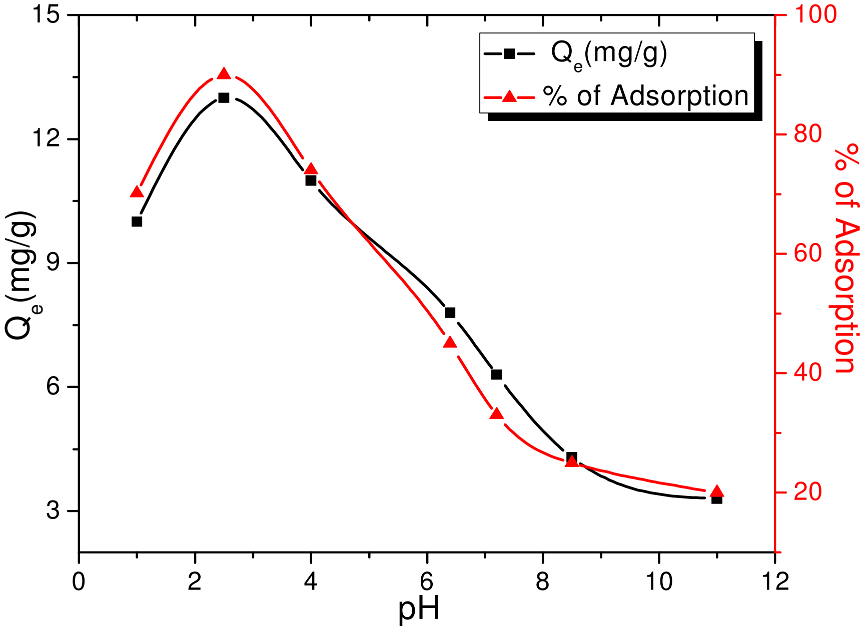

Fig.3.3. Effect of initial pH on adsorption of Au(III) ions on coal particles

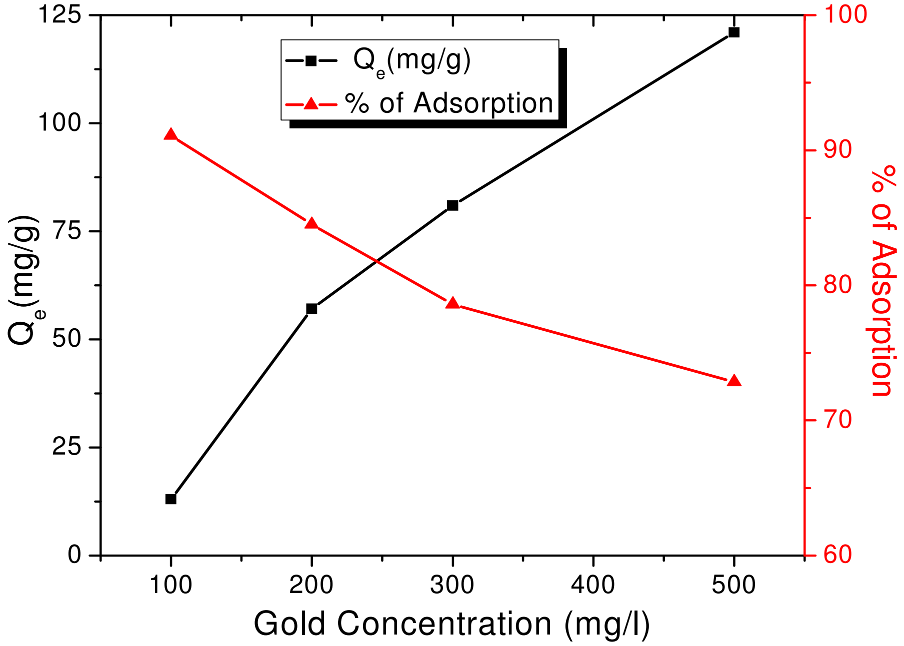

Fig.3.4 Effect of initial adsorbate concentration of Au(III) ions on adsorption capacity of coal particles

3.3.2.3. Effect of adsorbent mass

To study effect of amount of adsorbate on adsorption capacity at a constant concentration of Au(III), six different amounts of adsorbent ranging from 2 g/L to 30 g/L were selected. The relation between adsorption capacity and time at different adsorbent amount is shown in Fig.3.5. It was observed that percentage of Au(III) ion adsorption increased with increase in adsorbent dose. This trend is largely *attributed* to an increase in the adsorptive surface area and the availability of more active binding sites on the surface of the adsorbent due to increase number of coal particles. However, the equilibrium adsorption capacity showed an opposite trend. As amount of the adsorbent were increased from 2g/L to 30 g/L, the adsorption capacity decreased from 31.3 to 3.3 mg/g respectively. This may be due to overlapping or aggregation of adsorption sites as the coal amount in solution increases with constant Au(III) ion and volume of the solution. It leads to the less number of active sites available on the adsorbent per unit mass coal. coal particles. Thus with increasing adsorbent mass, the amount of Au(III) ion adsorbed onto unit mass of adsorbent gets reduced, causing a decrease in qe value with increasing adsorbent mass concentration. Furthermore maximum percentage adsorption of Au(III) ion on coal particles was 99%. It was observed at all the different adsorbent mass except 2g/L.

However, the time to reach the maximum adsorption was different for (A: 6, 10 and 15g/L) and (B: 20g/L and 30g/L). As in the case B, the amount of coal is very high compared to the coal amount in A, which leads to large significant increase in overall surface area for the coal particles.

3.3.2.4. Effect of contact time

The relation between adsorption capacity and contact time is shown in Fig. 3.6. The time variation plot indicates that adsorption of gold is rapid during initial stages but slows down gradually once equilibrium was attained and subsequently did not show any appreciable change with time.

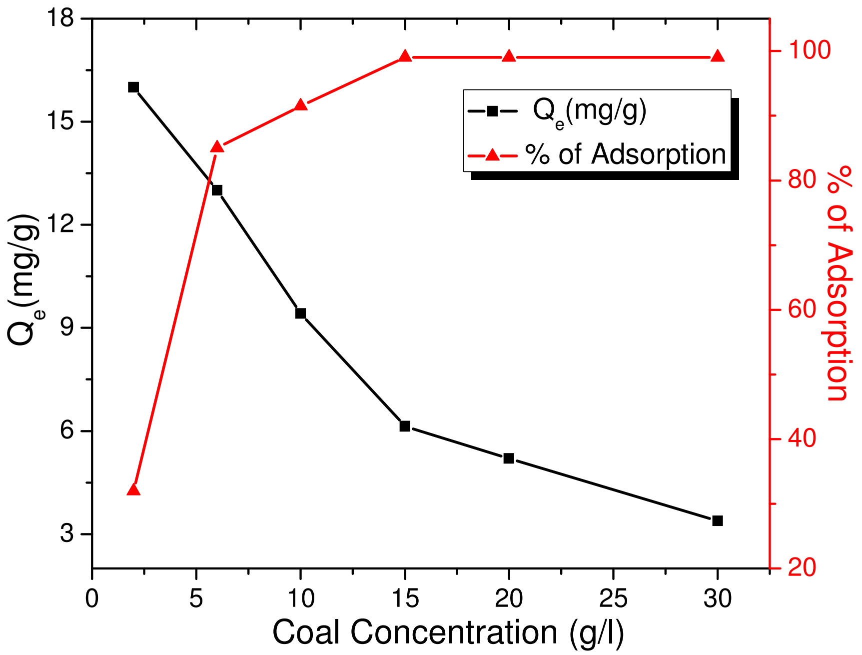

Fig.3.5 Effect of initial adsorbent concentration on adsorption of Au(III) ions

The attainment of adsorption equilibrium takes place within 40-50 min of contact between solid and liquid solution. This may be due to the availability of ample adsorption sites on coal particle during the preliminary stage of adsorption, after 40-50 min the adsorption sites get occupied by gold ions which lead to creation of a repulsive force between the adsorbate on the adsorbent surface and in bulk phase. It can be observed from Fig.3.6, that the amount of Au adsorbed varies with changing initial Au(III) concentration and increases with increase in initial concentration of Au(III). The adsorption attains a constant value after equilibrium due to the driving force offered by the increased solute concentration which is adequate to surmount the resistance to mass transfer between the solid and liquid phases. At this stage, the gold ions were transported to internal sites of the adsorbent through pore diffusion, which requires a longer contact time and is represented by the linear portions of Fig. 3.6.

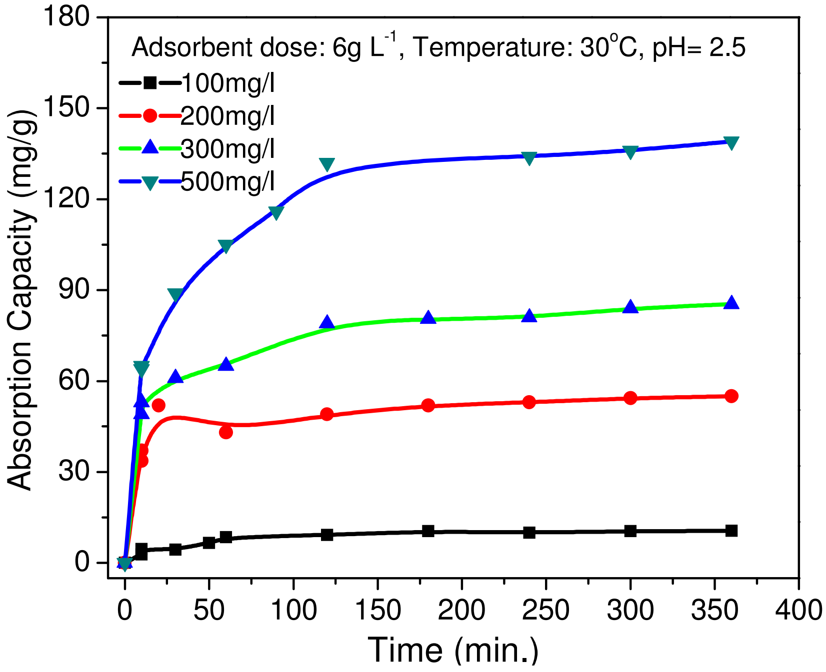

Fig.3.6.Effect of contact time on adsorption of Au(III) ions coal particles

3.3.2.5. Effect of Temperature

Temperature is a crucial parameter in adsorption reactions. The effect of temperature of solution on the adsorption of Au(III) on coal particles at different temperature is depicted in Fig.3.7. The adsorption capacity of the coal particles found to be marginally increased from 13.2 to 14.9 mg g^{-1} as the temperature was raised from 30 to 60 °C. According to the adsorption theory, adsorption decreases with increase in temperature and ions/molecules adsorbed earlier on a surface tend to desorb from the surface at elevated temperatures. But for coal particle, an unusual trend is noticed that uptake of Au(III) ions, causing adsorption to increase as temperature increases. In order to identify the *anomalies* of Au(III) adsorption on coal, thermodynamic factors were calculated. The thermodynamic factors, namely, the Gibb's free energy ($\Delta G°$, kJ mol^{-1}), enthalpy ($\Delta H°$, kJ mol^{-1}), and entropy ($\Delta S°$, J mol^{-1} K^{-1}) changes associated with Au(III)adsorption, were determined using the Gibb's free energy equation 3.7 and Van't Hoff equations as follows.

$$\Delta G^{o} = \Delta H^{o} - T\Delta S^{o} \tag{3.6}$$

$$\ln K_{c} = \frac{\Delta S^{o}}{R} - \frac{\Delta H^{o}}{RT} \tag{3.7}$$

where K_C is the distribution coefficient of adsorption, R is the universal gas constant (8.314 J mol^{-1} K^{-1}) and T is the adsorption temperature (K). The values of the equilibrium constant (K_C) for the adsorption of Au(III) ions on coal particle were calculated at different temperatures at equilibrium time (i.e. 50 min). The variation of K_C with the reciprocal of temperature is shown in (Fig.3.8) showing that K_C values increase with increase in adsorption temperature, thus implying a strengthening of the adsorbate-adsorbent interactions at higher temperatures. Value of ΔH° and ΔS° were computed from the slope and intercept of the linear variation of $\ln K_C$ with the reciprocal of temperature, $1/T$ (Fig.3.8) using Eq.(7). The endothermic nature of adsorption was established by the positive value of ΔH° (27.8 kJ mol^{-1}). The values of the free energy of adsorption for the present system ΔG° at temperatures 30, 45, and 60 °C were 0.9, 0.5 and -1.5 kJ mol^{-1}, respectively. The positive values of ΔG^{o} *indicate*non-spontaneous nature of *adsorption*process at the temperatures being determined and *negative values* of ΔG^{o} *point to spontaneous adsorption. Negative values* of ΔG^{o} may also be a result of an increase in the mobility of Au(III) ions with an increase in their kinetic energy and the enhanced rate of diffusion of Au(III) ions with the rise in temperature. The value of ΔG° becomes negative as the temperature increases, indicating an increasing driving force toward equilibrium, thereby resulting in a greater adsorption percentage of Au(III) at higher temperatures. The increase in the adsorption capacity of gold onto the adsorbents at higher temperature may be attributed to increased activation of the adsorbent surface.

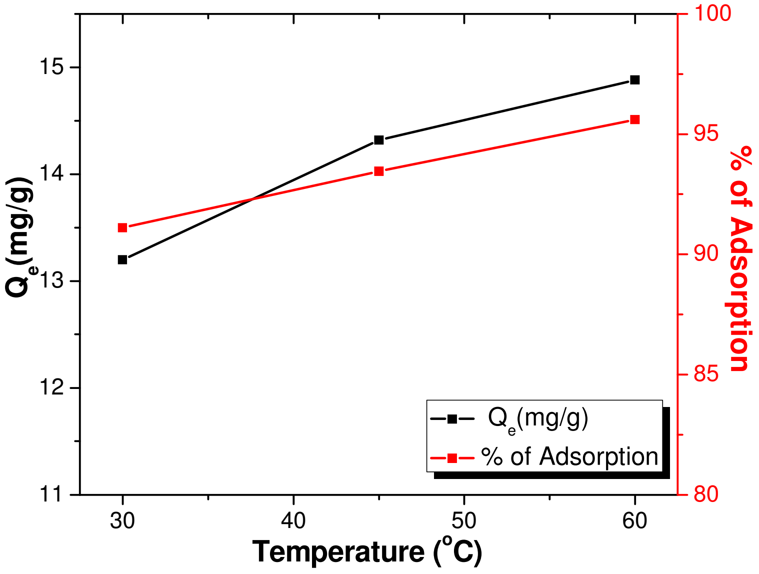

Fig. 3.7. Effect of temperature on adsorption capacity of gold ions on coal particles

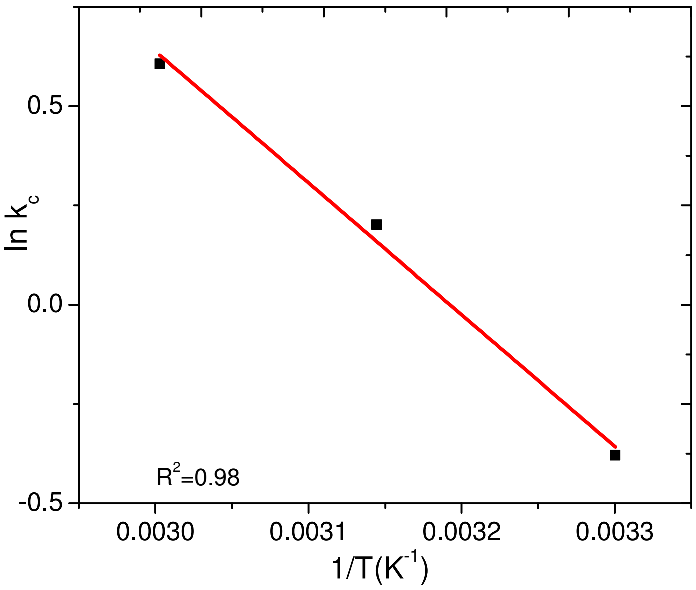

Fig.3.8:Plot of ln K_C versus 1/T for the adsorption of gold over coal particles.

The positive value of $\Delta S°$ (86.3 J mol^{-1} K^{-1}) point towards prevalence of some structural changes on the adsorptive site and an increase in the randomness at the solid/solution interface as a result of some rearrangement at the active adsorption sites. Since the adsorption process is endothermic; it follows that under these conditions the process becomes spontaneous because of the positive entropy change.

3.3.3. Equilibrium isotherm models

An adsorption isotherm describes the relationship between the amount of Au(III) ionadsorbed on adsorbent and the A(III) ion concentration remaining in solution at a constant temperature and pH. The isothermsalso provide information about the nature of interaction between adsorbed molecules and adsorbate surface. The data obtained from the batch adsorption experiments was analyzed andfitted to three equilibrium adsorption isotherm models i.e. Freundlich, Langmuir and Dubinin-Radushkevich (D-R). Frendulich Isotherm did not fit very well to the experimental data. However, Langmuir and D-R isotherms were found to be fitting very well to the experimental data and are discussed below.

3.3.3.1. Langmuir isotherm

The Langmuir isotherm assumes the formation of a monolayer adsorbate on the outer surface of the adsorbent with adsorption can only occur at a finite (fixed) number of definite localized sites that are identical and equivalent, with no lateral interaction even on adjacent sites. The model assumes uniform distribution of adsorption energies with no transmigration of adsorbed molecules in the plane surface (Langmuir, 1916). Its use was extended to empirically describe equilibrium relationships between a bulk liquid phase and a solid phase. Based upon these assumptions, Langmuir represented the following equation:

$$Q_e = \frac{Q_{max}.b.C_e}{1 + b.C_e} \tag{3.8}$$

where, Q_{max} is the maximum metal uptake (mg/g) by coal and b the Langmuir equilibrium constant (L/mg). The liner fit of experimental data to Langmuir equation is shown in Fig. 3.9. The Langmuir adsorption isotherm fits very well to the experimental data as R^2 for linear fit is 0.99. Langmuir constants, Q_{max} and b, were calculated from the linear plot and found to be 60 mg g^{-1} and 1.23 L mg^{-1}, respectively. High values of b are reflected in the steep initial slope of adsorption isotherm, indicating desirable high affinity. Thus, coal can act as good adsorbent for the Au(III) ions. The effect of isotherm shape is discussed from the direction of the predicting whether and adsorption system is "favorable" or "unfavorable". A dimensionless separation factor or equilibrium parameter, R_L, as an essential feature of the Langmuir isotherm to predict if an adsorption system is “favourable” or “unfavourable”, which is defined as (Hall et al., 1966):

$$R_L = \frac{1}{(1 + b.C_o)} \tag{3.9}$$

where C_0 is the initial Au(III) concentration ($mg.L^{-1}$) and b is the Langmuir isotherm constant. Value of $R_L < 1$ represents the favourable adsorption and value $R_L > 1$ represents unfavorable adsorption. The values of R_L is 0.008 for adsorption of Au(III) on the coal, were found to be within 0 and 1 which indicates a highly favorable adsorption.

3.3.3.2. Dubinin–Radushkevich (D–R) isotherm:

It was reported that the D-R isotherm model was applicable at low concentrations ranges and could be used to describe adsorption on both homogeneous and heterogeneous surface (Vijayaraghwan et al., 2006). The D–R equation has the following form:

$$\ln Q_e = \ln Q_s - \beta\varepsilon^2 \tag{3.10}$$

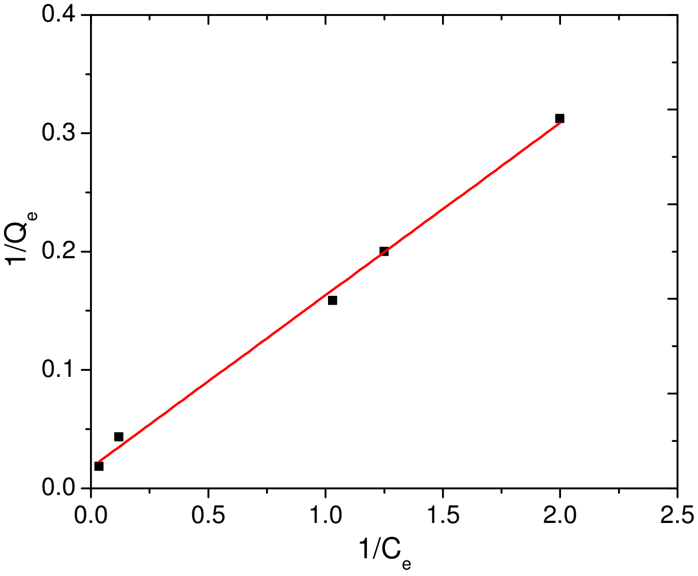

Fig. 3.9. Plot of Langmuir isotherm fits for Au(III) adsorption onto coal particles

where Q_e is the amount of metal ions adsorbed on per unit weight of adsorbent (mg/g), Q_s is the maximum adsorption capacity, β is the activity coefficient related to mean sorption energy, and ε is the Polanyi potential, which is equal given as:

$$\varepsilon = RT\ln(1 + {}^{1}/_{C_e}) \tag{3.11}$$

where R is the gas constant (J/mol K) and T is temperature (K).

The adsorption potential is independent of the temperature but varies according to the nature of adsorbent and adsorbate. The slope of the plot $\ln q_e$ versus ε^2 gives β (mol^2/J^2) and intercept yields the adsorption capacity Q_s (mg/g). The mean adsorption energy (E) is given by:

$$E = \frac{1}{(2\beta)^{1/2}} \tag{3.12}$$

The plot of $\ln Q_e$ against ε^2 for Au(III) adsorption on coal is shown in Fig 3.10. The experimental data fits very well to D-R model equation as R^2 is for the linear fit 0.98. The E values are 11.8 kJ/mol for Au(III) on the coal particles. The adsorption capacity q_s in the D–R equation is found to be 73.69mg/g for Au (III) ions. The numerical value of mean adsorption energy is in the ranges 1.00–8.00 and 9.00–16.00 kJ/mol for physical and chemical adsorption, respectively. It indicates that adsorption of Au(III) on coal particles is chemical in nature.

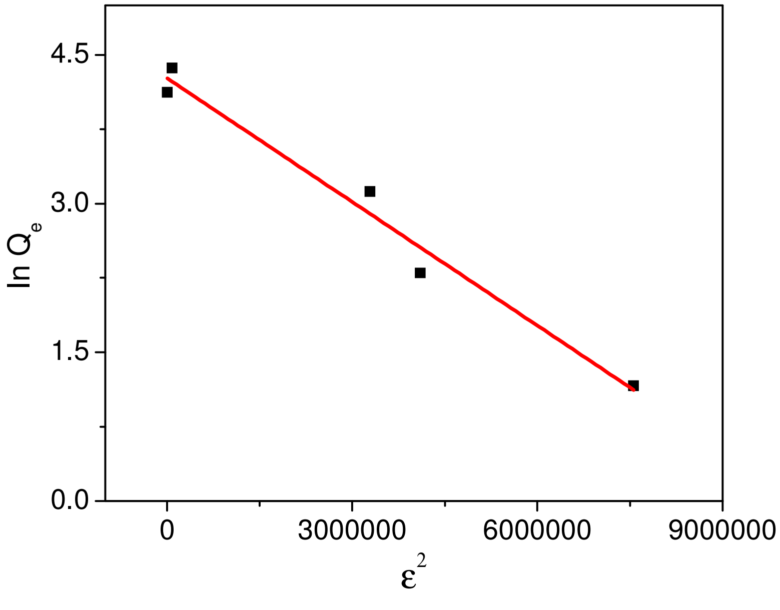

Fig. 3.10: Plot of D-R isotherm fits for Au(III) adsorption onto coal particles

3.3.4. Adsorption kinetics

In order to study the mechanism of adsorption and its potential rate-controlling steps such as mass transport and chemical reaction, two different models i.e. Pseudo-first-order (PFO) and pseudo-second-order (PSO) kinetic models were applied. It was found that PFO did not fits well to the experimental data, whereas PSO kinetic model was found to be fitting well to the experimental data and is discussed.

3.3.4.1. Ho’s pseudo-second-order (PSO)model

The kinetic data were further analyzed using Ho’s pseudo second- order kinetics (Choy and Mckay, 1999; Ho and McKay, 1999), which is represented by

$$\frac{t}{Q_t} = \frac{1}{k_2.Q_e^{\,2}} + \frac{1}{Q_e}t \tag{3.13}$$

$$h = k_2.Q_e^{\,2} \tag{3.14}$$

A plot between t/q versus t provides the value of the constants K_2 (g/mg min.) and also $q_{e,}$ (mg/g) can be calculated. Thus the rate constant K_2, initial adsorption rate h, and predicted q_e can be calculated from the plot of t/q versus time t using Eq. (13)

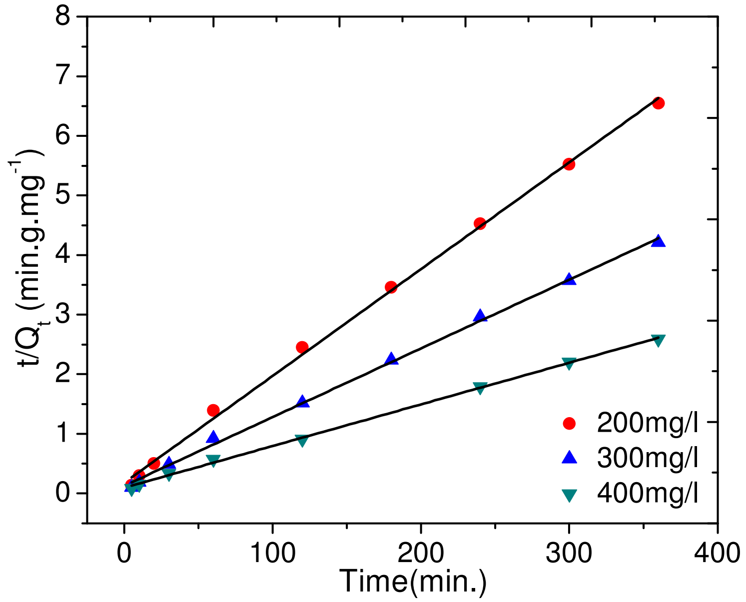

Fig.3.11: Pseudo-second-order kinetic plots for Au(III) adsorption on coal particles

Fig.3.11 shows the plot between t/q versus time t. The initial adsorption rate h, pseudo-second-order-rate constant K_2, amount of gold adsorbed at equilibrium q_e, and the linear regression correlation coefficient R^2values are given in Table 3.2.

Table 3.2: Pseudo-Second-Order Kinetic Parameters for the Adsorption of Au(III) onto coal particles

Gold Conc. (mg/l)	K_2 (min^{-1})	h (mg/g. min)	$q_{e, Exp}$ (mg/g)	$q_{e, Mod}$ (mg/g)	R^2
100	1.54	7.21	9.51	10.54	0.994

200	1.27	7.15	53	54.54	0.998
300	1.18	7.12	81	80.14	0.998
500	0.580	7.10	134	136.46	0.998

The higher values R^2 for PSO confirm that the adsorption process follows a pseudo-second-order mechanism. From Table 3.2, it was also observed that as Au(III) concentration increases h and K_2 decreases. This might be due to higher competition between the Au(III) ions for the surface active site.

3.3.4.2. Activation parameter

In any adsorption process, activation energy must be taken into account in order to understand the physical or chemical nature of the process. The activation energy of Au(III) adsorption onto the coal particles can be calculated by Arrhenius relationship (Zhu et al., 2009)

$$\ln K_2 = \ln A - \frac{E_a}{RT} \tag{3.15}$$

where A is the Arrhenius constant, R is the universal gas constant (8.314 J mol^{-1} K^{-1}), k_2 is second order rate constant and T is the temperature (K). When $\ln K_2$ is plotted against $1/T$ a straight line with slope $-E_a/R$ and intercept lnA is obtained. The plot of $\ln K_2$ versus 1/T (R^2 = 0.99024) is shown in Fig.3.12. The value of E_a as calculated from the slope of the plot was found to be 68 kJ/mol. The positive value of the activation energy indicates the presence of energy barriers in the adsorption of Au(III) on coal particle.

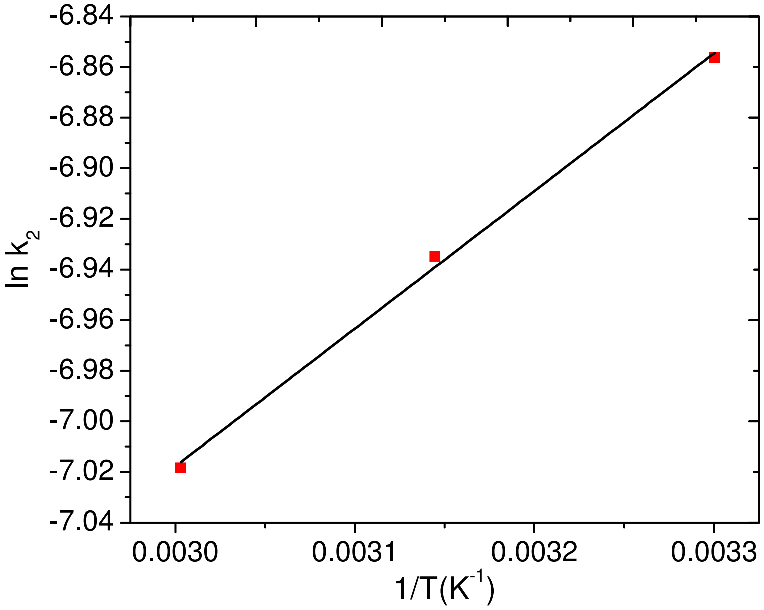

Fig.3.12. Plot of plot of $\ln k_2$ versus 1/T for adsorption of Au(III) on coal particles

The minimum energy that must be overcome in order to occur is therefore 68 kJ/mol. It is possible to obtain information about the type of adsorption (physical or chemical) from the magnitude of the activation energy. The physical adsorption processes usually characterized by low activation energies (in the range of 1–50 kJ mol^{-1}), while higher activation energies (60–800 $kJmol^{-1}$) advocate chemical adsorption (Roy et al., 2013). The value of the activation energy (68 kJ mol^{-1}) indicates that adsorption is chemical in nature.

3.4. Conclusions

From the studies following conclusions were drawn:

- Radiotracer technique was successfully used for investigating adsorption characteristics of Au(III) on coal particles at various conditions and eventually optimum conditions for maximum adsorption were obtained.
- At a constant adsorbate concentration, adsorbent amount, temperature and time of contact, the adsorption capacity of Au(III)on coal particles was found to increases with increasing pH, reached a maximum value at pH of 2.5 and thereafter further increase in pH resulted in gradual decrease in adsorption capacity or percentage.
- At a constant pH, adsorbent amount, temperature and contact time, the adsorption of Au(III) ions increased from 15 mg/g to 148 mg/g as the initial concentration of Au(III) ions increased from 100 mg/l to 500 mg/l.
- At a constant pH, adsorbate concentration, adsorbent amount and temperature, the adsorption of Au(III) rapidlyincreases initially with time but slows down gradually once equilibrium is attained. Subsequently, the adsorption did not increase appreciably change with time.
- There was a marginal increase in adsorption of Au(III) ions from 13.2 to 14.9 mg g^{-1} as the temperature was raised from 30 to 60 °C. Therefore adsorption has weak dependency on temperature.
- Among the adsorption isotherms studies, the Langmuir isotherm was demonstrated to provide the best correlation for adsorption of Au(III) onto coal particles. The applicability of the Langmuir isotherm dictates monolayer coverage of the ^{198}Au on surfaces of coal particles. The pseudo second-order kinetic model agrees very well with the dynamical behavior of ^{198}Au adsorption for concentrations range studied.
- The adsorption of Au(III) on to the coal particles was found to be chemical in nature as suggested by D-R isotherm and activation energy value.

- The thermodynamic parameters reveal that the adsorption is spontaneous and endothermic. The positive value of entropy indicates that increasing randomness at the solid/liquid interface during ^{198}Au adsorption. The activation energy of ^{198}Au adsorption was found to be 68 kJ mol^{-1} indicating chemically controlled process.
- Based on the obtained optimized conditions for adsorption, it can be concluded that coal particles have a considerable high percentage of adsorption (90 %) and thus could be used for preparation of radiotracer i.e.^{198}Au(III) labeled with coal particles for tracing coal in gasifiers or gas-solid fluidized bed system involving flow of coal.
- Based on the results of adsorption, radiotracer was prepared (^{198}Au(III) labeled coal particles) and used for measurement of RTD of coal particles in a pilot-scale gasifier. The mean residence times of coal particles and degree of axial mixing were estimated.

Chapter 4

Measurement of mixing time and holdup of solids in gas-solid fluidized bed using radiotracer technique

---

4.1. Introduction

A fluidized bed is a state of a two-phase mixture of particulate solid material and fluid (gas or liquid). It is formed when a quantity of a solid particulate substance is placed under appropriate conditions to cause the solid/fluid mixture to behave as a fluid. This is usually achieved by the introduction of pressurized fluid through the particulate medium. Fluidized bed systems are widely used in many modern technologies for efficient implementation of various physical and chemical processes. This is due to their many advantages such as high surface area contact between fluid and solid per unit bed volume, high relative velocities between the fluid and the dispersed solid phase, high degree of intermixing of the particulate phase and frequent particle-particle and particle-wall collisions. Because of these inherent advantages, fluidized beds have been used in technological processes such as cracking and reforming of hydrocarbons (oil), carbonization and gasification of coal, ore roasting, Fischer-Tropsch synthesis, polyethylene manufacturing, limestone calcining, aluminum anhydride production, granulation, vinyl-chloride production, combustion of waste, nuclear fuel preparation, combustion of solid, liquid and gaseous fuels, drying, adsorption, cooling, heating, freezing, conveying, storing and thermal treating of various particulate solid materials. The fluidized bed systems are operated either in batch or continuous mode depending upon the process requirement (Stepien and Sciazko, 2015).

The mixing of solid particles in continuous or batch fluidized bed system has been recognized as an important factor determining the heat and mass transfer rates as well as the overall reaction rates. This may have considerable effect on efficiency and quality of the product, and thus economy of the industry. Conventional tracer techniques such as colorimetry, thermometry and conductivity methods are commonly used for measurements of liquid mixing time in laboratory scale batch process systems. However, these techniques are not feasible to apply for measuring mixing of solids in pilot-scale solid-gas fluidized bed systems. Radiotracer techniques provide a practical means for measuring mixing times in industrial process systems because of their many advantages such as their high detection sensitivity, online detection, physico-chemical compatibility, availability of wide range of compatible radiotracers, and unambiguous detection (Pant et al. 200A; 2009B; 2012). Solid holdup is another very important parameter that characterizes the fluidization quality, mixing, and process efficiency in a fluidization system, and is defined as the volume fraction of gas present within the bed. Noninvasive measurement technique like γ ray attenuation method is suitable for this purpose, because it provides insight into the flow behavior and general hydrodynamic characteristics of multiphase flow and opaque systems (Yates at al., 2012; Bukur et al., 1996). Present chapter describes measurement of mixing times of solids at different operating condition and measurement of axial and radial distribution of solid holdup fraction in a pilot-scale batch fluidized bed system using radioisotope technique. The effects of gas superficial velocity (V_a) and bed height (BH) on solid holdup were investigated.

4.2. Experimental

4.2.1. Experimental setup

The schematic diagram of the batch type Fluidized Bed System (FBS) is shown in Fig. 4.1. The system consists of an acrylic cylinder of 0.15 m of internal diameter and 8 m of height, a distributor, feed transport system, a cyclone, and gas supply system. The bottom part of the system where fluidization occurs is called dense bed section while the top section of the cylinder is called as freeboard section and is connected to the cyclone. Sand particles of mean diameter of 223 micron and air were used as solid and gas phase respectively. When air flow is introduced through the bottom of the bed of solid particles at a critical value of gas velocity, the aerodynamic drag forces will be exactly equal to the downward gravitational forces, causing the particles to become suspended within the fluid. This condition is called fluidization and the bed is said to be fluidized. The minimum fluidization velocity (U_{mf}) of the system used in this work is 0.047 m/s.

4.2.2. Radiotracer experiments for mixing time measurement

Gold-198 radioisotope (gamma energy: 411 keV, half-life: 65 hr) was selected for labeling the sand particles and used as a radiotracer (Pant at al., 2009A; 2009B). Gold-198 was produced by first irradiating gold metal in DHRUVA reactor at Trombay, Mumbai and dissolving the same in aqua regia solution to produce hydrogen chloroauric acid solution of activity about 1.3 GBq in a volume of 1.2 ml. 0.03 Kg of sand particles were slowly poured into 100 ml aqueous solution containing 145 MBq activity and stirred intermittently for about half an hour. The supernatant solution was decanted and the sand particles were dried over a hot plate. These gold-198 labeled sand particles are used as radiotracer. 3 g of radiotracer having 11 MBq activity was used in each run. A series of tests were carried out at different fluidizing air velocity and static bed height.

All the detectors were calibrated prior to experiment to give the identical responses under similar conditions. The detector and the source were mounted in a fixed geometry as used in the actual experiment and the detector was connected to a pulse processing unit (PPU). The output signal of the detector was visualized on an oscilloscope screen after applying suitable operating voltage to the detector. The threshold level (lower level discriminator) was set to eliminate the electronic noise. The height of the output voltage pulse produced by the detectors maintained same by adjusting the gain. After calibration, it was ensured that all the detector gave similar counts rate for a given geometry and source. The experiments for mixing time measurement was started with instantaneous injection of radiotracer into the system through the feed line using pressurized-air. Seven different detectors mounted at different axial locations were used to record tracer concentration at an interval of 20 milliseconds. The detectors were collimated and connected to a computer controlled data acquisition system. The detector D1 was used to confirm and record the time of entry of radiotracer into the system, whereas detector D2 - D7 mounted at axial positions were used to record tracer concentration with time and estimate mixing time. The radiotracer concentration was monitored till the radiation level recorded by each detector becomes constant.

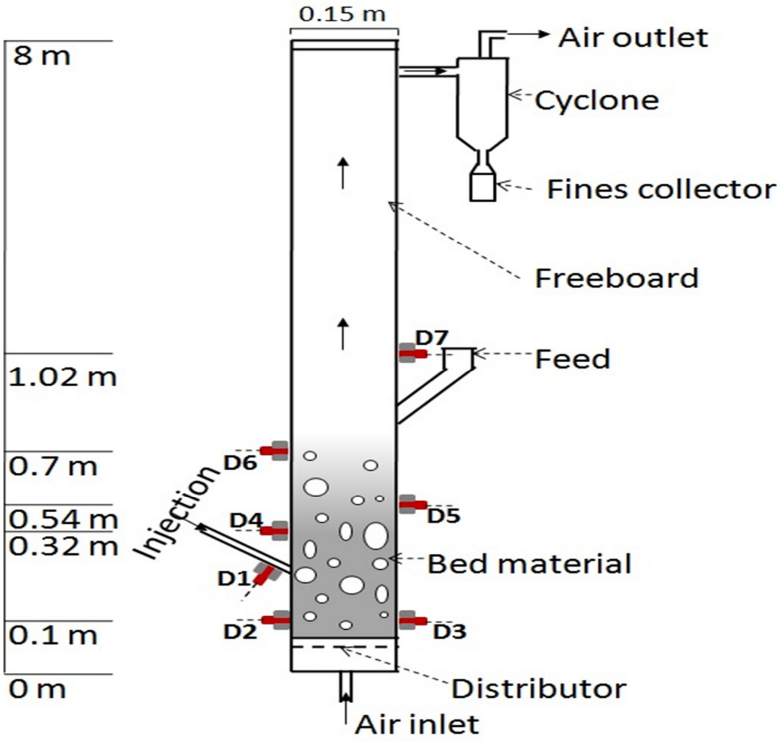

Fig. 4.1: Schematic diagram of gas-solid fluidized bed system and experimental setup for mixing time measurements

4.2.3. Experimental method for solid holdup measurement

The experimental setup for solid holdup measurements is shown in Fig. 4.2. Different axial positions were marked on the fluidizer column with the help of a graph paper. The radial/ chordal positions were marked on specially designed metal plates. Collimated sealed source of ^{137}Cs having 10 mCi activity and collimated NaI(Tl) detector were mounted on the metal plate and placed at both sides of test column by facing each other. The detector was connected to a counter and a data acquisition system with software interface to measure and record the photon counts in every 30 second. The holdup measurements were carried out at nine chordal positions and at three axial positions for different static bed heights (BH) (0.45 m and 0.8 m) and at different gas superficial velocities (V_a) (0.1m/s, 0.2m/s, 0.3m/s, 0.5m/s). The axial positions are represented as Level 1, Level 2, Level 3 and Level 4, which are at a height of 0.235 m, 0.335 m, 0.445 m and 0.873 m from the distributor plate and the chordal positions are represented as *r/R* ratio.

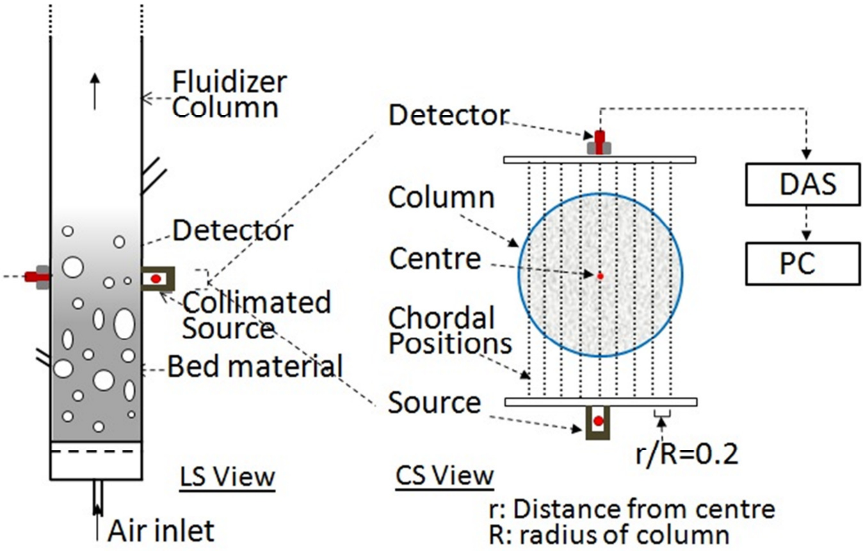

Fig. 4.2: Experimental setup for holdup measurement

Where *r* is perpendicular distance of chordal line from the centre of the column and *R* is the radius of the column. Hence *r/R* varies from -1 to +1 through zero. At each position the mean count was obtained by measuring three readings. The counts were measured for empty bed (I_a), packed bed at static condition (I_s) and fluidized bed (I_f).

4.3. Data Analysis:

4.3.1. Methodology for estimation of mixing time:

The steps include background correction, normalization with respect to the final counts as the each detector has different solid angle for the measurement (Brown et al., 2004). The equation used for the normalization is given below:

$$E(t) = C(t)/\bar{C}_f(t) \tag{4.1}$$

Where E(t) is the normalized tracer concentration, C(t) is tracer concentration at any point of time and $\bar{C}_f$(t): Average constant final concentration of the tracer.

Brown et al. (2004) had proposed that mixing time is the time after the injection of tracer, when tracer concentration of normalized curve is within ± 5 % of the final equilibrium value (Brown et al., 2002; Jafari and Mohammadzadeh, 2005; Othman and Kamarudin, 2012). However, in case of fluidized bed system, the flow dynamics is very fast. Hence, in present study, it is difficult to find directly the mixing time from a plot of E(t) versus t. Thus, in order to obtain accurate value of mixing time from the measured curves in this study, variance with respect to C(f) is plotted as a function of time and mixing time corresponding to 0.05 of variance is obtained. Thus the variance is given as:

$$\sigma^2 = (E-1)^2 \tag{4.2}$$

The different steps involved in the data treatment for the mixing time measurement is shown in the Fig. 4.3(a, b, c, d).A few representative plots of variance with time is shown in inset of Fig. 4.4 (a, b, c, d, e, f). The mixing times corresponding to 0.05 variances at various operating conditions are shown in Table 4.1. Mixing times were estimated from the measured normalized tracer concentration curves.

4.3.2. Principle and data treatment of solid holdup measurement:

When a narrow, parallel, mono-energetic γ-ray is transmitted through a medium, its attenuation depends on type and thickness of absorbing material and the number of photons registered per second is given by (Knoll, 2000):

$$I = I_0 e^{-\mu l} \tag{4.3}$$

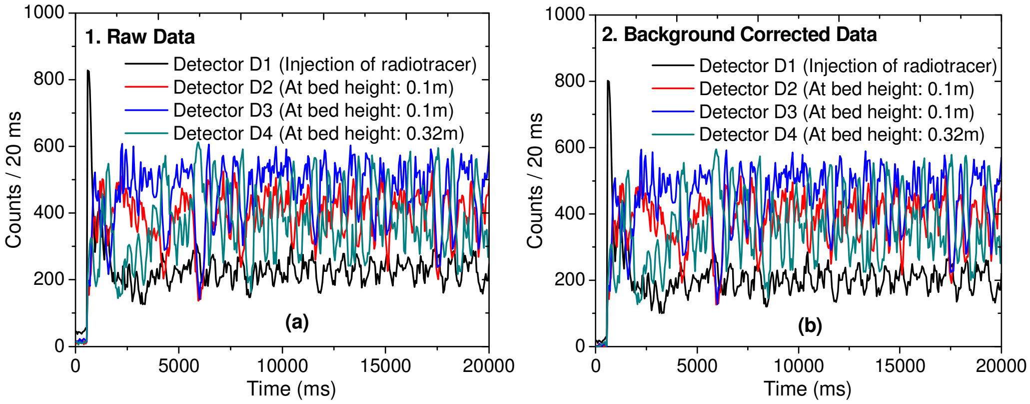

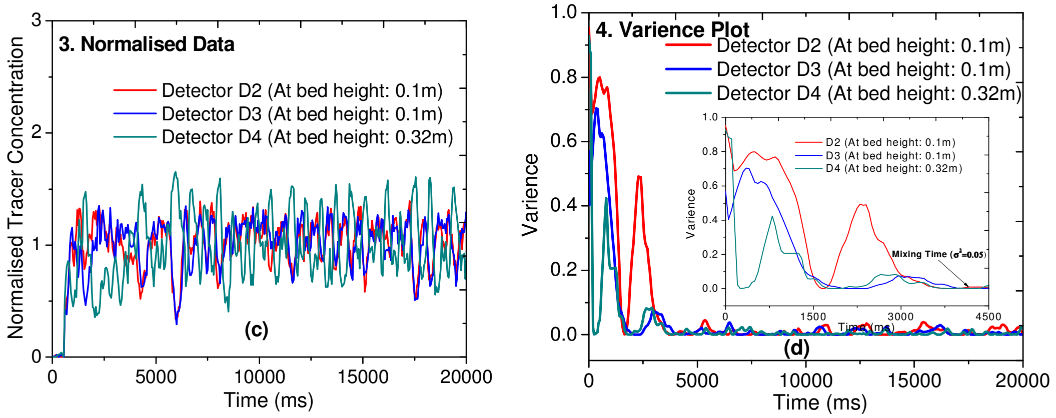

Fig. 4.3.(a,b,c,d): Graphical representation of mixing time data at different stages of data treatment

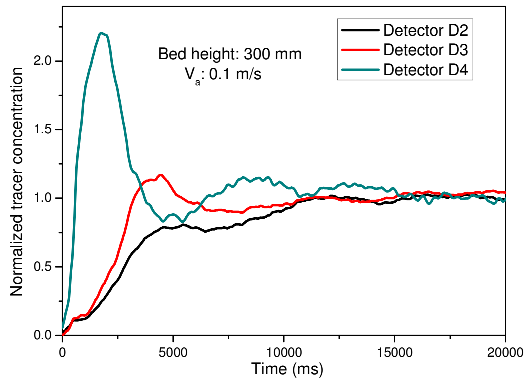

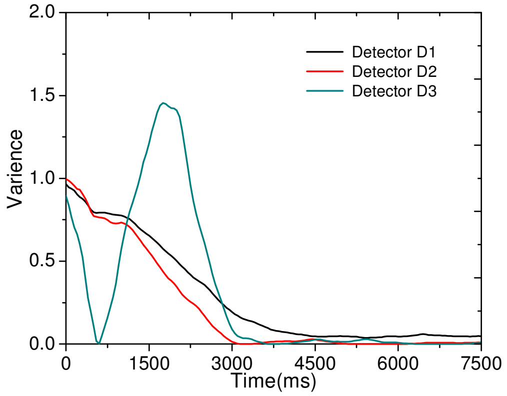

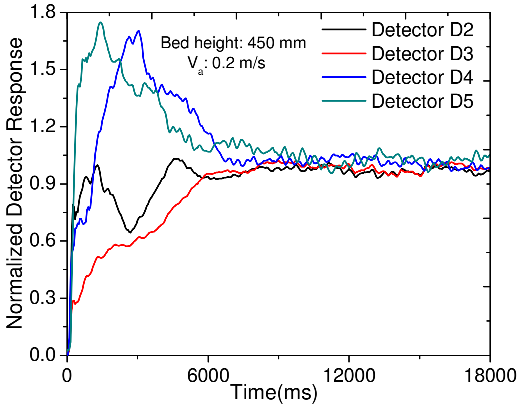

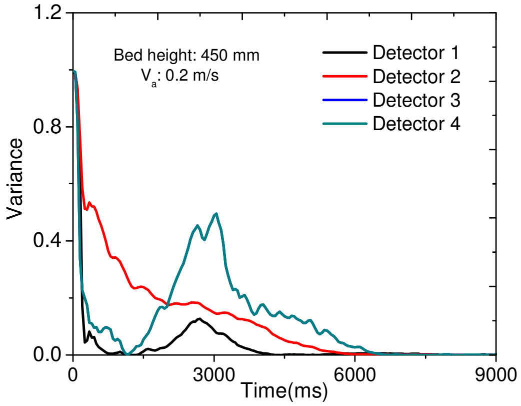

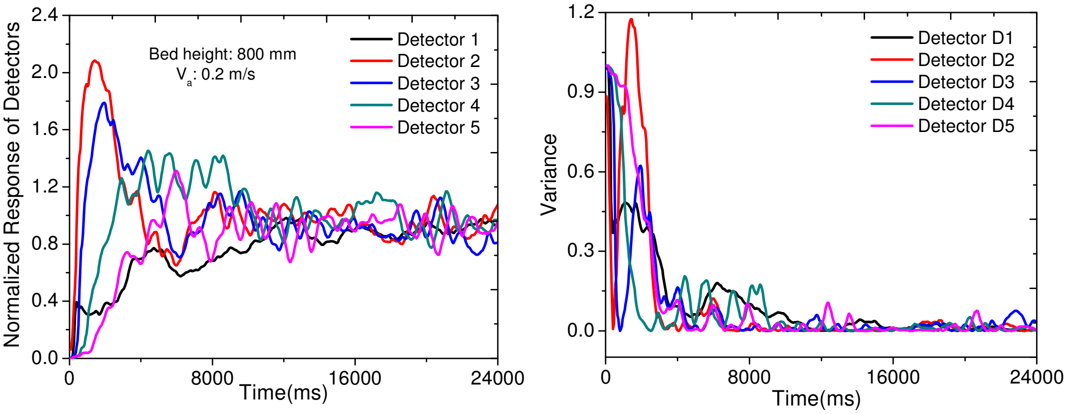

Fig. 4.4 (a, b, c, d, e, f): Normalized tracer concentration curve at different operating conditions and their corresponding variance plots

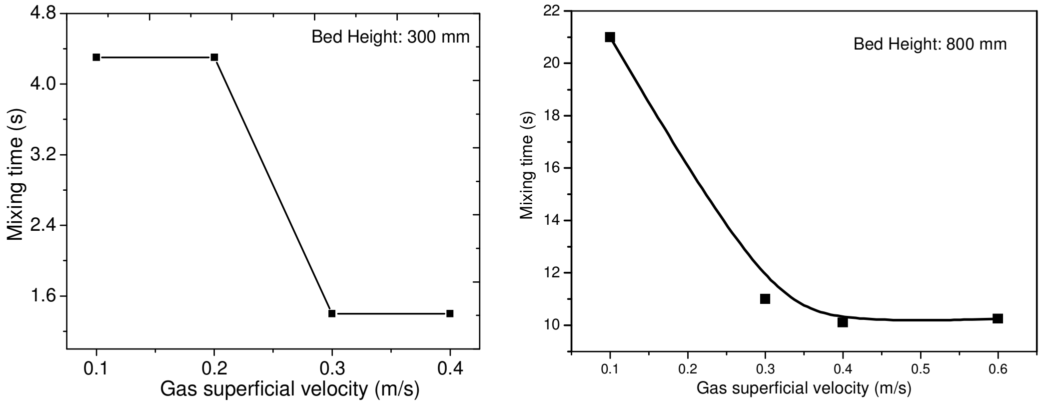

Fig. 4.5 (a,b): Variation of mixing time with gas superficial velocity at bed height 300mm and 800mm

Table 4.1: Mixing time for different bed heights and different gas superficial velocities

Run No.	Gas superficial velocity (m/s)	Static bed height (m)	Approximate expanded bed height (m)	Mixing time (s)
1	0.1	0.3	0.4-.6	4.3
2	0.2	0.3	0.42-0.65	4.3

3	0.3	0.3	0.45-0.7	1.4
4	0.4	0.3	0.45-0.7	1.4
5	0.1	0.45	0.5-0.6	6.45
6	0.2	0.45	0.6-0.7	6.45
7	0.3	0.45	0.7-0.85	4.9
8	0.1	0.8	0.9-1.1	21
9	0.3	0.8	0.9-1.3	11
10	0.4	0.8	1.2-1.5	10.1
11	0.6	0.8	1.1-2.0	11.25

Where, I_0, I, μ and l are initial intensity, intensity after transmission, attenuation co-efficient of medium and thickness of medium respectively. In the present system taking into consideration of two phase medium, i.e, air and sand; the attenuation coefficient at different measurement conditions can be found out and similar equation as Eq (4.3) can be derived for each condition (Kumar et al., 1997; Jin et al., 2005). Using the above principle in our experiment we can find out the voidage distribution of gas in the fluidized bed.

Assuming effective length and attenuation coefficient as constant

$$\text{Air only: } \ln\frac{I_a}{I_0} = -\mu_w l_w - \mu_a l \qquad (4.4)$$

Where I_0 = Total number of photons generated by the source

I_a = Detected number of photons attenuated by air

μ_a = Linear attenuation coefficient of air

l = Effective length of attenuation

μ_w = Linear attenuation coefficient of reactor wall

l_w = Thickness of the wall

$$\text{Sand only: } \ln\frac{I_s}{I_0} = -\mu_w l_w - \mu_{eff} l \tag{4.5}$$

Where I_s = Detected number of photons attenuated by solid particle bed

μ_{eff} = Effective linear attenuation coefficient of the solid particle bed

As we know that solid particle bed will have voidage between the particles filled with air.

$$\mu_{eff} = \epsilon_{a0}\mu_a + (1 - \epsilon_{a0})\mu_s \tag{4.6}$$

Where ε_{a0} = initial porosity of the bed when no air is flowing in the bed

μ_s = Linear attenuation coefficient of the solid particles

$$\text{Fluidized bed: } \ln\frac{I_f}{I_0} = -\mu_w l_w - \mu_{eff} l \tag{4.7}$$

Where I_f = Detected number of photons attenuated by fluidized bed

$$\mu_{eff} = \epsilon_a\mu_a + (1 - \epsilon_a)\mu_s \tag{4.8}$$

ε_a = porosity of the fluidized bed

By solving (4.4), (4.5) and (4.7) we get

$$\frac{\ln\dfrac{I_f}{I_s}}{\ln\dfrac{I_a}{I_s}} = \frac{\epsilon_a - \epsilon_{a0}}{1 - \epsilon_{a0}} \tag{4.9}$$

Where, ε_{ao}, ε_a are gas holdup fractions in static and fluidized bed respectively. From literature ε_{ao} is known to be 0.34 in case of sand at static condition. The solid holdup fraction is calculated by the following equation:

$$\text{Solid holdup fraction} = 1-\varepsilon_a \tag{4.10}$$

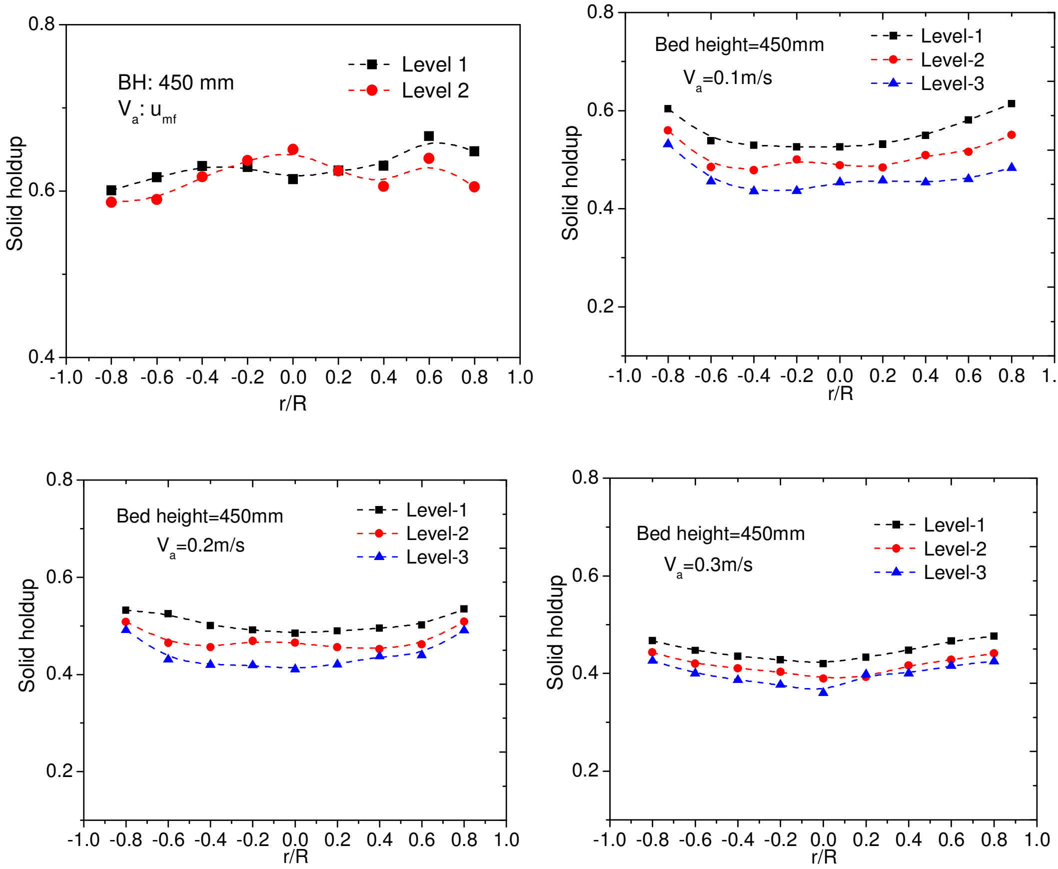

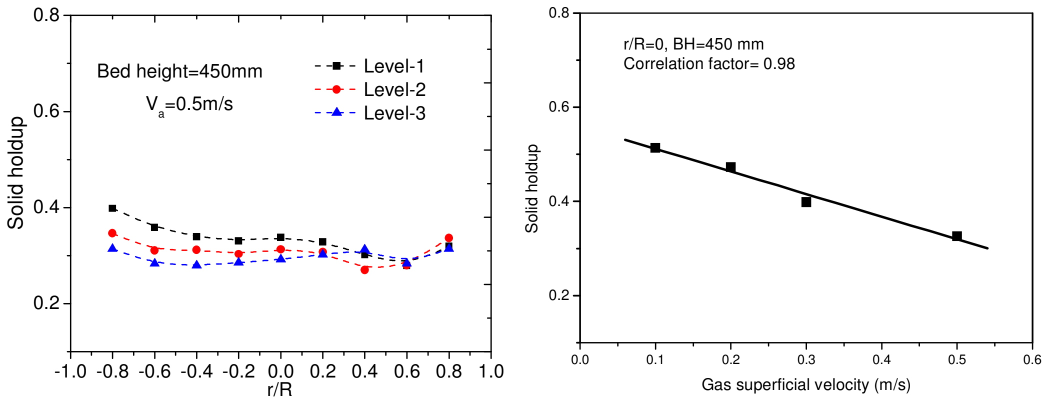

Fig.4.6: Radial solid hold up variation at different as velocity a) U_{mf}, b) 0.1m/s, c) 0.2m/s, d) 0.3m/s e) 0.5m/s, f) Average central point gas holdup variation at different gas superficial velocity

4.4. Discussion

The fluidization and mixing behavior of a fluidized bed mainly depends upon particle characteristics. Geldart proposed that the particles are classified into four groups i.e. Group A, Group B, Group C and Group D, based on their mean size and density (Geldart, 1973). Each of these groups exhibits a specific mixing behavior upon fluidization. Out of the above Groups, Group B particles having size ranging from 40 - 500 μm and density between 1.4 - 4 g cm^{-3}, fluidize with minimum fluidization velocity and are used in majority of gas-solid reactions in industry (Kunii and Levenspiel, 1991). Hence, in the present study, Group B particles (sand) having mean diameter of 223 micron were used. Mixing times were measured at three different static bed heights i.e. 0.3 m, 0.45 m and 0.8 m and five different gas velocities i.e. 0.1 m/s-0.6 m/s. At a fixed operating condition the observed mixing time value as obtained from variance versus time plot is given in Table 4.1. The effect of gas velocity on mixing time is shown in Fig. 4.5. It was observed that for 0.8 m bed height the mixing time decreases initially with increase in gas velocity up to 0.4 m/s and beyond this value there is no change. From the plot it can be concluded that for 800 mm bed height 0.3 m/s to 0.4 m/s gas velocity is suitable to get uniform mixing at less time. The measured mixing time values for different conditions are given in Table 4.1. It was observed that the mixing time increases with increase in the bed height. The radial distribution profile of average solid holdup fraction at minimum fluidization velocity (U_{mf}) for 0.45 m static bed height is shown in Fig. 4.6(a). It can be seen from the figure that there is not much change in the solid holdup fraction at different axial levels at U_{mf}. The radial distribution profile of average solid holdup fraction at different air velocity is given in Fig. 4.6(b-e). The radial variation of the solid holdup at 0.8 m static bed heights and air flow rate(Umf and 0.1m/s) is shown in the Fig.4.7.

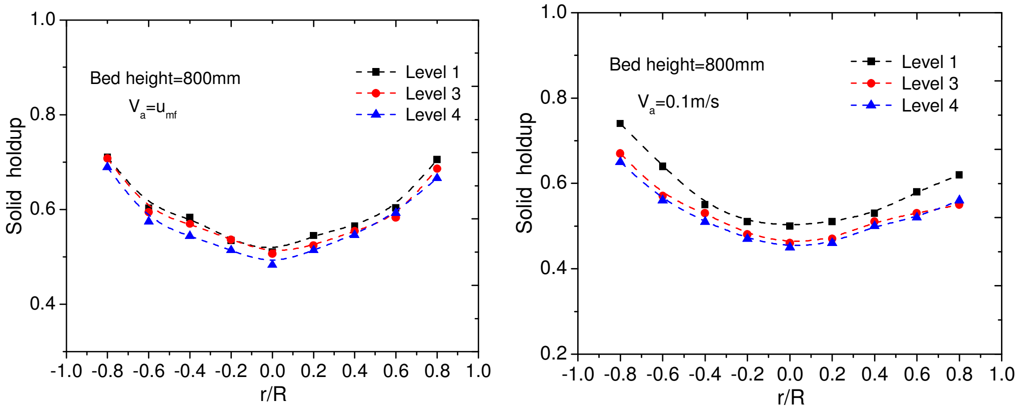

Fig.4.7.: Radial solid holdup variation at different height with BH: 800mm

The dip at the r/R=0 indicates that the air flow in the center is higher and hence the solid holdup is also less. This may be due to wall effects present in the smaller column. The solid holdup at the equidistant point from the r/R=0 have nearly same value. This provides information about the air distribution at radial positions which seems to be more over uniform (Efhaima, 2016). It was also observed that the solid holdup fraction decreases at higher axial height. The solid holdup fraction was measured at different gas superficial velocities at the centre of column (r/R: 0) for fixed bed height and axial level and is shown in Fig. 4.6(f). As can be seen from the figure the relationship between solid holdup fractions with gas superficial velocity is linear with correlation factor 0.98 and the solid holdup fraction decreases with increase in gas superficial velocity.

4.5. Conclusions

Radiotracer technique was successfully employed to measure mixing and solid holdup in a gas-solid fluidized bed system. It was observed that the increase in fluidization velocity up to 0.4 m/s facilitates mixing by decreasing the mixing time. The mixing time was observed to be higher for higher bed heights. The holdup fraction of solid was found to be more towards the wall compared to the centre of the column. The solid holdup decreases linearly with increase in gas velocity. The solid holdup decreases at higher axial heights and it increases marginally for higher bed height.

Chapter 5

Measurement of the flow dynamics of the coal particles in cold and hot flow fluidized bed gasifier using radioactive particles

---

The gasifier involves flow of two different phases i.e. solid (coal) and gas (air/steam) and understanding of dynamics of these two phases is important to assess the performance of the system as well as for scale up of the process at different scale of the gasifiers. The gasifier is designed and expected to behave as a well-mixed flow system for solids and any deviation from the well-mixed flow condition will deteriorate the performance and efficiency of the gasifier.

The mixing of the solid and gas phases within the gasifier has prime importance for the efficient gasification of the coal particles. The key component that guides the uniform distribution of gas across the fluidized bed is the design gas distributor and thereby helps in achieving good mixing of solids. Therefore, the efficiency of the fluidization process depends upon the design and performance of the distributor, which need to be evaluated before scale up. The qualitative information about the performance of distributor in a transparent Perspex cold fluidized bed system could be obtained either by observing the mixing/churning phenomena visually or by photographic techniques. However, it is always desirable to know the performance quantitatively. The good mixing and minimum weeping governs the selection of a distributor for actual hot operations in full-scale fluidized bed system. The analytical approach to evaluate the performance of a distributor and overall mixing behavior of the fluidized bed is to measure and analyze the residence time distribution (RTD) of the solid phase.

Two pilot-scale of Fluidized-Bed Gasifier (FBG) were designed to study the various design and operation aspects of coal gasification/combustion process. The two different studies were carried out in pilot scale coal gasifiers based on basic fluidized bed reactor (FBR) design. The objectives of the two study were (a) To know the dynamics of the solids i.e. mixing of solids in presence of gas phase with two different types of air distributors i.e. flat plate and conical distributor used independently in the system and compare their performance in cold flow gasifier (b) The suitable air distributor selected in the previous study (i.e. study-a) was used to study the flow dynamics of the gasifier in hot condition i.e. real operating condition of the gasifier.

Chapter 5(a)

Evaluation of efficiency of Two Different Air Distributors Used in a Pilot-Scale Cold Flow Fluidized Bed Gasifier Using Radiotracer Technique

---

5(a).1.Introduction:

Two different air distributors were designed and proposed to use for distribution of gas phase (air) in the fluidized bed gasifier system. It was desired to know the dynamics of the solids i.e. mixing of solids in presence of gas phase with two different types of air distributors i.e. flat plate and conical distributor used independently in the system and compare their performance. The primary function of the air distributor is to fluidize the coal particles uniformly the quality of the mixing can be measured quantitatively by measuring the RTD of solid phase. Ideally the RTD of the solid phase in FBG should be like continuously stirred tank reactor i.e perfect mixer. Any anomaly in the distributor performance and fluidization process will be reflected in measured RTD. From the measured RTD, flow abnormalities, if any, are identified and mean residence time (MRT) of the process material is measured. In addition to this, the modeling of the RTD data provides information about flow patterns and detailed flow structure within the system. Radioisotope tracers are very effective tool to measure residence time distribution (RTD) of process material in pilot-scale as well as the full scale industrial. In this study the residence time distribution measurement was done to measure the efficacy of the measurement of the solid particles using radioactive coal particles.

5(a).2. Fluidized Bed Gasifier and Distributors

The schematic diagram of the pilot-scale fluidized bed system is shown in Fig. 5(a)-1. The plant consists of various subsystems such as a fluidizer, freeboard, cyclone, a feeding system, an air supply system and an ash extraction system. The compressor supplies air to an air header, which in turn distributes and supplies air for fluidization and to the feed transportation system. The air flows can be controlled and measured as per the requirement using the air flow meters. The different design parameter of the fluidized bed gasifier is listed in the Table 5(a)-1.

The provision for changing the distributor has been made so that both conical and flat plate distributors could be tested. The outlet of the freeboard section is connected to the cyclone. The fines captured within the cyclone are collected in the collection vessel at the bottom of the cyclone. The solids are continuously fed into the bed using a feeding system (hopper) and extracted from the bottom using a rotary extractor. The pressure inside the system during normal operation ranges from 0.5-0.6 kg/cm^2.

Table 5(a)-1: Design parameters of the cold flow FBG model

Parameters	Value
Fluidizer inner diameter	0.65 m
Fluidizer height	1.5 m
Free board inside diameter	0.88 m
Free board height	1.1 m
Bed material	Coal
Fluidizing agent	Air
Operating pressure	0.5-0.6 kg/cm^2

Two different distributors i.e. flat plate and conical distributors were independently used in the system. The distributors are shown in Fig. 5(a)-2 and Fig. 5(a)-3, respectively.

Flat plate distributor has a outer diameter of 1100 mm and inner diameter of 1030mm. The peripheral ring contains 32 holes of diameter of 15mm with the thickness of 6mm. It has 235 bubble caps in its core at 20mm triangular pitch and the length of the hole is 2mm. The length of the bubble cap is 70mm with outer diameter of 12mm and inner diameter of 6mm.

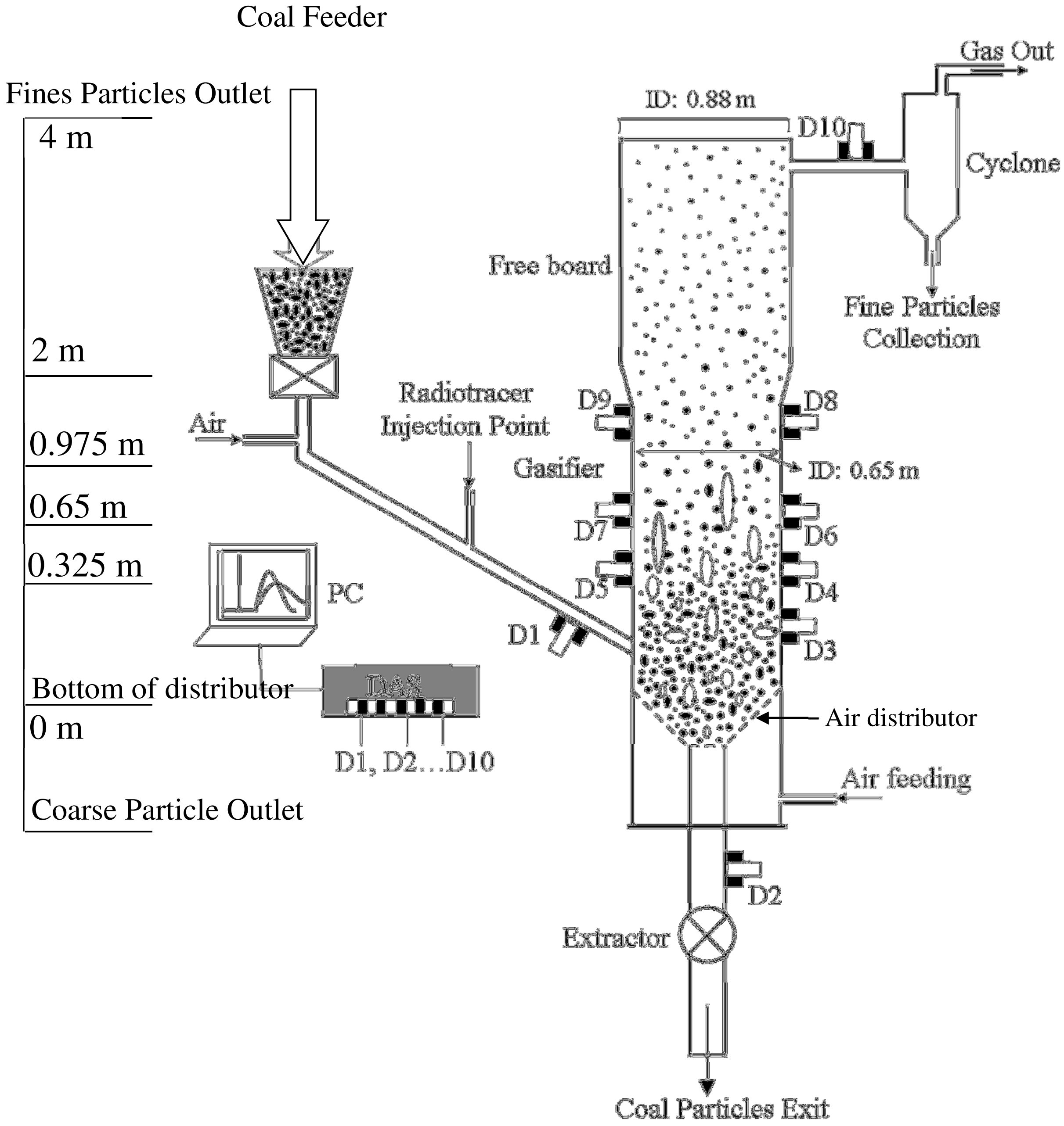

Fig.5(a)-1 Schematic diagram of fluidized reactor and experimental setup

Conical distributor with cone diameter of 650 mm and height 520 mm has outer diameter of 1100 mm. The total number of holes in this distributor is 941 with diameter of 2mm. It has 149 holes at 3 mm pitch, 246 holes at 3 pitch, 205 holes at 5 pitch, 188 holes at 7mm pitch and 153 holes at 10.5mm pitch on planes which are 80mm, 160mm, 240mm, 320mm and 400 mm distance from the bottom of the distributor.

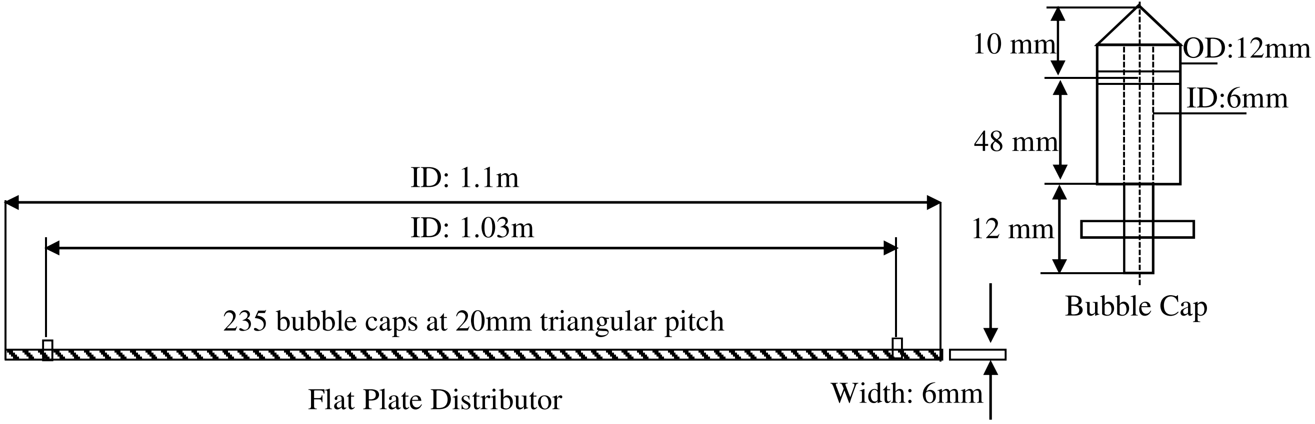

Fig. 5(a)-2: Flat plate distributor

5(a).3. Preparation of radiotracer:

The preparation of radiotracer for this study involves labelling of coal particles with suitably selected radioisotope. The one of the important parameter for tracer particle selection is coal particle size distribution. The detailed chemical and physical analysis of coal particles is done reported elsewhere in literature (Goswami et al., 2017). The labelling of coal particles involves two steps. In step one, is preparation of radioactive solution and in the second step labelling of radiotracer into the coal particles. In this study the Au-198 ($t_{1/2}$= 2.78 days, γ: 411 KeV (100%)) was found to be suitable radiotracer owing to its nuclear properties. The preparation of Au-198 from inactive Au-197 involves slow neutron irradiation of the inactive target. Upon the neutron irradiation gold goes through Au-197(n,γ) Au-198 nuclear reaction.

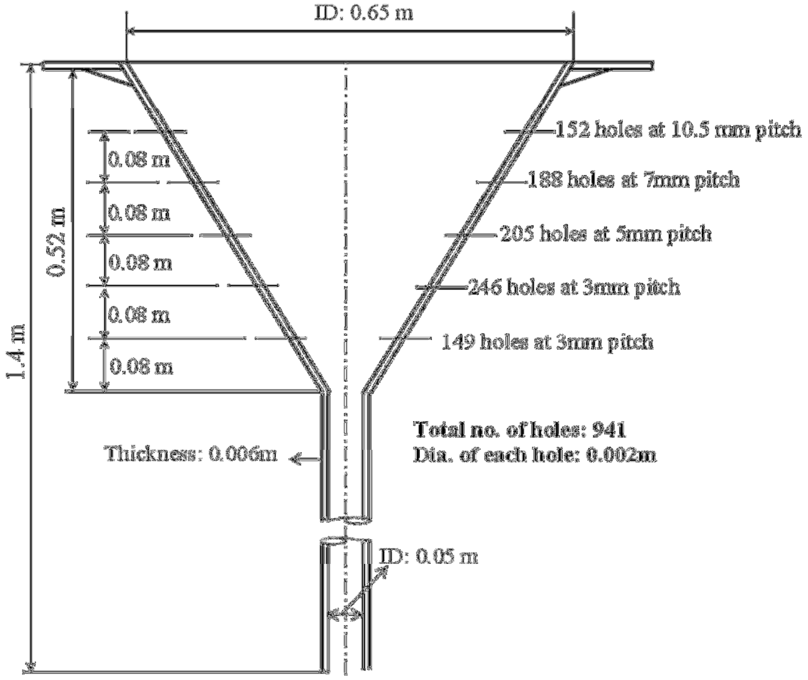

Fig. 5(a)-3: Conical plate distributor

Subsequently, dissolution of radioactive gold metal in aqua regia (3:1 mixture of HCl and HNO_3) is done. In this process radioactive metal is converted into water soluble terachloroaurate ion. After the preparation of the radioactive gold, it needs to be transferred from liquid phase to solid phase coal particles. The various factors affecting the transfer of the gold ions from radioactive solution to the coal particles have been discussed in the literature (Goswami et al., 2017). As reported in the literature, when liquid gold solution pH is in the range of 2-3, about 90% of the radioactive gold is transferred from liquid to coal particles. Therefore, the pH of the aqueous solution having volume 500 ml and radioactivity of 4.5 mCi was adjusted in range 2.5-3 using 1M NaOH and 1M HCl solution. Then, about 75 grams of coal particles were suspended in the solution for a period of 40-45 minutes. Subsequently, the mixture was allowed to settle and water in present the mixture decanted. The welted solid particles were dried over a hot plated at temperature about 50^{o}C to remove the excess of water present in the coal particles. The dried and labelled coal particles were used as radiotracer in this study. The labelled coal particles are divided in the three equal parts, so that 25 grams of coal particles is having about 1mCi of activity. The labelled coal particles were sufficient to carry out three RTD runs. For the further study, the same methodology was employed for the preparation of the radiotracer.

5(a).4.Radiotracer experiment, analysis and modelling:

A fixed quantity of the coal particles into the system at predefined bed height, air at a certain flow rate was fed into the system and fluidization was achieved. After the fluidization, the coal particles were continuously fed and extracted from the system at the same rate and amount of the coal particle in the bed was maintained to be constant. The radiotracer was injected as pulse into the system after the system achieved steady state condition. In each experiment about 75 gm of coal particles having activity of about 100-120 MBq was used as radiotracer.The radiotracer was instantaneously injected into the feed pipe using a specially fabricated injection arrangement and monitored at ten different locations in the FBG using lead collimated scintillation detectors (D1, D2, D3, D4, D5, D6, D7, D8, D9, D10 and D11) as shown in Fig. 5(a)-1. All the detectors except D2 were collimated using lead collimators of thickness 25 mm. The D2 detector was collimated with a collimator having thickness of 50 mm to avoid detection of stray radiations from within the system. The detection geometries of detector D3, D4, D5, D6, D7, D8, D9 and D11 were identical as all of them were mounted at various axial locations along the fluidizer. Whereas, the detection geometries at detector locations D1, D2 and D10 were different as the size of the standpipes was different at these locations. Prior to the experiment, all the detectors were calibrated to give the identical responses under similar conditions.All the detectors were connected to a multichannel computer controlled data acquisition system (CCDAS) set to record tracer concentration data at an interval of every 30 seconds. The tracer concentration data acquired as a function of time was saved as an ASCII file in the computer for further analysis. The radiotracer concentration curve monitored at bottom of the gasifier with different distributer is shown in the Fig. 5(a)-4 and 5(a)-5. The radiotracer data was analysed using the same methodology as mentioned in section data treatment and analysis of chapter 2. The treated data is shown in the Fig. 5(a)-6 and 5(a)-7.

The treated data was used to estimate the MRT and dead volume of the reactor by the detector placed at the bottom of the reactor and MRT of the fine particles was also estimated as given in the Table 5(a)-2 and 5(a)-3 respectively. The treated data was first simulated using continuously stirred tank in series model, the model simulated and experimental curve comparison is shown in the Fig. 5(a)-8. Subsequently, modified tank in series model i.e. gamma distribution model was used to simulate the experimental RTD curve and found to be fitting very well to the experimental curve [Fig. 5(a)-9].

5(a).5.Results and Discussion

5(a).5.1.Uniformity in fluidization

In order to investigate the uniformity of fluidization across the diameter of the system, the tracer concentrations was recorded at four different heights i.e. 325mm, 650mm, 975 mm, 2000 mm. At a height of 325 mm, only one detector (D3) was used whereas at other heights two detector (D4D5D11, D6D7 and D8D9), mounted diametrically opposite to each other were used.

The detection geometry at all the seven locations (D3-D9 and D11) was maintained identical and all the detectors were calibrated to give identical responses. The comparison of intensity of tracer concentration provides information about radial distribution or uniformity of fluidization across the diameter. If the two curves recorded in a plane, superimpose on each other, then the radial distribution is estimated to be good.

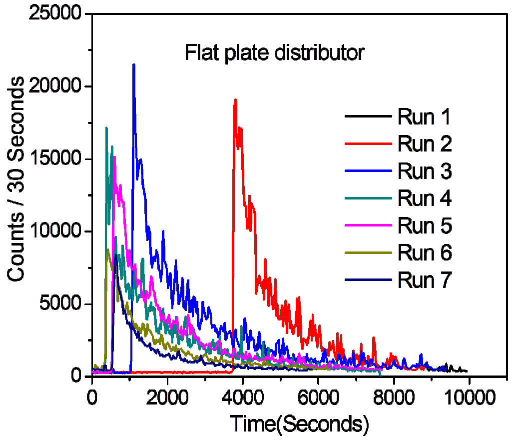

Fig.5(a)-4.Untreated tracer concentration curves recorded by detector D2 (With flat plate distributor)

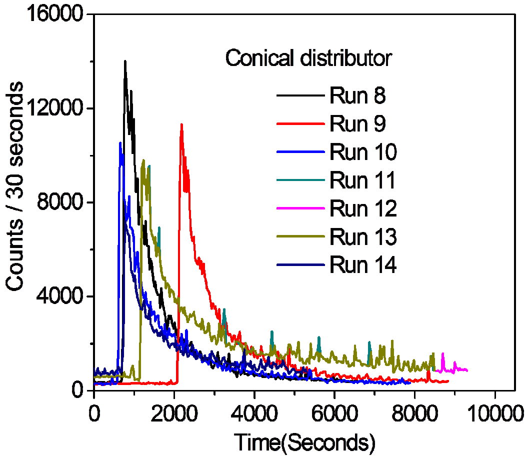

Fig.5(a)-5. Untreated tracer concentration curves recorded by detector D2 (With conical distributor)

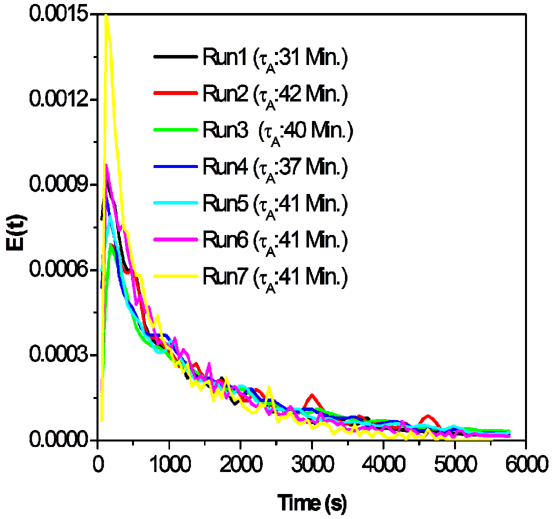

Fig. 5(a)-6. Treated RTD curves recorded by detector D2 (With flat plate distributor)

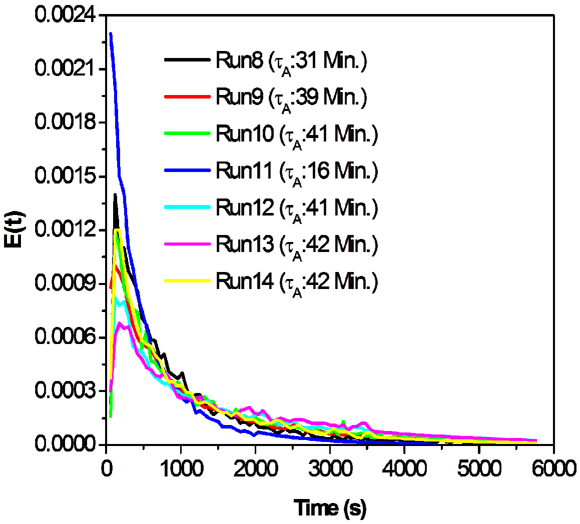

Fig.5 (a)-7. Treated RTD curves recorded by detector D2 (With conical distributor)

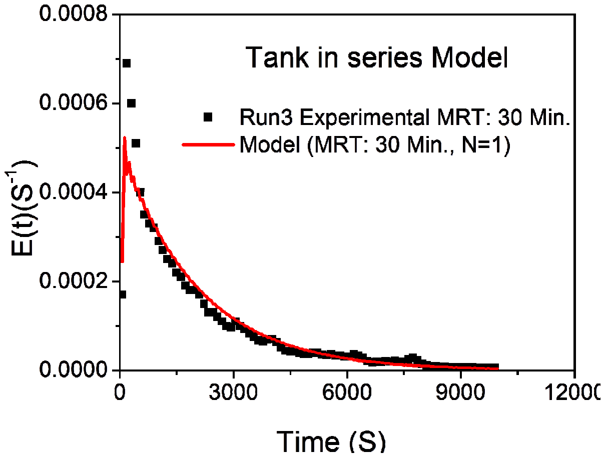

Fig. 5(a)-8: Comparison of tank in series model and experimentally measured RTD

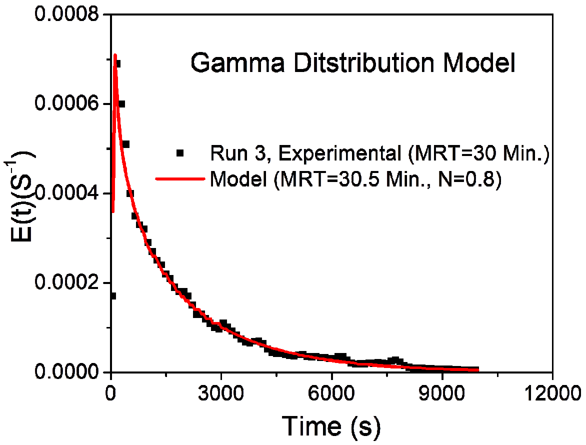

Fig. 5(a)-9: Comparison of gamma distribution model and experimentally measured RTD

Any deviation in two curves will indicate poor radial distribution of solids across the bed. The treated tracer concentration curves recorded by detector pairs i.e. D4D5, D6D7 and D8D9D11 are shown in Fig.5(a)-10 and Fig.5(a)-11. The radial orientation of the detectors is shown in Fig. 5(a)-1. The comparison of curves recorded by three different pairs of detectors mounted at three different axial locations shows that the tracer concentration curves superimpose on each other indicating uniform solid concentration across the planes. It has been observed that the intensity of recorded tracer concentration curves at three different axial locations is different. At the lower axial location (D4D5D11), the intensity is much higher than the middle (D6D7) and top (D8D9) axial locations [Fig.5(a)-10 and Fig. 5(a)-11]. This is because the solid holdup (tracer concentration) is much higher at the bottom level than the two other axial locations. This indicates that at bottom axial location (D4D5D11), the bed remains in bubbling fluidized state, whereas at middle axial position, the condition of partial fluidization occurs. The low intensity of tracer concentration curves recorded by D8D9 indicate very low solid holdup that at that axial plane and is due to fines being entrained to the cyclone. At the lower axial location (D4D5D11), the intensity is much higher than the middle (D6D7) and top (D8D9) axial locations [Fig.5(a)-10 and Fig. 5(a)11]. This is because the solid holdup (tracer concentration) is much higher at the bottom level than the two other axial locations. This indicates that at bottom axial location (D4D5D11), the bed remains in bubbling fluidized state, whereas at middle axial position, the condition of partial fluidization occurs. The low intensity of tracer concentration curves recorded by D8D9 indicate very low solid holdup that at that axial plane and is due to fines being entrained to the cyclone.

5(a).5.2. Mean residence time, dead volume and flow pattern of bulk flow

It is required operate the system with a certain theoretical mean residence time (τ) of the particles within the system and thus accordingly bed weight and coal feed rates adjusted.

Table 5(a)-2. Operating parameters and analysis of RTD measured by detector D2 at the bottom exit of the fluidized bed system

Run No.	Type of distributor	Bed height (mm)	Initial bed weight (kg)	Final bed weight (kg)	Coal feed rate (kg/h)	Air velocity (m/s)	Bottom extraction rate(kg/h)	Cyclone extraction rate (kg/h)	PSD of Tracer (mm)	τ (Min.)	$\bar{t}$(Min.)	% DV	Model parameters	
													$\bar{t}_m$	N
1	Flat plate	1D	200	260	517	0.72	457	30	0.5-4	27	23.5	13	20	0.86
2	Flat plate	1D	180	190	260	0.72	227	28	0.5-4	43	27	37	28	0.84
3	Flat plate	1D	180	180	260	0.80	233	27	0.5-4	41	34	17	33.5	0.80
4	Flat plate	1.5D	260	210	380	0.79	383	30	0.5-4	37	28	24	26	0.80
5	Flat plate	1D	180	200	260	0.78	237	20	1-2	44	27	39	26	0.83
6	Flat plate	1D	180	200	260	0.78	237	20	2-3	44	23	48	22.7	0.73
7	Flat plate	1D	180	200	260	0.79	237	20	0-1(50%)+ 4 (50%)	44	16	64	15.6	0.60
8	Conical	1D	220	120	328	0.75	358	20	0.5-4	31	15	52	15.4	0.70
9	Conical	1D	220	200	328	0.82	313	25	0.5-4	38	20	47	17.7	0.86
10	Conical	1.5D	300	340	460	0.80	412	30	0.5-4	42	21.5	49	20	0.65
11	Conical	1D	220	120	655	0.76	548	40	0.5-4	15	10	33	8	0.98
12	Conical	1D	220	250	328	0.80	307	14	1-2	43	29	33	27	0.74
13	Conical	1D	220	250	328	0.80	307	14	2-3	43	30	30	29.6	0.82
14	Conical	1D	220	240	328	0.80	302	17	0-1(50%)+ 4 (50%	42	19	55	18	0.70

Table 5(a)-3: Results of mathematical modeling of tracer distribution curve measured by detector D10 mounted at top exit of the system

Run No.	Type of distributor	Bed height (mm)	Initial bed weight (kg)	Final bed weight (kg)	Coal flow rate (kg/h)	Air velocity (m/s)	Bottom extraction rate(kg/h)	Cyclone extraction rate (kg/h)	PSD of Tracer (mm)	$\bar{t}_{Expt.}$ (Min.)	Model parameters	
											$\bar{t}_m$	N
1	Flat plate	1D	200	260	517	0.72	457	30	0.5-4	58	55	0.86
2	Flat plate	1D	180	190	260	0.72	227	28	0.5-4	63	59	0.84
3	Flat plate	1D	180	180	260	0.80	233	27	0.5-4	45	40	0.95
4	Flat plate	1.5D	260	210	380	0.79	383	30	0.5-4	-	-	-
5	Flat plate	1D	180	200	260	0.78	237	20	1-2	29	29	0.85
6	Flat plate	1D	180	200	260	0.78	237	20	2-3	36	35	0.99
7	Flat plate	1D	180	200	260	0.79	237	20	0-1 (50%) + 4 (50%)	35	33	0.97
8	Conical	1D	220	120	328	0.75	358	20	0.5-4	46	46	0.96
9	Conical	1D	220	200	328	0.82	313	25	0.5-4	55	51	0.90
10	Conical	1.5D	300	340	460	0.80	412	30	0.5-4	45	55	0.86
11	Conical	1D	220	120	655	0.76	548	40	0.5-4	39	38	0.98
12	Conical	1D	220	250	328	0.80	307	14	1-2	58	58	0.99
13	Conical	1D	220	250	328	0.80	307	14	2-3	56	56	1.0
14	Conical	1D	220	240	328	0.80	302	17	0-1 (50%) + 4 (50%)	41	39	0.94

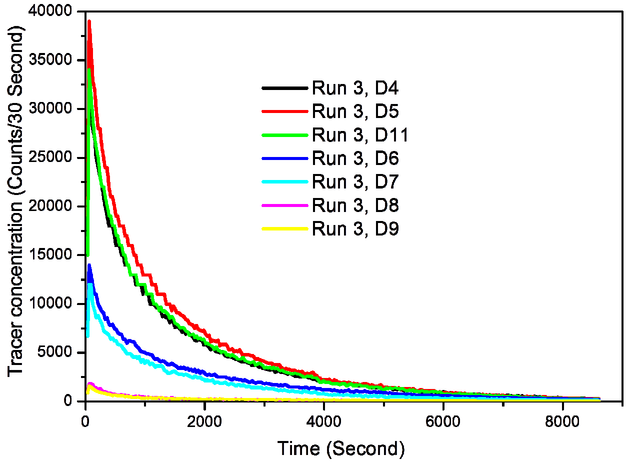

Fig.5(a)-10. Comparison of tracer concentration curves recorded at different axial positions in the fluidizer with flat plate distributor

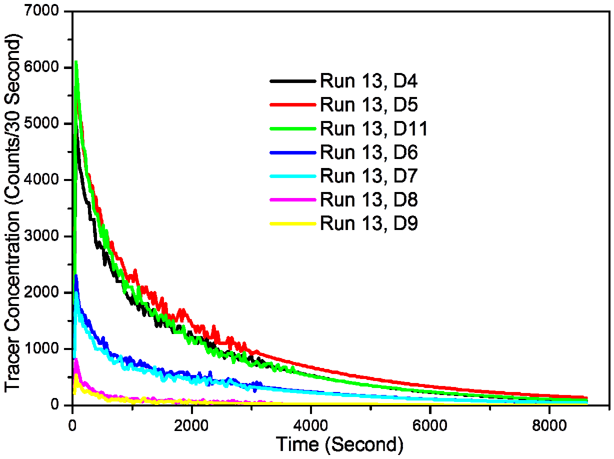

Fig.5(a)-11. Comparison of tracer concentration curves recorded at different axial positions in the fluidizer with conical distributor

The comparison of theoretical and experimentally determined MRTs shows that there is significant difference between the two indicating presence of dead volume inside the fluidized bed. This implies that coal particles are not homogeneously distributed inside the bed during fluidization. Based on the comparison of the MRTs, the percentage of dead volume (% DV) within the fluidized bed is estimated and the values are given in Table **5(a)-2.** It has been observed that for flat plate distributor with PSD of 0.5-4 mm, the dead volume values ranged from 10-36%, whereas for conical distributor with PSD 0.5-4 mm, the values of dead volume ranged from 30-55% (IAEA, 1990; 2004B). This indicates that the percentage of dead volume within the fluidizer is lesser with flat plate distributor than the conical distributor. It has also been observed that with other tracer particle sizes (1-2mm, 2-3mm and 0-1mm (50%) +4 mm (50%)), the extent of dead volume is higher in flat plate distributor than the conical distributor.At a constant bed height (1D) and particle size distribution (0.5-4 mm), it has been observed that MRT is higher at higher fluidization velocity for both the distributors. There is no significant change in MRT with increase in bed height from 1D to 1.5D in case of both the distributors (Fig. 5(a)-12, Fig.5(a)-13). In order to investigate effect of particle size distribution (PSD) on dynamics of coal particles, experiments were required to be conducted with different particle size distributions other than the normal PSD (0.5-4 mm).

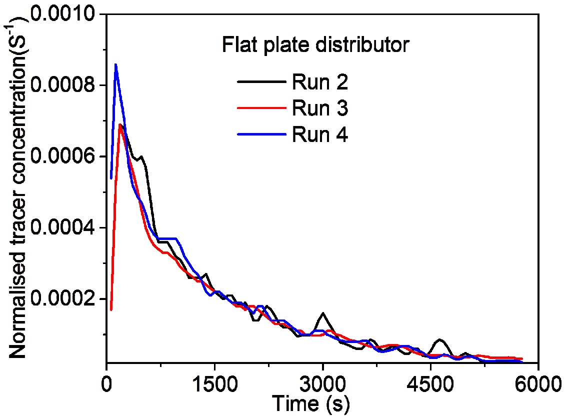

Fig.5(a)-12. Effect of bed height on RTD (Flat distributor)

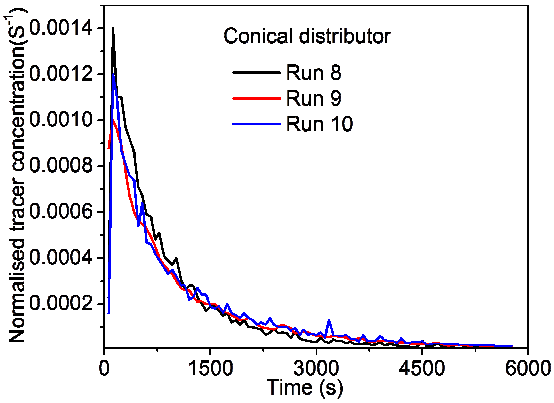

Fig.5(a)-13. Effect of bed height on RTD (Conical distributor)

But it was not practically feasible to carry out such experiments as the quantity of coal particles of the desired particle sizes distribution was huge. In order to get some information about effect of PSD on dynamics of solids, experiments were carried out with different PSD of tracer. In addition to PSD of 0.5-4 mm, RTD experiments were also carried with other ranges (1-2mm, 2-3 mm and 0-1mm (50%) +4 mm (50%)) of PSD of tracer. In case of flat plate distributor, the MRTs of coal particle extracted from bottom of the system with PSD of tracer 1-2, 2-3, 0-1 (50%) +4 (50%) mm, were estimated to be 27, 23 and 16 minutes, respectively (Fig.5(a)-12). Whereas, with conical distributor, the MRTs were determined to be 29, 30, 19 minutes with tracer PSD of 1-2, 2-3, 0-1 (50%) +4 (50%) mm, respectively

(Fig.5(a)-13). It is observed that the courser particles come out early through the bottom extractor and as the PSD decreases, MRT increases.

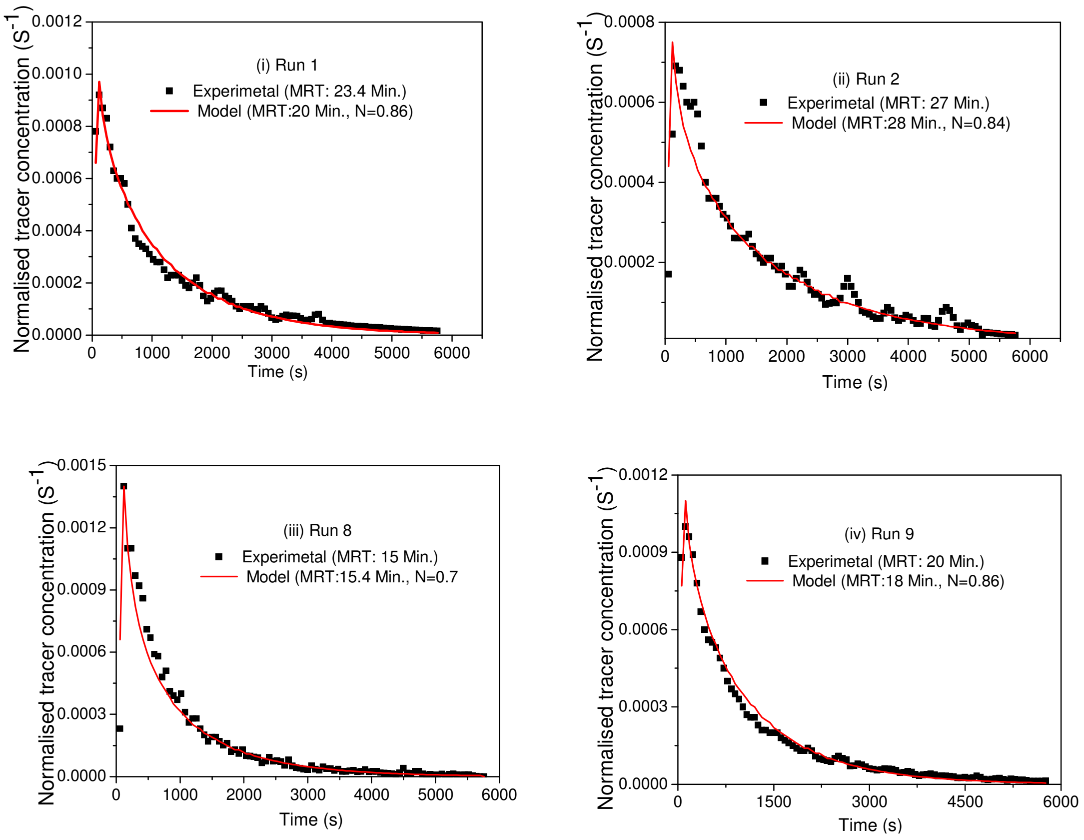

Fig.5(a)-14: Comparison of experimental and model simulated curves of bulk flow of coal particles exiting bottom of the reactor (i, ii) Flat plate distributor (iii, iv) Conical distributor

The RTD curves measured by detector D2 mounted at extractor bottom were analyzed using modified tank-in-series model as described above and model parameters i.e. model predicted MRT ($\bar{t}_m$) and Tank Number (N) were obtained. The model is found to be fitting very well to the experimental RTD curve as shown in the Fig 5(a)-14. The values of these parameters are given in Table 5(a)-1. It has been observed that the model obtained MRTs (($\bar{\mathrm{t}}_{\mathrm{m}}$) are in good agreement with the experimentally determined MRTs ($\bar{t}$). The value of Tank number (N) obtained in model simulation at different operating conditions ranges from 0.6-0.98 indicating bypassing of a fraction of the bulk flow. This implies that a fraction of the particles do not participate in mixing and spend minimum time within the system. It is observed that for flat plate distributor with PSD 0.5-4 mm, the values of the N ranges from 0.8-0.86, whereas for conical distributor, the values of N with PSD 0.5-4 range from 0.7-0.86. This implies that bypassing is more with the conical distributor than the flat plate distributor. However, with PSD of 1-2mm, 2-3 mm and 0-1mm (50%) +4 mm (50%), almost identical values of N have been obtained in case of both the type of distributors.

5(a).5.3.Mean residence time and flow pattern of fine coal particles:

During fluidization, a fraction of the fine particles is entrained with air and get separated in the cyclone. These fines are collected at the bottom of the cyclone, whereas, the remaining fraction of the fines flow out of the system from bottom along with the bulk flow. The knowledge of residence time and flow characteristic of fines is also important for evaluation of performance of a fluidized bed gasifier, therefore, it was important to measure RTD of fines entrained along with air and characterize their flow behavior. The detector D10 was mounted at the exit of the free board to measure RTD of fines (Fig.5(a)-15 – Fig.5(a)-19) and measured MRTs are given in Table 5(a)-3.

It is observed that at the same operating conditions, the MRTs of fines are greater than the MRTs of the bulk flow being extracted from bottom of the system (Table 5(a)-2,

Table 5(a)-3). It was not possible to estimate theoretical MRT of fines inside the system because of non-availability of values of exact weight of fines and their feed rate. Two tracer experiments were carried out with PSD of 0-1mm (50%)+4mm (50%) and 1-2 mm for each distributor and It was observed that with both the PSD, MRT of fines is more in case of conical type distributor (Run5, Run12 and Run7, Run14).

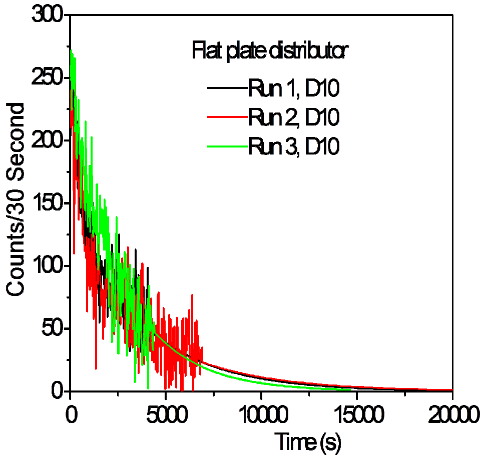

Fig.5(a)-15.Tracer distribution curves of fines recorded by detector D 10

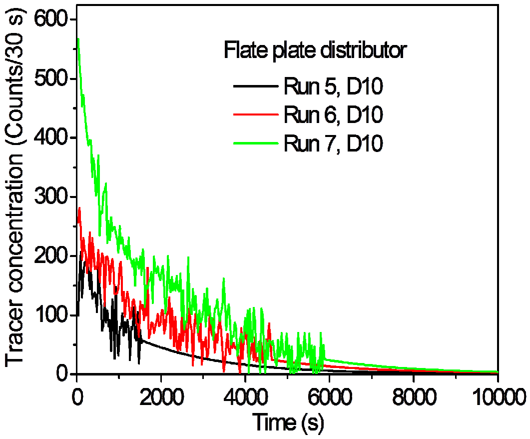

Fig.5(a)-16. Tracer distribution curves of fines recorded by detector D10 with different PSD of tracer D10

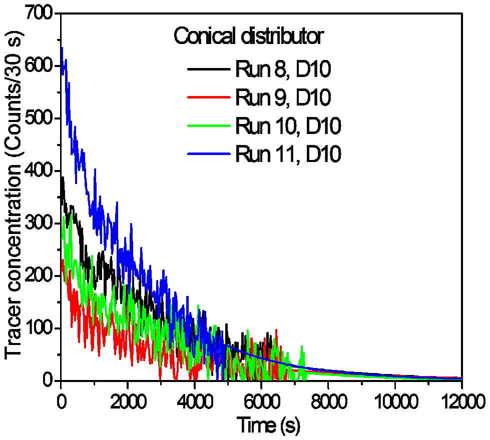

Fig.5(a)17.Tracer distribution curves of fines recorded by detector D 10 with PSD 0.4-5 mm

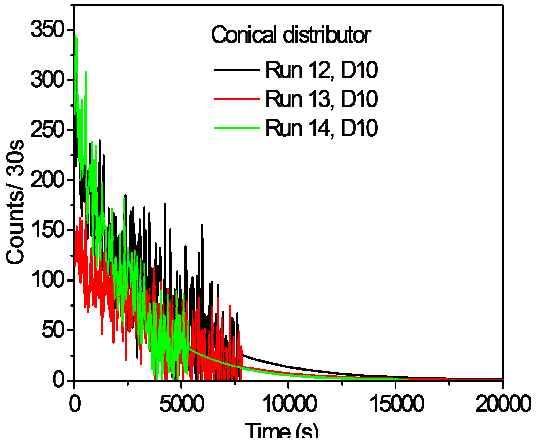

Fig.5(a)-18.Tracer distribution curves of fines recorded by detector D 10 with different tracer PSD

The RTD curves of fines measured by detector D10 were also analysed using the above-described tank-in-series model. The experimental RTD was found to be fitting well to the model simulated data as few representative plots are shown in the Fig.5(a)-20. The results of the model simulation are presented in Table 5(a)-3. The values of tank number obtained at different operating condition ranged from 0.84-1. In most of the runs, the value of N has been close to unity indicating well mixed flow behaviour of fines flowing out from top of the system in case of both the distributors.

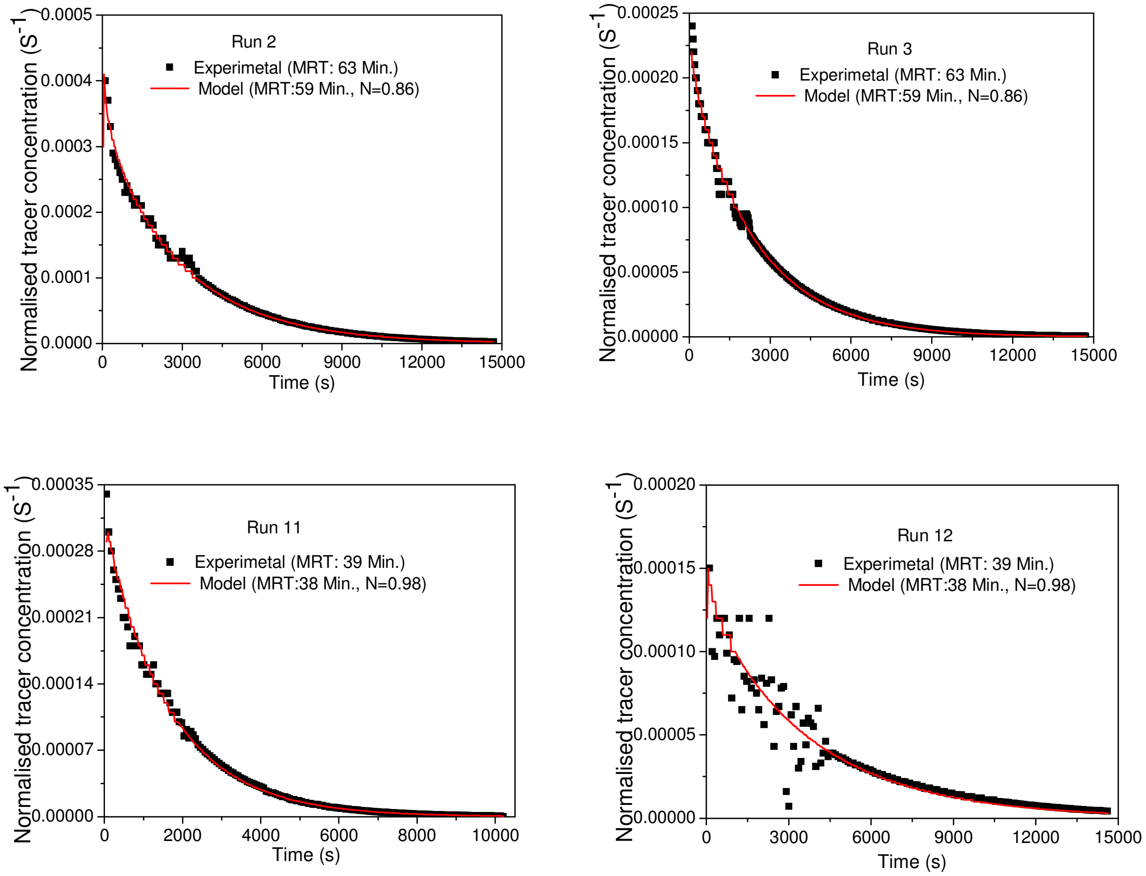

Fig.5(a)-19: Comparison of experimental and model simulated curves of fine coal particles exiting bottom of the reactor (i, ii) Flat plate distributor (iii, iv) Conical distributor

5(a).5. Conclusions

Form this study, following conclusions were drawn.

- The mean residence times of bulk flow flowing out from the bottom of the system have been determined from the measured RTD curves and compared with actual theoretical MRTs. The experimentally determined MRTs with flat plate distributor ranged from 16-34 minutes at different operating and tracer particle size distributions. Whereas MRTs with conical distributor ranged from 10-30 minutes. It has been observed that measured residence times are lesser that the actual theoretical MRTs. The comparison of MRTs indicated presence of dead volume within the fluidized bed and was estimated to be about 15-61% at different operating conditions and process conditions. This indicates that a fraction of the radiotracer bypasses the system and exit without mixing within the bulk flow. This means channeling or bypassing of a fraction of the bulk flow. The amount of dead volume is lesser with flat plate distributor as compared to that of conical distributor.
- The mean residence of fines flowing out from top of the system was also determined from the measured tracer concentration curve and were found to be 29-63 minutes with flat plate distributor and 39-58 minutes with conical distributor at different operating and process conditions. The MRTs of fines with the system is more than the MRTs of bulk flow (coarser particles).
- Tank-in-series model was used to simulate the measured RTD data and comparison of the model simulated RTD curves fitted very well to the experimentally measured curves. This indicates that tank-in series model describes the flow of solids in the

fluidized bed system. After simulation, the values of model parameter (N) obtained indicated bypassing of a fraction of the bulk flow as the values were found to be less than unity.

- Almost similar results were obtained in analysis of RTD curves measured within the bed using detector D3 and at the bottom of the extractor using detector D2 at 1D bed height.
- The coarser particles come out early through the bottom extractor and as the MRT increases with decrease in PSD.
- The analysis of RTD experiments carried out with two different air distributors indicated that flat plate distributor is marginally better that the conical distributor as the amount of dead volume and extent of bypassing appears to be higher with conical distributor. This implies that mixing is better with flat plate distributor.

Chapter 5(b)

Flow Dynamics of Coal Particles in Pilot-Scale Fluidized Bed Gasifier using Radiotracer Particles

---

5(b).1. Introduction:

In the previous study, the efficacy of fluidization of two different air distributors in cold flow condition was measured in cold flow condition and quantified using the radiotracer techniques. It was found that the flat plate bubble cap distributor is having better performance than the conical distributor. However, the study was not carried out under the real condition such as high temperature and pressure in a fluidized bed gasifier.

In the literature, the RTD study measurement of the solid particles in the small scale laboratory fluidized bed reactor (FBR) is reviewed by Berruti et al., 1995 and Harris et al. 2002. In these two papers, it is reported that different authors have used different tracers such as chemical, magnetic, subliming, colouring, fluorescent tracers (Christopher et al., 2002). In these studies experimental RTD of FBR is aimed to study overall hydrodynamics of the solid particles at different operating conditions and design parameters. As reported by Roy, 2017, the hydrodynamics of the solid phase in FBR is highly complex and scale dependent. Hence, before the implementation of the process at industrial scale, it should be studied at laboratory and pilot scale having conditions as close to the existent fluidized gasifier. The practical means to study the solid phase particles in large scale systems is using radiotracers (Pant et al 2001; IAEA, 2004). The conventional tracers are not suitable for the large scale systems (IAEA, 2008B; Kalga et al., 2012; Roy et al., 2017). The reported studies had been done on large scale FBR for

RTD measurements using radiotracer are summarized in the Table 5(b)-1 (Lin et al., 1999; Pant et al., 2009A; 2014; Rao et al., 2012). In this study major difference compared to previous reported study is type of air and steam distributor used to fluidize the coal particles i.e. flat plate bubble cap distributor.

The key component that decides the quality of the fluidization in the FBR is the air and steam distributor (Pant et al, 2014; Roy et al., 2017). Therefore, it is valuable to study the flow dynamics of the coal particles in the same FBG with flat plate bubble distributor at the gasifying conditions of the FBG. In the present study, the effect of different operating conditions such as bed height, temperature, size of the coal particles on the RTD of solid phase were studied. In addition to the above, a phenomenological model was purposed to visualize the flow behaviour of the coarse coal particles and to estimate the degree of bypass of coal particles if there exits any in the system.

5(b).2. Fluidized Bed Gasifier System:

The pilot scale fluidized bed gasifer (FBG) consists of various subsystems such as a fluidized bed, freeboard, cyclone, feeding section, air-steam supply system and ash extraction system. The Fig. 5(b)-1 shows layout of the facility in the present study and Table 5(b)-2, presents the most important parameters of gasifier under the study. The detail of the plant is described in the previous publication of Pant and et al. 2009. The major difference between of the reported and present study is the type of the distributor. In the previous study conical distributor was used for the fluidization and gasification, where as in the present study flat plate bubble cap distributor is used to carry out the fluidization and gasification process. The air and steam used as gasifying agent and coal particle size distribution given in Table 5(b)-3 used as radiotracer.

5(b).3.Radiotracer experiment:

Preparation of the radiotracer was done using as discribed in the chapter 5(a) section 5(a).3. A series of thirteen experiments were carried out at different operating and process conditions given in Table 5(b)-5 and 5(b)-6. About 25 gm of coal particles labeled with Gold-198 radioisotope was used as a radiotracer. About 37 MBq activity was used in each experiment. The radiotracer was instantaneously injected into the feed pipe using a specially fabricated injection arrangement and monitored at different locations in the FBG using lead collimated scintillation detectors as shown in Fig.5(b)-1. All the detectors were connected to a computer controlled multi-channel data acquisition system (CC-MIDAS) set to record tracer concentration data at an interval of every 30 seconds. The tracer concentration data acquired was a function of time was saved as an ASCII file in the computer for further analysis. The radiotracer concentration curves recorded at two locations were shown in Fig 5(b)-2(i) and Fig 5(b)-3(i).

5(b).4.Data analysis and model simulation*:*

The experimentally measured data was treated for the basic correction mentioned in the section of data treatment and analysis in chapter 2. The treated radiotracer curves are shown in the Fig 5(b)-2(ii) and Fig 5(b)-3(ii). Experimentally measured residence time distribution curves of the coal particles is simulated by appropriate flow model to characterize the non-ideal flow pattern present in the Fluidized bed gasification (FBG) reactor.

In FBG wide range of coal particles are present in the system. Typically, the bulk of the coal particles come out from the bottom of the FBG, whereas the extremely fine particles exists the FBG from the top of the bed. To describe the overall flow behavior of the coal particles inside the FBG, it is important to simulate the RTD curves observed at top and bottom of reactor. In literature, to describe the non-ideality present in the flow of the coal particles, axial dispersion model (ADM) and tank in series model (TISM) are used extensively (IAEA, 2004A; 2008A). In the FBG, the designed flow of the coal particles is as perfect mixer. Therefore, ADM will not be sufficient to describe the flow of coal particles inside the FBG. A tank in series model will be most suitable to describe the flow of coal particle in the system as compared to the former model for the both fine and bulk particles (Lin et al., 1999). The simulation of the experimental RTD data was done using DTSpro Software (PROPEPI/SYSNTEC, 2000). This software allows construction of basic and complex network of the elementary models such as plug flow, ADM, TISM, perfect mixing in series with exchange and perfect mixing cells in series exchanging with a dead zone and optimization of the parameters (Caludel et al., 2003). In the present study, first model is tried to simulate the bulk flow of the coal particles coming out from the bottom of the system using TISM. The experimentally observed and treated RTD curves for bottom of the reactor is shown in Fig.5(b)-2(ii).

Table 5(b)-1: Comparison of the present study with reported RTD studies carried out in the FBR using radiotracers

Authors	**System Dimension**	**Operating Conditions**		**Fluid Distributor Type**	**Flow model used for simulation**	**Major Findings of the Study**
		P (Bar)	**T (^{o}C)**			
Lin et al. (1999)	H: 22.8m, B: 0.2m, L: 4m	92	505	Not mentioned	Tank in series	• Recirculation rates of solid particles in the stand pipe of boiler were estimated. • Significant Reduction in the recirculation rate was observed as the load of boiler decreases. • The experimental model was found to suitable for the representation of the flow of particles in standpipe and boiler
Pant et al. (2009A)	ID_F: 200mm ID_{FB}: 250mm H_{FBR}: 2m	1.1-1.2	1000 And Ambient	Conical	Modified Tank in series	• Au-198 and La-140 adsorbed over the coal particles are found to be suitable for the tracing of the solid phase • RTD of the coarser particle indicated that a small fraction of coal particle bypassing without adequate mixing gasification in FBG. • Amount of bypassing is grater at the ambient conditions as compared to the hot condition. • It is not possible to quantify the amount of the bypassing using the model
Pant et al. (2014)	ID_F: 650mm ID_{FB}: 880mm H_{FBR}: 2.5m	1	Ambient	Conical	Modified Tank in series	• Bypassing of the coarser coal particles from the bottom of the reactor was found • Significant amount of the dead volume is present in the system • Proposed flow model is describing the flow behavior of the coal particles in the gasifier.
Present Study	ID_F: 200mm ID_{FB}: 250mm H_{FBR}: 2m	3	1000-800 and Ambient	Flat plate with bubble caps	Phenomenological	• Presented in the Paper

H: Height of the reactor, L: Length of the reactor, B: Breath of the reactor, ID_F: Internal diameter of the fluidized bed section, ID_{FB}: Internal diameter of the free board section, H_{FBR}: Height of the reactor

Table 5(b)-2: System parameters of the fluidized bed gasifier

Parameters	Value
Fluidizer inner diameter	0.20m
Fluidizer height	1.0m
Free board inner diameter	0.25m
Free board height	1.5m
Bed material	Coal
Gasification agent	Air + Steam
Distributor	Bubble cap flat plate
Operating temperature	1050°C (Max.)
Operating pressure	3 Atm.(Max.)
Regime of fluidization	Bubbling

Table 5(b)-3: Coal particle size distribution

Particle size range (mm)	% of weight
3-4 (Coarse)	17
2-3(Coarse)	40
1-2(Coarse)	33
0.5-1 (Fine)	10

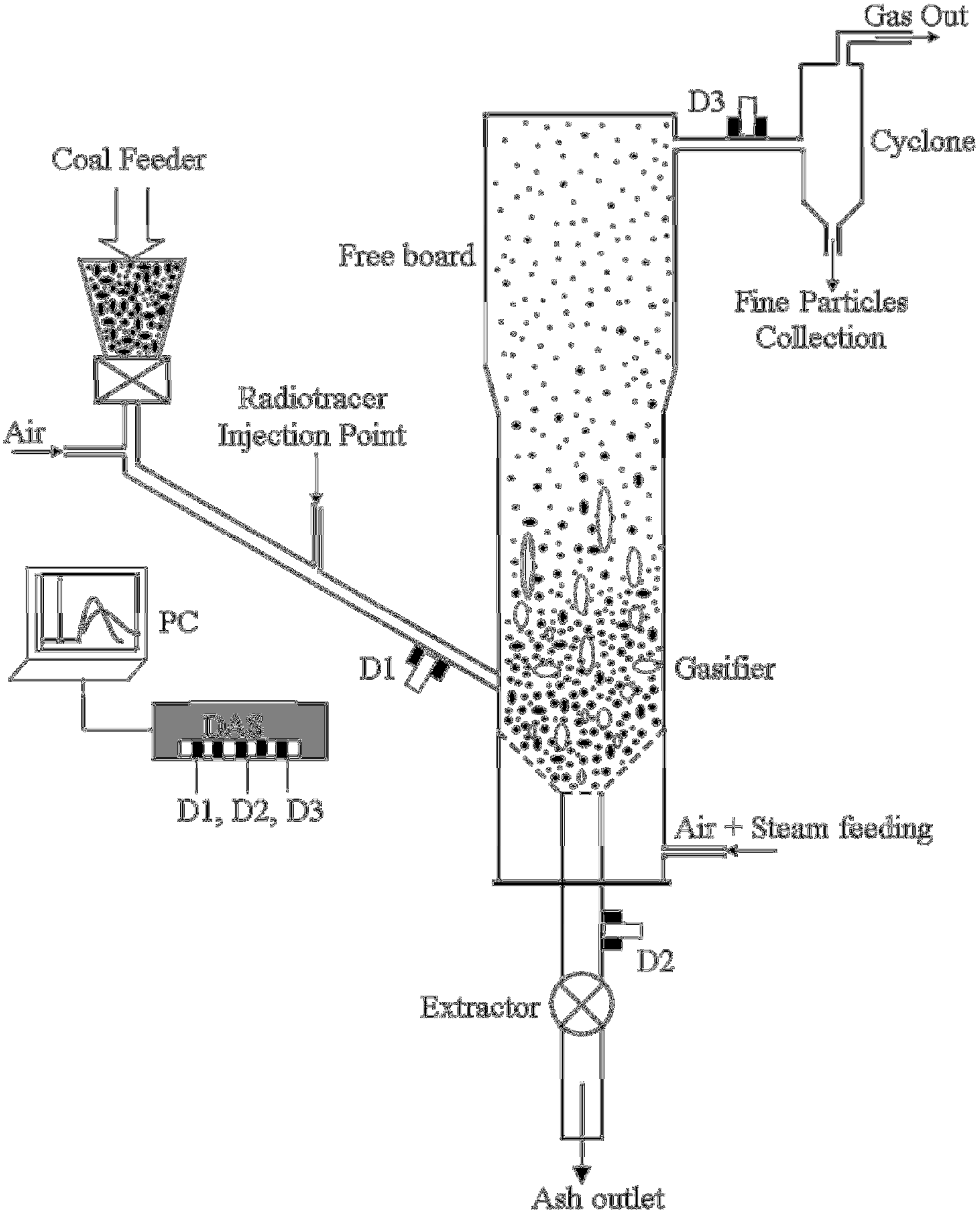

Fig. 5(b)-1. Schematic diagram of FBG and experimental setup

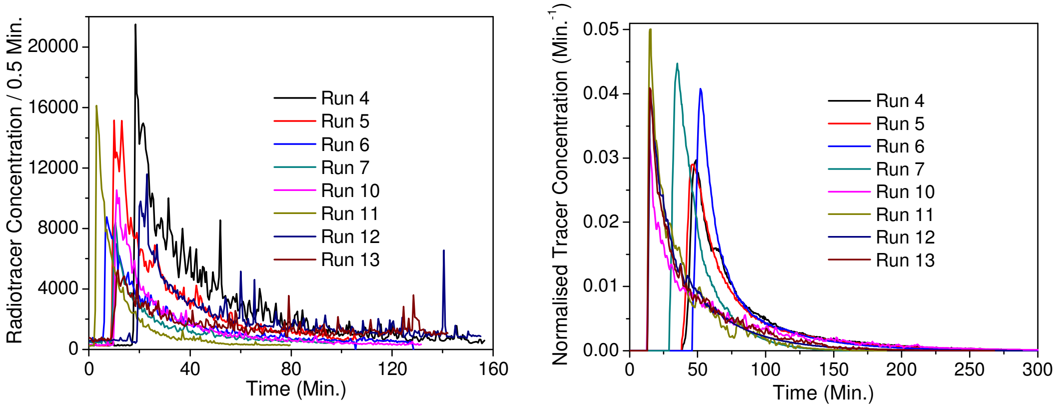

Fig 5(b)-2. (i) Untreated (ii) Treated , radiotracer concentration curve of the bulk of the coal particle

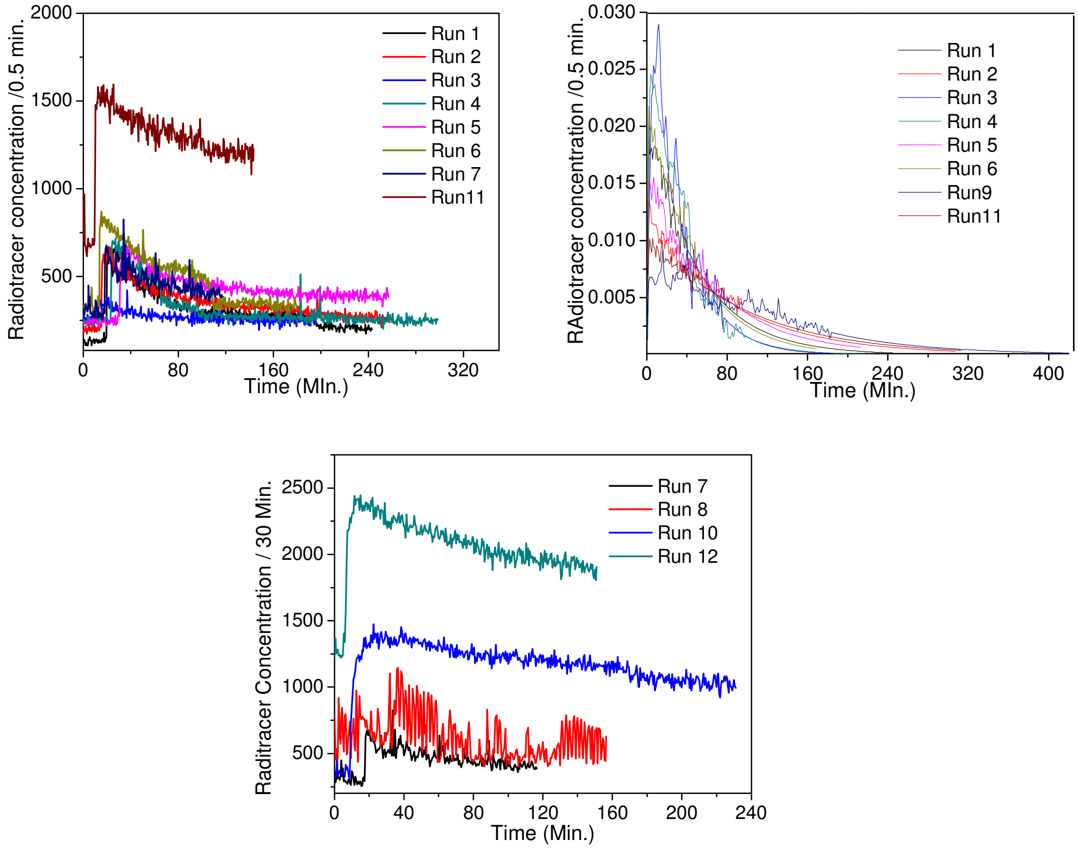

Fig 5(b)-3. (i) Untreated (ii) Treated, radiotracer concentration curve of the bulk of the coal particles (iii) untreatable data

It can be observed from the graphs that the breakthrough or first observance of the tracer starts after time delay. This delay in time suggests that a plug flow component in series should be attached before the TISM to simulate the data. The block diagram of plug flow in series combined with TISM and its parameters is given in Table 5(b)-4. Several attempts were made to simulate the experimental RTD curve. The comparison of the experimental RTD and model simulated curve corresponding to the minimum value of the errors is shown in the Fig.5 (b)-4(i). The combined model used to simulate the experimental RTD data should fit reasonably well to the peak and tail portion of the experimental curve. From the Fig.5 (b)-4(i), it can be concluded that this model is fitting reasonably well to the tail portion, whereas the fitting of the peak portions is not good enough. This fact suggests that a different model should be selected for the flow representation of the coal particles inside the FBG.

As reported in the literature that modified TISM i.e. gamma distribution model can be used to simulate the experimental RTD curve in the situation, where the TISM is not able to fit (Pant et al., 2009A, 2014; Rao et al., 2012; Roy et al., 2017). Therefore, in the second attempt to simulate the experimental RTD curve of the coal particles is done using combination of plug flow component in the series with the gamma distribution model. The block diagram of model and its parameters is given in Table 5(b)-4. Similar to the TISM, several attempts were tried to simulate the experimental RTD curve. The curve representing minimum value of the error and best fit is shown in Fig.5(b)-4(ii). It can be clearly observable from the Fig.5 (b)-4(ii), neither the peak and nor the tail portion of the curve fits to the experimental RTD curve. Therefore, it is concluded that this model is also not suitable for describing the flow of coal particles inside the FBG in the present study.

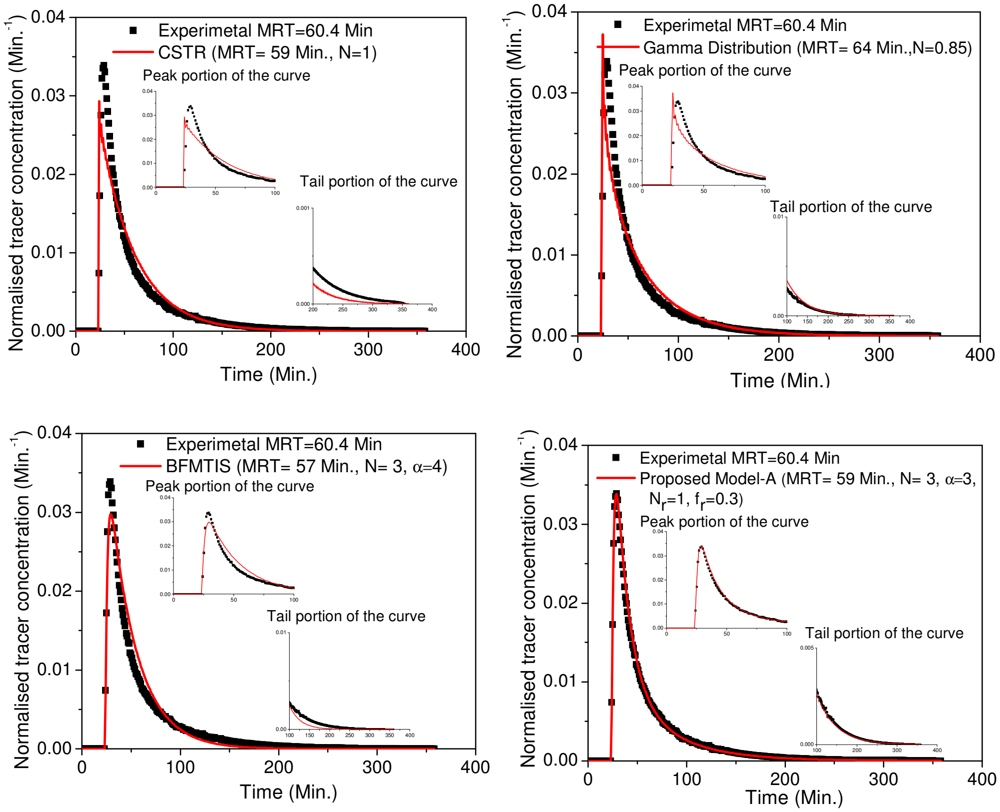

Fig.5(b)-4. Comparison of the different models used to simulate the experimental RTD curves

In the quest to describe the flow behavior of the coal particles inside the FBG, a third model was tired. In the operation of the fluidized bed reactor, the coal particles are fed in to the bed and thereafter the fluid is passed from the bottom of the column through a distributor. After, a certain velocity of the fluid, the coal particles experience a drag force by the fluid is enough to lift the particles and particles move in the bed along with fluid particles. The particles are lifted upward by the drag force in the bed due to the fluid upward movement. However, the gravitational force is always acts downwards to the particles, which pulls them back to the bed. These two forces determine the nature of the flow of coal particles in the FBG. As the particle height in the bed increases the gravitational force becomes dominant and particles comes into the bed. If drag force is dominant, the particles moves in upward direction. Due to these two forces the particles are constantly in to and fro motion in the FBR. The backflow mixed tank in series model (BFMTISM) is suitable to depict the above situation (Utgikar, 2009). Hence, the plug flow combined with BFMTISM is used to simulate experimental RTD curves of the FBG and the block diagram of the model is shown in Fig.5 (b)-3. The best fit corresponding to the minimum error using this model is shown in the Fig.5 (b)- 4(iii). From the Fig.5 (b)- 4(iii) clearly indicates that the peak portion of curve gives the reasonable enough fit, however the tail portion does not fits well. Nonetheless, this model seems to be close enough to represent the physical phenomenon occurring in the FBG.

Lastly, the minor modification in the above model should be enough to describe the flow of the coal particles. As reported in the literature, there exists solid particles internal recirculation inside the FBG (Berutti et al., 1988; Dagugupati et al., 2010; Roy et al, 2017). Therefore, an internal recirculation leg was attached to the above model. The modified model (Proposed model-A) block diagram and its model parameter are given in Table 5(b)-4. The best fit of the model simulated curve corresponding to the minimum error is shown in the Fig. 5(b)-4(iv). The both peak and tail portion are now found to be fitting very well to the experimental RTD curve. In addition to this, model represents an overall physical picture of the coal particles flow behavior in the FBG. All the RTD runs carried out in the hot condition were found to be fitting very will to the experimentally measured RTD curves. The various model parameters of the best fit are given in the Table 5(b)-5.

Table 5(b) - 4. Models used to simulate the experimental RTD curves recorded at bottom (Bulk flow) and top outlet (Fine particles) of the FBG

Models used to simulate the bulk flow of the coal particles coming out from bottom of the reactor			
Sr. No.	Model	Block diagram	Model Parameters
1	Tank in series model in series prefixed in series with plug flow component	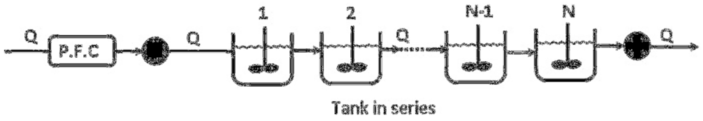	τ_P, τ, N: Interger
2	Gamma Distribution Model prefixed in series with plug flow component	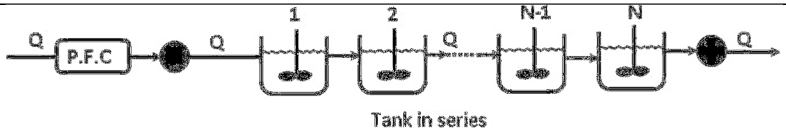	τ_P, τ, N: Rational
3	Back flow mix tank in series model prefixed in series with plug flow component	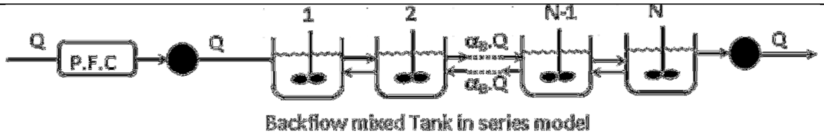	τ_P, τ, N: Integer, α
4	Proposed Model -A	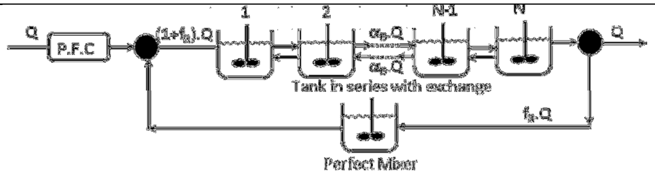	τ_P, τ_T, N_B: Integer, α, f_R, N_R , τ_R
5	Proposed Model-B	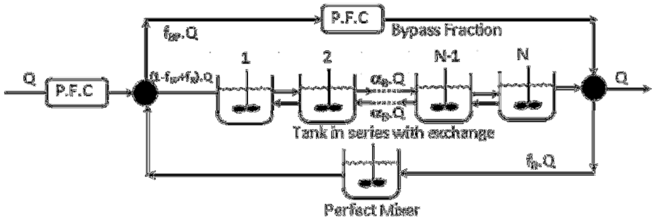	τ_P, τ_T, N_B: Integer, α, f_R, N_R , τ_R, $f_{BP,}$
Models used to simulate the fine particles of the coal particles coming out from bottom of the reactor			
1	Tank in series model	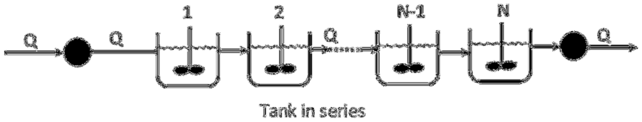	τ, N: Interger

The runs carried out at ambient condition (Run 10 to 13), were not found to be fitting well to the model simulated data by proposed model-A.A sharp peak exiting at the beginning of the RTD curve was the only part in the curve not fitting to the model simulated curve Fig.5 (b)-5(i). It could be due to the bypass of the coal particles as it is present at the beginning of the curve. This bypass fraction needs to be accommodated in the model. The modified model block diagram used for the simulation (Proposed model-B) of the coal particles at ambient condition and its parameters are given in Table 5(b)-5. The comparisons of experimental and model simulated data using this model are shown in Fig.5 (b)-5(ii). The modified model was found to be fitting well to peak and tail portion of the experimental curve as shown in the Fig.5 (b)-5(ii). All the model parameter of simulation using this model is given in the Table 5 (b)-5. The corresponding best fit experimental and model simulated curves for hot condition using proposed model-a are given in Fig. 5(b)-6(i-ix), whereas best fit model simulated curves using proposed model-b is given in Fig. 5(b) 6(ix-xii).

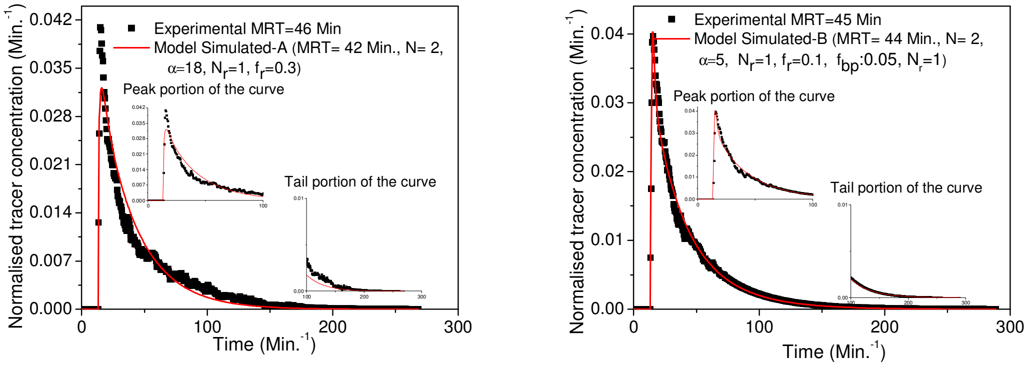

Fig. 5(b)-5. Cold flow bulk particles flow behaviour modelled data with proposed model-A and B respectively

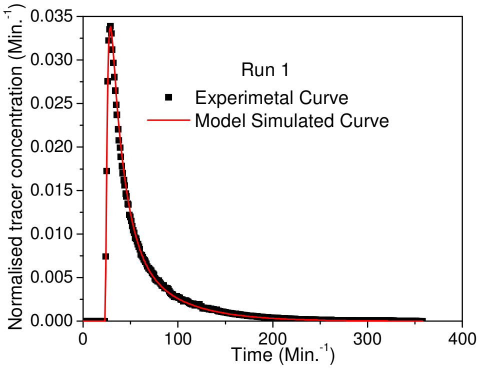
Run 1
Experimetal Curve
Model Simulated Curve
Normalised tracer concentration (Min.$^{-1}$)
0.000
0.005
0.010
0.015
0.020
0.025
0.030
0.035
Time (Min.$^{-1}$)
0
100
200
300
400

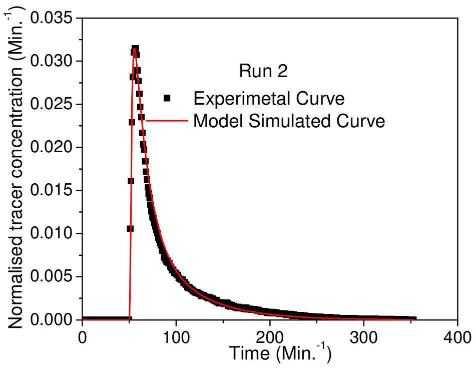
Run 2
Experimetal Curve
Model Simulated Curve
Normalised tracer concentration (Min.$^{-1}$)
0.000
0.005
0.010
0.015
0.020
0.025
0.030
0.035
Time (Min.$^{-1}$)
0
100
200
300
400

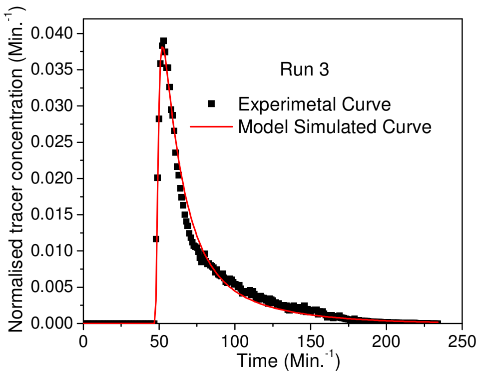
Run 3
Experimetal Curve
Model Simulated Curve
Normalised tracer concentration (Min.$^{-1}$)
0.000
0.005
0.010
0.015
0.020
0.025
0.030
0.035
0.040
Time (Min.$^{-1}$)
0
50
100
150
200
250

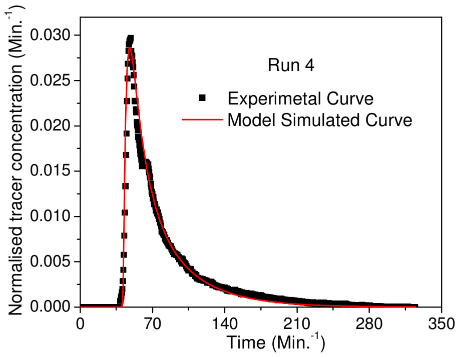
Run 4
Experimetal Curve
Model Simulated Curve
Normalised tracer concentration (Min.$^{-1}$)
0.000
0.005
0.010
0.015
0.020
0.025
0.030
Time (Min.$^{-1}$)
0
70
140
210
280
350

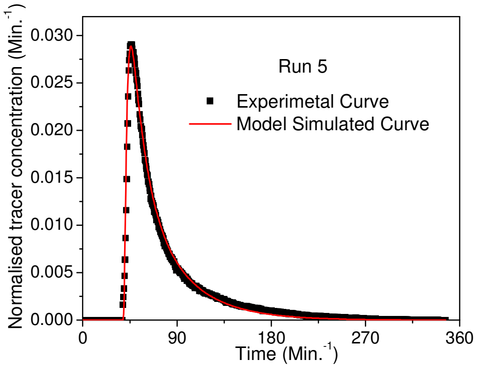
Run 5
Experimetal Curve
Model Simulated Curve
Normalised tracer concentration (Min.$^{-1}$)
0.000
0.005
0.010
0.015
0.020
0.025
0.030
Time (Min.$^{-1}$)
0
90
180
270
360

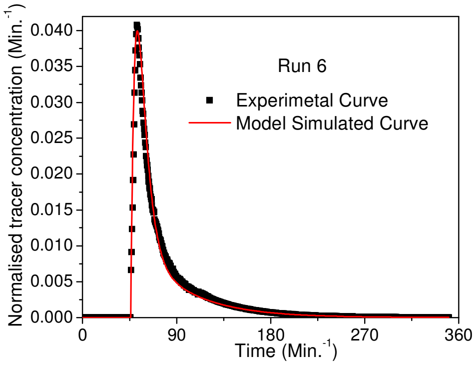
Run 6
Experimetal Curve
Model Simulated Curve
Normalised tracer concentration (Min.$^{-1}$)
0.000
0.005
0.010
0.015
0.020
0.025
0.030
0.035
0.040
Time (Min.$^{-1}$)
0
90
180
270
360

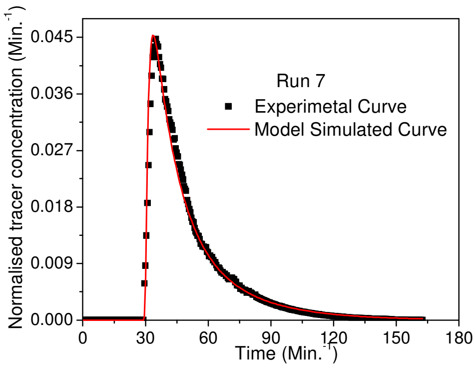
Run 7
Experimetal Curve
Model Simulated Curve
Normalised tracer concentration (Min.$^{-1}$)
0.000
0.009
0.018
0.027
0.036
0.045
Time (Min.$^{-1}$)
0
30
60
90
120
150
180

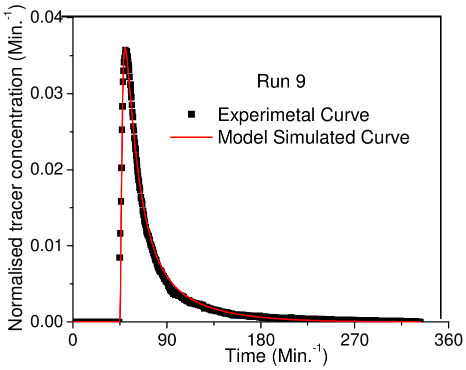
Run 9
Experimetal Curve
Model Simulated Curve
Normalised tracer concentration (Min.$^{-1}$)
0.00
0.01
0.02
0.03
0.04
Time (Min.$^{-1}$)
0
90
180
270
360

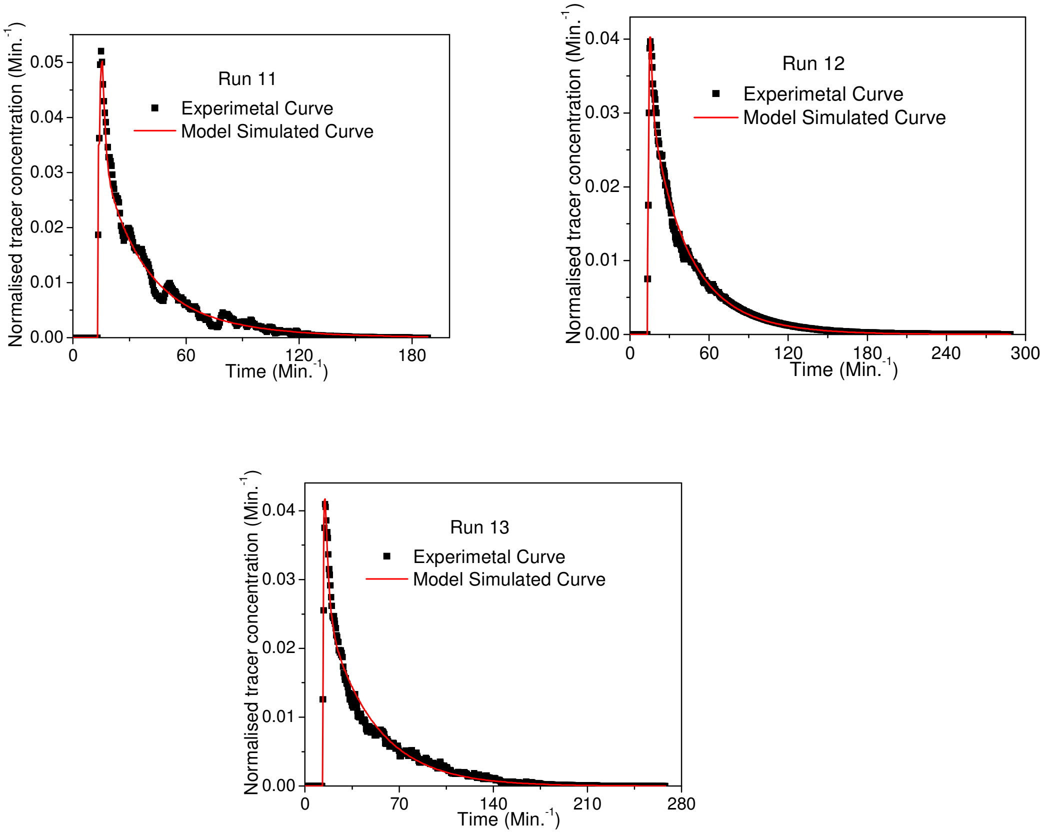

Fig 5(b)-6: Experimental and model simulated curve bulk coal particles coming out at bottom of the FBG hot and cold Condition

The radiotracer concentration curve recorded by the D3 at top of the FBG is shown in Fig. 5(b)-3(ii). It repents the RTD of the fine particles present in the FBG. The experimental RTD curves of the fine particles were simulated using the TISM. The block diagram of the model and its parameters are given in Table 5(b)-4. Moreover, the curves are found to be fitting very well to both hot and cold flow experiments. The comparison of the experimental and model simulated RTD curve of hot and ambient condition runs are shown in the Fig.5(b)-7 (i,ii). It can be clearly seems that the both peak and tail portion of the model simulated curve are found to be fitting very well to the experimental RTD curve. The model parameters of simulation corresponding to the best fit and minimum error are given in Table 5(b)-6. The best fitted experimental and model simulated curves using this model are shown in Fig. 5(b)-8(i-xiii). Therefore, it can be concluded that simple tank in series model is good enough to describe the flow behaviour of the fine particles inside the FBG.

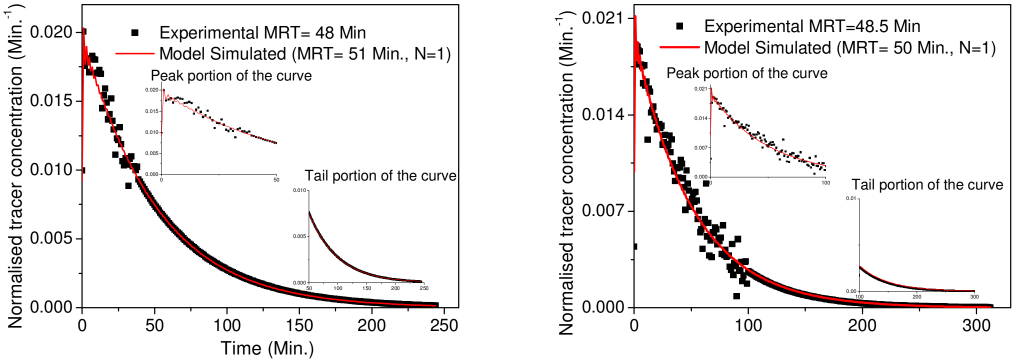

Fig.5(b)-7. Experimental and Model simulated curve of fine particles flow for at hot and cold flow condition

5(b).5. Results and Discussion

In the present study thirteen runs were carried out at different operating conditions using above methodology. The different operating and experimental parameters include variation of air and steam velocity, the bed height of the coal particles, different size of labelled coal particles, operating temperature of the FBG and few runs at ambient conditions.

5(b).5.1. Flow behaviour of the bulk of the coal particles exiting at bottom of the FBG:

The RTD curves observed at the different operating condition are shown in the Fig. 5(b)-2. The mean residence time of the bulk of the coal particles observed at the different conditions is given in the Table 5(b)-5.

Table 5(b)-5. Operating parameters and analysis of RTD measured by detector D2 at the outlet of the system

Run No.	Temp. (^{0} C)	Air+ Steam velocity (m/s)	Bed Height	Bed material Weight (kg)	Coal size (mm)	Feed rate (kg/h)	Extraction rate (kg/h)			Tracer particle size (mm)	$\bar{t}_b$ (Min.)	Model Parameters								
							Bottom ash	Cyclone-1	Cyclone-2			τ_P	τ_B	N_B	α_B	f_R	τ_R	N_R	f_{BP}	τ_T
1	1000	1.75	1D	12	0.5-4	25	4	4.8	2	0.5-4	60.4	23	19.5	3	3	0.3	30	1	--	59
2	1000	1.75	1D	12	0.5-4	25	4	4.8	2	0.5-1	85	50	21	6	7	0.25	30	1	--	88
3	1000	1.75	1D	12	0.5-4	26	4	4.8	2	2-3	67	47	18.5	4	6	0.3	29	1	--	79
4	1000	1.75	1D	12	0.5-4	27	4	4.8	2	3-4	83	38	27	7	5	0.25	20	1	--	79
5	1000	1.5	1D	12	0.5-4	21	5	3.1	2	0.5-4	79	38	24	5	5	0.22	18	1	--	75
6	1000	2	1D	12	0.5-4	29	5	4	2	0.5-4	55	46	17	2	6	0.3	28	1	--	60
7	1000	1.75	1.5D	14	0.5-4	31	5	5	2.5	0.5-4	78	43	20	2	4	0.25	33	1	--	76
8	900	1.75	1D	12	0.5-4	28	5	4	2	0.5-4	51	29	16.5	3	6	0.2	20	1	--	53
9	850	1.75	1D	12	0.5-4	41	12	7	3.5	0.5-4	23	8	9	6	7	0.2	15	1	--	24
10	Ambient	0.65	1D	12	0.5-4	10	10	5	3	0.5-4	55	13	40	1	5	0.15	25	1	0.05	63
11	Ambient	0.65	1D	12	0.5-4	10	10	5	3	0.5-4	39	13	22	1	5	0.15	30	1	0.05	45
12	Ambient	0.65	1D	12	0.5-4	9	9	5	3	0.5-4	45	13	28	2	5	0.1	25	1	0.05	44
13	Ambient	0.65	1D	12	0.5-4	9	9	5	3	0.5-4	48	13	33	2	8	0.1	25	1	0.1	46

D: inner diameter of the fluidizer section, τ_P: time of plug flow component, τ_B:time spent in the bed, N_B: Tank no. of bed, α_B: Back mixing ratio of bed material, f_R: Recycle fraction of flow, $\boldsymbol{\tau_R}$**:** time of recycle, N_R: Tank no. of recycle, τ_T: Total time spent in the system, , f_{BP}: Fraction of bypass

Table 5(b)-6. Operating parameters and analysis of RTD measured by detector D3 at the outlet of the system

Run No.	Temp. (^{0} C)	Air+ Steam velocity (m/s)	Bed Height	Bed material Weight (kg)	Coal size (mm)	Feed rate (kg/h)	Extraction rate (kg/h)			Tracer particle size (mm)	$\bar{t}_f$ (Min.)	Model Parameters	
							Bottom ash	Cyclone-1	Cyclone-2			τ_T	N_B
1	1000	1.75	1D	12	0.5-4	25	4	4.8	2	0.5-4	48	51	1
2	1000	1.75	1D	12	0.5-4	25	4	4.8	2	0.5-1	75	79	1
3	1000	1.75	1D	12	0.5-4	26	4	4.8	2	2-3	34.3	32	2
4	1000	1.75	1D	12	0.5-4	27	4	4.8	2	3-4	34.6	33	2
5	1000	1.5	1D	12	0.5-4	21	5	3.1	2	0.5-4	56	57	1
6	1000	2	1D	12	0.5-4	29	5	4	2	0.5-4	38	37	1
7	1000	1.75	1.5D	14	0.5-4	31	5	5	2.5	0.5-4	86	90	1
8	900	1.75	1D	12	0.5-4	28	5	4	2	0.5-4	--	--	--
9	850	1.75	1D	12	0.5-4	41	12	7	3.5	0.5-4	--	--	--
10	Ambient	0.65	1D	12	0.5-4	10	10	5	3	0.5-4	--	--	--
11	Ambient	0.65	1D	12	0.5-4	10	10	5	3	0.5-4	50.6	52	1
12	Ambient	0.65	1D	12	0.5-4	9	9	5	3	0.5-4	--	--	--
13	Ambient	0.65	1D	12	0.5-4	9	9	5	3	0.5-4	48.5	50	1

D: inner diameter of the fluidizer section, τ_P: time of plug flow component, τ_B:time spent in the bed, N_B: Tank no. of bed, α_B: Back mixing ratio of bed material, f_R: Recycle fraction of flow, $\boldsymbol{\tau_R}$**:** time of recycle, N_R: Tank no. of recycle, τ_T: Total time spent in the system, , f_{BP}: Fraction of bypass

The effect of coal particle size distribution on the MRT of the bulk of the coal can be done using two methodologies. One of the ways is to have desired size sieved bed material and subsequently, the tracer to same particle size used to trace. The second approach involves, the bed material broad distribution of the coal particles, however the tracer particles of certain size is only labelled with radioactivity. The labelled particles of certain size only track motion of the similar size particles. The later approach is more realistic way to study flow dynamics of the different size coal particles in a pilot scale FBG. Four runs with different particles sizes were carried out (Run 1-4). The tracer particle sizes used in these runs were listed in the Table 5(b)-5. The MRT of the mixture of the particles was found to be lower than that of the uniformly sized particles**.** This indicates that a heterogeneous tracer particle is having less MRT than the uniformly sized coal particles. However, in uniformly sized particles, finer and coarser particles have higher residence time as compared to the average sized coal particles. It clearly indicates that a finer and coarser particle spends more time in FBG as compared to the average sized coal particles. Moreover, air and steam velocity varied from 1.5-2 m/s, MRT of the coal particles in the bed decreases with increase in the gas and steam flow rate as observed in Run 1, 5 and 6 (Table 5(b)-5). The effect of bed height on the MRT of the solid particles is studied in RTD Runs 1 and 9 at bed height of 1D (20 cm) and 1.5D (30 cm). The MRT values of the coal in the FBG were found to be increasing with increase in bed height. This is due to the fact that solid fraction of the coal particles in the FBG increases with increase in the bed height. The effect of temperature was studied at three different operation temperatures i.e. 1000^{o}C, 900^{o}C and 850^{o}C. MRT of the coal particles was found to be decreasing marginally, when operating temperature of the FBG is decreased from 1000^{o}C to 900^{o}C. However the MRT of the coal particles was found to be decreased significantly from 900^{o}C to 850^{o}C as given in the Table 5. The significant change in the MRT from 900°C to 850°C is not only due to the temperature change, but also due to uncontrolled operational parameters such as coal feed rate and variable bed height as observed during experimentation. The four runs carried out at ambient condition are given in the Table 5(b)-1. We cannot compare these runs with the hot conditions run as important operating parameters such as air and steam velocity are not same.

The value of N of the mixture of particles was found to be lowest as compared to uniform sized coal particles. It could be due to the heterogeneity introduced by the size distribution of the coal particles in FBG. This creates high randomness in the particle flow inside the FBG and consequently increased in the mixing. The finer and coarser particles shows higher tank no as compared to the mixture of the coal particles. This clearly indicates that the finer and coarse particles have lower mixing behaviour as compared to the mixture of the particles. But, the average sized coal particles; tank no. is much closer to the mixture of particles. This can be explained by the major component of the averaged sized coal particles present in the bed of FBG as compared to the fine and coarser particles. The values of N were found to be decreasing with increase in air and steam velocity and bed height of coal particles in the FBG. The increase in gas flow rate enhances the amount of fluid in the bed and heterogeneity of the phases. This consequently, in turn increases the degree of mixing or lower N. As the bed height in the FBG increases, increases the coal particle-particle collision is observed due increase in the number of the coal particles. This increment in the collision increases the randomness of the particles and decreases the N. In addition to this, N was found to be decreasing with increase in the temperature from 850°C to 900°C. However, from 900 to 1000°C, they are found to be constant. It suggests that on increasing the temperature, the degree of back mixing increases to an extent and then becomes constant.

The fractions of the internal recycle (f_r) of the finer and coarser particles are also found to be lower than the averaged sized particles. This indicates that finer and coarser particles will leave the internal recirculation of system earlier than the averaged sized particles. The value of $f_r$was found to be changing marginally with increase in fluid velocity and bed height of the coal particles. However, it was found to be increasing with increase in the temperature. The higher temperature introduces thermal stress in system which enhances the breakdown of the particles, which in turn increases the rate of internal recirculation. The value of the degree of backflow ratio (α) observed at different conditions is reported in the Table 5(b)-5. It follows the similar trend as the value of N was found at different operating conditions.

Four RTD runs were carried out at low temperature 40^o-100^oC. These were carried out at two different coals feed rates. The $f_r$was found to be less than the hot condition runs as at lower temperature thermal stress are not present. This indicates that the generation of fine particles in the case of the hot condition is higher than the cold conditions runs. The fines particles contribute to high degree of recycle in the hot condition as given in the Table 5(b)-5. A degree of bypass of the coal particles was present in the ambient condition, which was not present in the hot condition runs. The amount of coarse particles present in the bed at cold conditions is higher than the hot conditions. The bubble space present between the coarse particles is higher than the fine particles. These air gapsbetween coarse particles acts as easy escape path for the particles resulting bypassingin ambient flow conditions.

5(b)5.2. Flow behaviour of the fine particles inside the FBG:

The experimental RTD curves of the fine particles at different operating conditions are shown in the Fig.5-3(ii). If we compare this curve with the typical curve of the bulk coal particle exit. It can be said that there is no time delay present in the fine particles RTD curve. It suggests that as soon as tracer is injected in the system a small portion of this reaches the top outlet. We could able to treat the Run 7, 8, 10 and 12. As in the run no 7 and 8, the signal recoded is having large fluctuations and even after smoothing proper tail could not be fitted. Whereas, fluctuations in run 10 and 12 RTD curves much less than former runs. However, the tail fitted curve was gives MRT, which is not acceptable. The effect of tracer particle size, bed height, air velocity and temperature on the flow behaviour of the fine particles was studied. The effect of tracer particle size on the MRT of the fine particles was studied in Run 1 to Run 4. The MRT of the particles was found to be decreasing with decreasing particle size. The fine particles (0.5-1mm) can be easily fluidized and mixed with in the entire FBG in negligibly small time and take longer time to exist. On comparing, the normal distribution (0.5-4mm) of the coal tracer particles with the different range of the particles, the MRT of normal range was between the fine particles and coarse particles. Whereas the MRT of the Tracer particles size 2-3mm, is close enough to the normal range of the particles (0.5-4mm). As, this size range coal particle fraction was the one major part of the coal particle size distribution. The effect of the air and steam velocity on the MRT of the fine particles is studied in Run 1, 5 and 6. The air velocity was varied from 1.5 to 2 m/s. The MRT of fine particles were found to increase marginally as the steam and air velocity was increased. The RTD curve monitored at different temperature is shown in the Fig. 5(b)-3(c) (Run 7 and 8). It was observed from the experimental curves that these runs cannot be recorded with good signal to noise ratio and above the background level. The fine particles may get stuck to the fine out let in these runs. Hence, it is not possible to conclude about effect of temperature on the flow of the fine particles. If we observe the effect of the bed height on the MRT of the fine particles, the increase in the amount of coal particles in the bed increases the solid holdup in the bed. Consequently, MRT of the coal particles should increase as given in the Table 5(b)-6 (Run 1 and Run 9). The MRT of the fine particles at ambient conditions ranged from 48-50 min. These results cannot be compared with the hot flow condition. As the air and steam velocity used in cold condition is different from the hot flow condition.

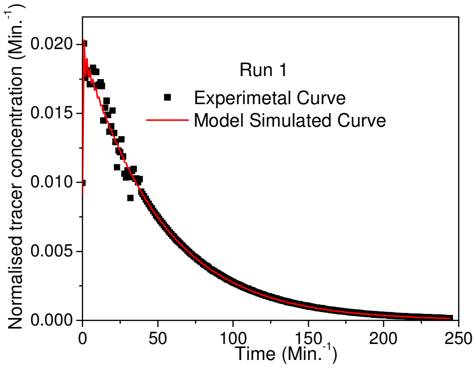

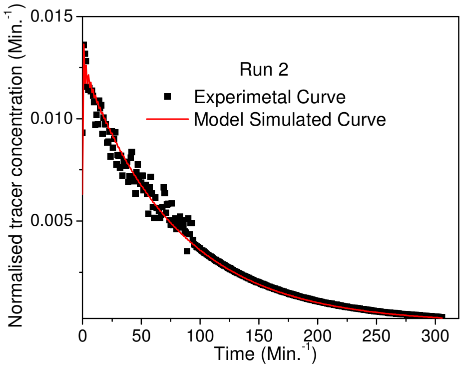

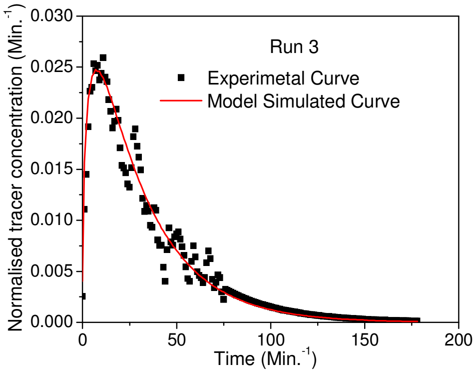

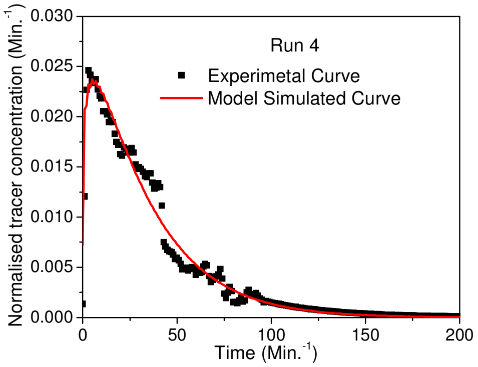

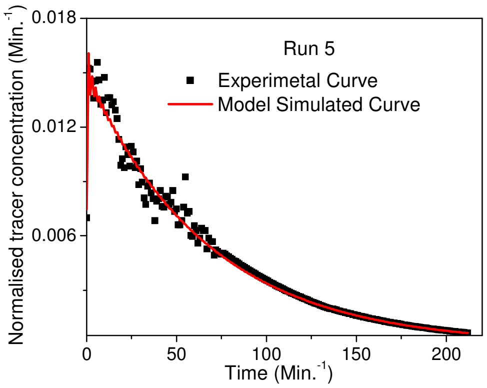

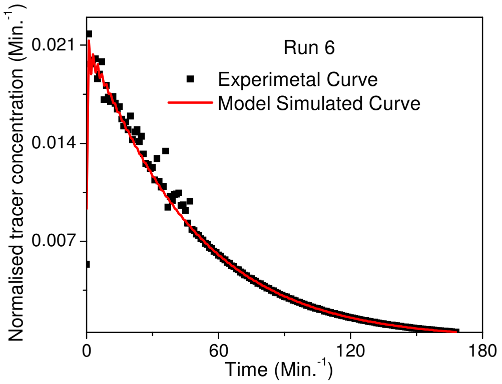

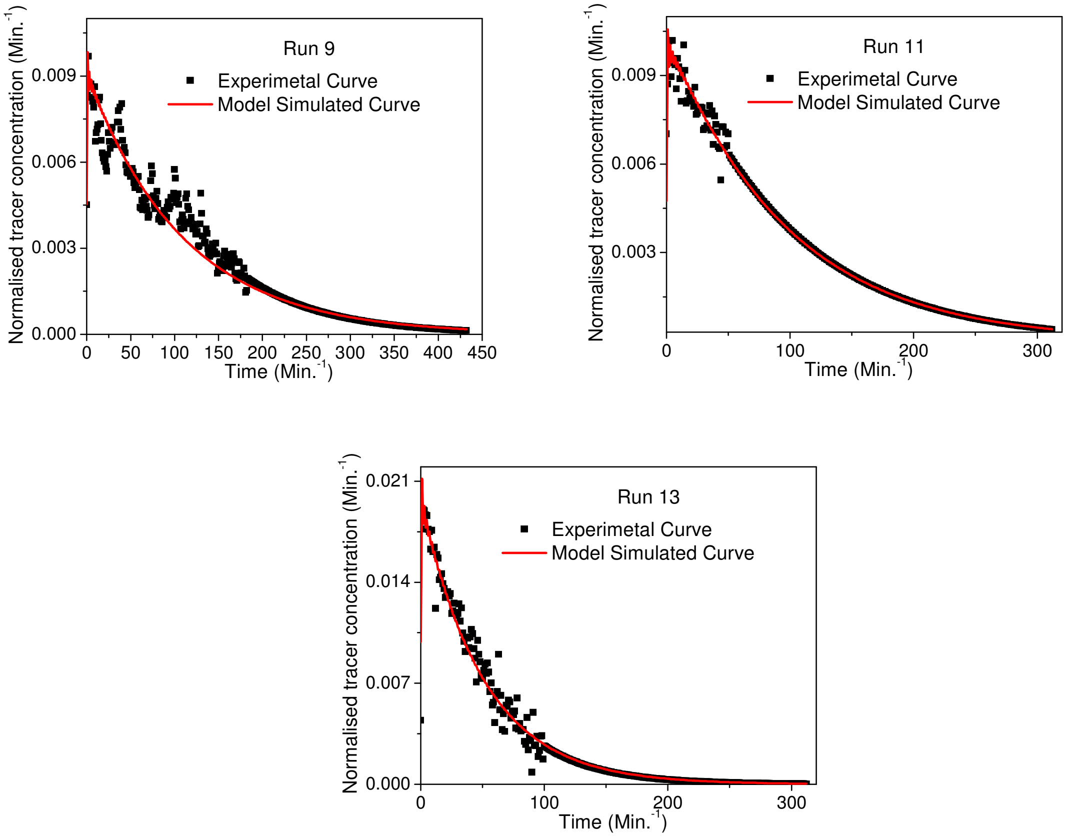

Fig 5(b)-8: Experimental and model simulated curve fine coal particles coming out at top of the FBG at hot and cold Condition

The model simulated parameter tank no. (N), signifies the degree of the mixing of the fine coal particles within the bed. The tank no. is found to be 1 at most of the hot flow and cold flow conditions except when the large size tracer particles were used (Run 3 and 4), value of N is 2. This suggests that the fine particles are mixed with the whole FBG within fraction of the second. When the coarse particle tracers are used, the higher value of N suggests that the fine particle tracing is not done initially. But after some time the generation of the fine particles occurs due to attrition of the particles and particle-particle collision. Therefore, the tracing of the fine particles was not possible at initial stages. But, it traces the generation of the fine particles during the course of the operation. From above results, it can be concluded that behavior of the fine particles with in the FBG is like prefect mixer.

5(b).6. Conclusions:

The following conclusions were drawn from the radiotracer study carried out in pilot-scale fluidized bed coal gasifier:

- Radiotracer technique for measurement of RTD of the coal particles and study of flow behavior of a pilot-scale FBG was successfully applied to study flow dynamics of coal particles.
- The mean residence time (MRT) of the coal particles was not found decreasing with increase in the air and steam velocity and decrease in bed height of the coal particles. Moreover, with mixture of particles the MRT of the coal particles is lower than uniformly sized particles.
- The degree of mixing of the coals particles increases with increase in the bed height, air and steam velocity and increase in the hertogenity of the coal particle size.
- Different complex network of elementary models representing physical flow of the coal particles were successfully implemented to understand the flow of coal particles inside the fluidized bed gasifier.
- Flow of the bulk particles exiting bottom of the FBG at hot and cold conditions were simulated using proposed model A and B respectively. There is a good agreement between the experimental and model simulated RTDs was found.

- Flow of the fine particles exiting top of the FBG, simple tank in series model founds good agreement between the experimental and model simulated RTD curves.
- Bypassing of coal particles exiting bottom of the FBG was found at only cold conditions runs. The percentage of the bypass was estimated using proposed model-B in the range of 5-10%.
- The results of the study could be used to improve the design of the existing FBG to improve the mixing of the coal particles inside the gasifier. Moreover, the results could also be used for scale-up of coal gasification process.

References:

1. Abdul R. R., Fazalul R. M. H., Chan K.S., 2004. Monitoring Liquid/Gas Flow Using Ultrasonic Tomography. Proc. 3rd International Symposium on Process Tomography in Poland. Lodz, Poland. 130-133.
2. Aktas S., Ozlem E., Zeytuncu B., Marcali M. H., 2015. Studies of gold adsorption from chloride media. Mineral Research. 18(3), 660-667.
3. Al-Hasan, M., Al-Qodah Z., 2007. Characteristics of gas-solid flow in vertical tube. In 9th International Symposium on Fluid Control Measurement and Visualization, FLUCOME, 1, 264-271.
4. Barreira A., Patierno M., Bautista C. R., Impacts of pollution on our health and the planet: The case of coal power plants, UN Environment Report, https://wedocs.unep.org/bitstream/handle/20.500.11822/22218/Perspective_No_28_web.pdf?sequence=1, (Accessed on November, 2018).
5. Berruti F., Liden A.G., Scott D.S., 1988. Measuring and modelling residence time distribution of low density solids in fluidized bed reactor of sand particles, Chem. Eng. Sci. 43(4), 739-748.
6. Bidin A.R., Green R.G., Shackleton M.E., Stott A.L., Taylor R.W., 1995. Electrodynamic Sensors for Process Tomography. In: Williams, R. A. and Beck, M. S. (Eds). Process Tomography: Principles, Techniques and Applications. Oxford: Butterworth-Heinemann. 101-117.
7. Biggs R. D., 1963. Mixing rates in stirred tanks. AIChE Journal 9(5), 63-640.

8. Biswal J., Pant H.J., Goswami S., Samantray J. S., Sharma V.K., Sarma K.S.S., 2018. Measurement of flow rates of water in large diameter pipelines using radiotracer dilution method, Appl. Radiat. Isotope, 59, 194-200.
9. Brown D.A.R., Jones P.N., Middleton J.C., 2004. Experimental methods, Part A: measuring tools and techniques for mixing and flow visualization studies. In: Atiemo-Obeng VA, Kresta SM (eds) Paul EL. Wiley-Interscience, Handbook of industrial mixing, 145–202.
10. Buffham, B. A. and Gibilaro, L.G., 1968. A generalization of the tanks in series mixing model, AIChE J., 14 (5), 805-806.
11. Bukur D.B., Daly J.G., Pate S.A., (1996) Application of γ-ray attenuation for measurement of gas holdups and flow regime transitions in bubble columns. I&EC Research 35(1), 70–80
12. Chan A.M.C., Banerjee S., 1981. Design aspects of gamma densitometers for void fraction measurements in small scale two-phase flows, Nucl. Instrum. Methods 190, 135-148.
13. Chaouki J., Larachi F., Dudukovic M. P., 1997B. Non-invasive Monitoring of Multiphase Flows. Elsevier, Amsterdam.
14. Chaouki J., Larachi F., Dudukovic M.P., 1997A, Non-Invasive Tomographic and Velocimetric Monitoring of Multiphase Flows. I&EC Research 36(11), 4476-4503.
15. Charlton, J.S., Hurst, J.A. (1994). Radioisotope techniques for problem solving in the offshore oil and gas industry. National executive management seminar, Thailand.
16. Charlton, J.S., 1986. Radioisotope tracer techniques for problem solving in industrial plants, Leonard Hill, Glasgow and London.

17. Cherry S. R., Sorenson J. A., Phelps M. E., 2012. Physics in Nuclear Medicine (Fourth Edition), Elsevier, Philadelphia, U.S.A.

18. Choppin G., Liljenzin J., O., Rydberg J., Ekberg C., Radiochemistry and Nuclear Chemistry (Fourth Edition) 2013, Butterworth-Heinemann, USA, 239-295.

19. Choy, K.K.H., McKay, G., Porter, J.F., 1999. Sorption of acidic dyes from effluents using activated carbons. Resour Conserv Recy. 27, 57-71.

20. Christophe B., Duquenne A. M., Gabriel W., 2002. Measuring techniques in gas–liquid and gas–liquid–solid reactors, Chem. Eng. Sci. 57, 3185–3215.

21. Claudel, S., Fonteix, C., Leclerc, J.P., Lintz, H.G., 2003. Application of the possibility theory to the compartment modeling of flow pattern in industrial processes. Chem. Eng. Sci. 58, 4005–4016.

22. Coal reserves in India, Ministry of coal, Government of India (MoC-GOI), https://coal.nic.in/ content/coal-reserves (Accessed on November, 2018).

23. Collin, A., K.-E. Wirth, and M. Stroeder, 2009. Characterization of an annular fluidized bed, Powder Technol. 19 (1-2), 31-35.

24. Czerwinski, A., Voulgaropoulos, A., Mark, H. B., 1984. A radiotracer method for the study of ruthenium adsorption on polysulfur nitride. J. Radioanal. Nucl. Chem.85(3), 173-180.

25. Daggupati S., Mandapati R. N., Mahajani S. M., Ganesh A., Pal A. K., Sharma R. K., Aghalayam P.,2010. Compartment Modeling for Flow Characterization of Underground Coal Gasification Cavity, Ind. Eng. Chem. Res. 50, 277–290.

26. Danckwerts P.V., 1953. Continuous flow systems: distribution of residence times, Chem. Eng. Sci. 2 (1) 1–13.

27. Daniels, A.R., 1996, Dual Modality Tomography for the Monitoring of Constituent Volumes in Multi-Component Flows. Sheffield Hallam University: Ph.D. Thesis.

28. Dash A., Knapp Jr F. F., Pillai M. R. A., 2013. Industrial radionuclide generators: a potential step towards accelerating radiotracer investigations in industry, RSC Adv., 3, 14890-14909.

29. Davidson, J. L., Ruffino, L. S., Stephenson, D. R., Mann, R., Grieve, B. D. and York, T. A., 2004. Three-Dimensional Electrical Impedance Tomography Applied to a Metal-Walled Filtration Test Platform, Meas. Sci. Technol. 15, 2263–2274.

30. Demori, M., Ferrari V., Strazza D., Poesio P., 2010. A capacitive sensor system for the analysis of two-phase flows of oil and conductive water, Sens. Actuators, A Phy. 163 (1), 172-179.

31. Dickin, F. J., Wang, M., 1995, Impedance Sensors-Conducting System. In: Williams, R. A. and Beck, M. S. (Eds). Process Tomography: Principles, Techniques and Applications. Oxford: Butterworth-Heinemann. 63-84.

32. Emun F., Gadalla M., Majozi T., Boer D., 2010. Integrated gasification combined cycle (IGCC) process simulation and optimization, Comput. Chem. Eng., 34 331–338.

33. Fano, U., 1953. Gamma ray attenuation Part-1: Basic process, Nucleonics. 11 (8), 8–12.

34. Fischer, C., Peglow M., Tsotsas E., 2011. Restoration of particle size distributions from fiber-optical in-line measurements in fluidized bed processes, Chem. Eng. Sci. 66(12), 2842-2852.

35. Fogler, H.S., 2005, Elements of Chemical Reaction Engineering (4th Edition), Prentice Hall.

36. Foldiak, G., 1986. Industrial Application of Radioisotopes, Elesevier.

37. Godfroy L., Larachi F., Kennedy G., Grandjean B.P.A., Chaouki J., 1997, Online Flow Visualization in Multiphase Reactors Using Neural Networks. Appl. Radiat. Isotop. 48, 225-235.

38. Goel M., Kumar B., Charan S.N., 2009. Carbon Capture and Storage R&D Technologies for Sustainable Energy Future, Narosa Publishing House, New Delhi, 3–14 .

39. Goswami S., Pant H.J., Ambade R.N., Paul B., Varshney L., Dash A.,2017. Study of adsorption characteristics of Au(III) onto coal particles and their application as radiotracer in a coal gasifier, Appl. Radiat. Isotot. 122, 127–135.

40. Goswami S., Sharma V. K., Samantray J. S., Pant H. J., 2014. Sediment transport investigation near Sagar Island in Hooghly Estuary, Kolkata Port, Kolkata, J. Radioanal. Nucl. Chem. 300, 107-113.F

41. Green R.G., Rahmat M. F., Evans K., Goude A., Henry M., Stone, J.A.R., 1997. Concentration Profiles of Dry Powders in a Gravity Conveyor Using an Electrodynamic Tomography System, Meas. Sci. Techno. 8(2), 192-197.

42. Grodstein, G.W., 1957, X-ray attenuation coefficients from 10 keV to 100 MeV. NBS Circular 583.

43. Grootjes A.J., Aranda G., van der Meijden C.M., van der Drift A., Vreugdenhil B.J., 2015. Gasification of low rank coals, Proceedings of the Seventh International Conference on Clean Coal technology(CCT2015), Karakow, Poland.

44. Guerreto, H.N., 1978. Topics in Two-phase heat transfer and flow, ASME Winter Annual Meeting, San Francisco 199-206.

45. Hall, K. R., Eagleton, L. C., Acriros, A., Vermeulen, T., 1966. Pore-and Solid-Diffusion Kinetics in Fixed Bed adsorption under constant pattern conditions. Ind. Eng. Fundam.5(2), 212-223.
46. Harnby N., Edwards M.F., Nienow A.W., 1997. Mixing in the Process Industries, Butterworth-Heinemann, Oxford, UK.
47. Harris A.T., Davidson J.F., Thrope R.B.,2002. A novel method for measuring the residence time distribution in short time scale particulate system, Chem. Eng. Sci. 89, 127-142.
48. Hayashi, J. I., Hosokai, S., Sonoyama, N., 2006. Gasification of low-rank solid fuels with thermochemical energy recuperation for hydrogen production and power generation. Process Saf. Environ. Prot. 84(6), 409–419.
49. Henderson, C., Clean coal technologies. IEA clean coal centre report: CCC/74. Graham & Trotman, London, 2003.
50. Himmler, K., Schierholz, W., 2004. Mischvorg¨ange: klassische methoden und computational fluid dynamics in der industriellen Praxis. Chemie-Ingenieur- Technik 76 (3), 212–219
51. Ho, Y.S.; McKay, G., 1999. Pseudo-second order model for sorption processes. Process Biochem. 34, 451–465.
52. Hoyle B.S., 1996. Process Tomography Using Ultrasonic Sensors, Meas. Sci. Technol. (7) 272-280.
53. Huber, A.A., Kirk, R.J., Pietruszkiewicz, J. and Smith, R.S., 1984, An Assessment of Integrated Gasification Combined Cycle Power Generation, Coal Technology 84, Nov. 13-15.

54. IAEA/RCA/RAS/8012-P1, 2015. Protocol for preparation of radioactive gaseous tracers Methyl Bromide-82 and Argon-41 and Krypton-85, Vienna, Austria.
55. Idakiev V., Mörl L., 2013. Study of residence time of disperse materials in continuously operating fluidized bed apparatus, Journal of Chemical Technology and Metallurgy, 48(5), 451-456. Ind. Rev. Chem. Eng. 17, 165–252.
56. International Atomic Energy Agency (IAEA) 1996. Residence time distribution software analysis user’s manual, Computer Manual Series No. 11, Vienna.
57. International Atomic Energy Agency (IAEA), 1990. Guide book on Radioisotope Tracers in Industry, Technical Report Series No.316, IAEA, Vienna, Austria.
58. International Atomic Energy Agency (IAEA), 1991. Use of artificial tracers in hydrology, Proceedings of an Advisory Group Meeting held in Vienna, IAEA-TECDOC-601, Vienna, Austria.
59. International Atomic Energy Agency (IAEA), 2001. Radiotracer technology as applied to industry, Tecdoc-1262, IAEA, Vienna, Austria.
60. International Atomic Energy Agency (IAEA), 2001. Radiotracer technology as applied to industry, TECDOC-1262, Vienna, Austria.
61. International Atomic Energy Agency (IAEA), 2003. Manual for reactor produced radioisotopes, IAEA-TECDOC-1340, Vienna, Austria.
62. International Atomic Energy Agency (IAEA), 2004C, Radiotracers and labeling compounds for applications in industry and environment, 16-19 June, 2004.IAEA Report for CM, Poland.
63. International Atomic Energy Agency (IAEA), 2008C. Report of the CM on Radiotracer and sealed source techniques for sediment management, Vienna, Austria.

64. International Atomic Energy Agency (IAEA), 2009. Leak detection in heat exchanger and underground pipeline using radiotracer, Training course series 30, IAEA, Vienna, Austria.

65. International Atomic Energy Agency (IAEA), 2013. Radiotracer generators for industrial applications, IAEA Radiological Technology Series No.5, Vienna, Austria.

66. International Atomic Energy Agency (IAEA), 2014. Radiotracer and sealed source application in sediment transport studies, Training course series No. 59, Vienna, Austria.

67. International Atomic Energy Agency, 2001. Radiotracer technology as applied to industry, TECDOC-1262, Vienna, Austria

68. International Atomic Energy Agency, 2004A. Integration of tracing with computational fluid dynamics for industrial process investigation, Tecdoc-1412.IAEA, Vienna, Austria.

69. International Atomic Energy Agency, 2004B. Radiotracer applications in industry - A guidebook, Technical Report Series No. 423, IAEA, Vienna, Austria.

70. International Atomic Energy Agency, 2007. Signal Processing and Electronics for Nuclear Spectrometry, IAEA-TECDOC-1634, Vienna, Austria.

71. International Atomic Energy Agency, 2008A. Radiotracer residence time distribution method for industrial and environmental applications, Technical Report Series No.31, IAEA, Vienna, Austria.

72. International Atomic Energy Agency, 2008B. Industrial Process Gamma Tomography: IAEA TECDOC-1589, International Atomic Energy Agency, Vienna, Austria.

73. International Commission on Radiological Protection (ICRP), 1991. Recommendations of the International Commission on Radiological Protection. Pergamon Press, Oxford.

74. International Energy Agency (IEA), Energy and Air Pollution World Energy Outlook Special Report (2016), p. 43. Available at: http://www.iea.org/publications/freepublications/publication/WorldEnergyOutlookSpecialReport2016EnergyandAirPollution.pd, (Accessed on December, 2018).

75. IPG (2003): International Power Generation, July 2003, 39.

76. Jafari M, Mohammadzadeh J.S.S., 2005. Mixing time, homogenization energy and residence time distribution in a gas-induced contactor, Chem. Eng. Res. Des. 83(5), 452–459.

77. Jay R. B., Lynn M., Jeffrey H., Massood R., 2002. Major environmental aspects of gasification-based power generation technologies, Gasification Technologies Program, National Energy Technology Laboratory, U.S. Department of Energy, U.S.A.

78. Jin H., Yang S., Guo Z., Guangxiang H., Tong Z., 2005. The axial distribution of holdups in an industrial-scale bubble column with evaluated pressure using gamma-ray attenuation approach, Chem. Eng. J., 115, 45–50

79. Jung, S.H., Kim, K., Ryu, J.H., Choi, S.H., Kim, J. B., Moon, J.H., Jin, J.H., 2010. Preparation of radioactive core-shell type ^{198}Au@SiO$_2$ nanoparticles as a radiotracer for industrial process applications. Appl. Radiat. Isot., 68, 1025–1029.

80. Kalaga, D. V., Reddy R. K.; Joshi, J.B., Dalvi, Sameer V.; Nandkumar, K.2012. Liquid phase axial mixing in solid–liquid circulating multistage fluidized bed: CFD modeling and RTD measurements, Chem. Eng. J. 191, 475-490.

81. Karcz J., Szoplik J., 2008. Mixing time of a non-Newtonian liquid in an unbaffled agitated vessel with an eccentric propeller. Chem. Pap. 62 (6), 70–77.

82. Karthikeyan, G., Andal, N.M., Anbalagan, K., 2005. Adsorption studies of iron(III) on chitin, J. Chem. Sci., 117(6), 663–672.

83. Kevin R.L., Eugene V.M., Mark K.H., 2002. Ultrasonic Lamb Waves Tomography, Inverse Problems, 18, 1795–1808.

84. Key world energy statistics-2017, Technical Report, International Institute of Energy (IIE), Paris, France, 2017, 30-31.

85. Kling, K., 2003. Quantitative measurements of micro- and macromixing in a stirred vessel using planar laser-induced fluorescence, J Visual. 6 (2), 165–173.

86. Knoll, G.F, 2000. Radiation detection and measurement. John Wiley & Sons, New York.

87. Knowlton T.M., Karri S.B.R., Issangya A., 2005. Scale-up of fluidized-bed hydrodynamics, Powder Technol. 150, 72 – 77.

88. Kramers H., Baars G., Knoll W., 1953. A comparative study on the rate of mixing in stirred tanks. Chem. Eng. Sci. 2 (1), 35–42.

89. Kumar S. B., Davood M., Dudukovic M. P., 1995. A γ-ray tomographic scanner for imaging voidage distribution in two-phase flow systems, Flow Meas. Instrum. 6(1), 61-73.

90. Kumar S.B., Dudukovic M.P., Toseland B.A., 1997. Measurement technique for local and global fluid dynamic quantities in two and three phase systems. In: Larachi F, Dudukovic MP, Chaouki J (eds) Non-invasive monitoring of multiphase flows, Elsevier Science B V, Amsterdam, 1–36.

91. Kunii D., Levenspiel O., 1991. Fluidization Engineering (2nd Ed), Butterworth-Heinemann (USA).

92. Kunni D., Levenspiel O., Fluidization Engineering, Butterwoth-Heinemann, USA, 2013, ISBN: 978-0-08-050664-7.

93. Langmuir I., 1916. The constitution and fundamental properties of solids and liquids. J. Am. Chem. Soc., 38(11), 2221–2295.

94. Leclerc, J.P., Detrez, C., Bernard, A., Schweich, D., 1995. DTS un logiciel d'aide à l'élaboration de modèles d'écoulement dans les réacteurs. Revue de l'Institut Français du Pétrole, 50, 5, 641-656.

95. Lee, K., Yianneskis, M., 1997. A liquid crystal thermographic technique for the measurement of mixing characteristics in stirred vessels, Chem. Eng. Res. Des. 75, 746–754.

96. Levenspiel, O., 1999. Chemical Reaction Engineering, 3rd Edn., John Wiley & Sons, Inc., New York, pp:257-282.

97. Levenspiel, O., 2012. Tracer Technology: Modeling the Flow of Fluids, Fluid mechanics and its application 96, Springer, New York, ISBN 978-1-4419-8073-1, https://doi.org/10.1007/978-1-4419-8074-8.

98. Levenspiel, O., Smith, W.K., 1957. Notes on the diffusion-type model for the longitudinal mixing of fluids in flow, Chem. Eng. Sci. 6 (4-5), 227-235.

99. Lin W., Weinell C. E., Hansen P. F.B., Dam-Johansen K., 1999. Hydrodynamics of a commercial scale CFB boiler with radioactive tracer particles, Chem. Eng. Sci. 54, 5495-5506.

100. Link, J.M., Godlieb W., Tripp, Deen N.G., Heinrich S., Kuipers J.A.M., Schönherr M., Peglow M., 2009. Comparison of fibre optical measurements and discrete element

simulations for the study of granulation in a spout fluidized bed, Powder Technol. 189(2), 202-217.

101. Ma Z., Turchi C. S., 2011. Advanced supercritical carbon dioxide power cycle configurations for use in concentrating solar power systems, presented at the Supercritical CO_2 Power Cycle Symposium Boulder, Colorado, https://www.nrel.gov/docs/fy11osti/50787.pdf, (Accessed on November, 2018).
102. Machowska H., Knapik E., 2011. Coal gasification clean technology, Chemik, 65(10), 946-953.
103. Marcali, M. H., Aktas S., 2011. Gold uptake from chloride solution by lewait Tp 214 and activated rice husk. Int. J. Miner. Process., 101, 63-70.
104. Martin D. , 2000. Interpretation of Residence Time Distribution Data, Chem. Eng. Sci., 55, 5907-5917.
105. Mayr B., Horvat P., Moser A., 1992. Engineering approach to mixing quantification in bioreactors. Bioprocess. Eng. 8, 137–143.
106. Meggitt, B.T., 2010. Fiber Optics in Sensor Instrumentation. In Instrumentation Reference Book (Fourth Edition), Boston: Butterworth-Heinemann, 191-216.
107. Michelsen, M.L., 1972. A Least-Squares Method for Residence Time Distribution Analysis, Chem. Eng. J., 4, 171-179.
108. Minchener, J., Coal gasification for advanced power generation. Fuel, 2005, 84, 2222–2235.
109. Mondel P., Dang G.S. ,Garg M. O., 2011. Syngas production through gasification and cleanup for downstream applications — Recent developments, Fuel Process. Technol. 92 (2011), 1395–1410.

110. Munawer M.H., 2018. Human health and environmental impacts of coal combustion and post-combustion wastes, J Sustain Min. 17(2), 87-96.

111. Muthukumar U., Chandapillai J., Saseendran S., 2010. Flow Measurement in Hydro-electric Stations Using Tracer Dilution Method – Case Studies, IGHEM-2010, Oct. 21-23, 2010, AHEC, IIT Roorkee, India.

112. Nauman E. B., 2008. Residence time theory, Ind. Eng. Chem. Res. 47, 3752-3766.

113. Nauman, E.B., Buffham, B.A., 1983. Mixing in continuous flow systems, New York: John Wiley & Sons.

114. Othman N., Kamarudin S.K., 2014. Radiotracer technology in mixing processes for industrial applications. The Scientific World J., 1–15.

115. Ozeroglu, B. C., Keceli, G., 2009. Kinetic and thermodynamic studies on the adsorption of U(VI) ions on densely crosslinked poly(methacrylic acid) from aqueous solutions. J. Radiochim. Acta., 97, 709–717.

116. Palige, J., Majkowska, A., Herdzik, I., Ptaszek, S., 2011. 68Ge/68Ga radioisotope generator as a source of radiotracers for water flow investigations, Nukleonika, 56 (1), 77-80.

117. Pant H.J., Goswami S., Samantray J.S., Sharma V.K., Maheshwari N.K., 2015. Residence time distribution measurements in a pilotscale poison tank using radiotracer technique. Appl. Radiat. Isot. 103, 54–60.

118. Pant H.J., Sharma V.K., Kamudu M.V., Prakash S.G., Krishnamoorthy S., Anandam G., Rao P.S., Ramani N.V.S., Singh G., Sonde R.R., 2009A. Investigation of flow behavior of coal particles in a pilot-scale fluidized bed gasifier (FBG) using radiotracer technique. Appl. Radiat. Isot. 67:1609–1615

119. Pant H.J., Sharma V.K., Kamudu M.V., Prakash S.G., Krishnamoorthy S., Anandam G., Ramani N.V.S., Singh G., 2009B. Measurement of circulation rates of coal particles in standpipe of a circulating fluidized bed system (CFBS) using radiotracer technique, J. Radioanal. Nucl. Chem. 280(1), 47–56.

120. Pant H.J., Sharma V.K., Singh G., Raman V.K., Bornare J., Sonde R.R., 2012. Radiotracer investigation in a rotary fluidized bioreactor, J. Radioanal. Nucl. Chem. 294(1), 59–63.

121. Pant, H. J., Kundu, A., Nigam, K. D. P., 2001. Radiotracer applications in chemical process industry, Rev. Chem. Eng. 17, 165-252.

122. Pant, H.J, Yelgoankar, V.N, 2002. Radiotracer investigations in aniline production reactors, Appl. Radiat. Isot. 57 (3), 319-325.

123. Pant, H.J., Goswami, S., Biswal, J., Samantaray, J.S., Sharma, V.K., Singhal, S., 2016. Radiotracer investigation in a glass production unit, Appl. Radiat. Isot. 116, 41-50.

124. Pant, H.J., Kundu, A., Nigam, K.D.P., 2001. Radiotracer applications in chemical process industry, Rev. Chem. Eng. 17 (3), 165-252.

125. Pant, H.J., Sharma, V.K., 2015. Radiotracer investigation in an industrial-scale oxidizer, Appl. Radiat. Isot. 99, 146-149.

126. Pant, H.J., Sharma, V.K., Goswami, S., Samantray, J.S., Mohan, I.N., Naidu, T., 2014. Residence time distribution study in a pilot-scale gas–solid fluidized bed reactor using radiotracer technique, J. Radioanal. Nucl. Chem. 302 (3), 1283-1288.

127. Pant, H.J., Sharma, V.K., Kamudu, M.Vidya, Prakash, S.G., Krishanamoorthy, S.G., Anandam, G., N.V.S., Singh, G., 2009C. Measurement of circulation rates of coal

particles in standpipe of a Circulating Fluidized Bed System (CFBS) using Radiotracer Technique, J. Radioanal. Nucl. Chem., 28(1), 47-56.

128. Pant, H.J., Sharma, V.K., Vidya Kamudu, M., Prakash, S.G., Krishanamoorthy, S., Anandam, G., Seshubabu Rao, P., Ramani, N.V.S., Singh, G., Sonde, R.R., 2009A. Investigation of flow behaviour of coal particles in a pilot-scale fluidized bed gasifier (FBG) using radiotracer technique, Appl. Radiat. Isot. 67(9), 1609-1615.

129. Park H. S., Chang H. C., 2007. Design and Application of a Single-Beam Gamma Densitometer for Void Fraction Measurement in a Small Diameter Stainless Steel Pipe in a Critical Flow Condition, Nucl. Sci. Technol., 39(4), 349-358.

130. Phillips J., Different type of gasidiers and their integration with gas turbines, A Report from EPRI, CA, 2003. https://netl.doe.gov/File%20Library/Research/Coal/energy%20 systems/ turbines/handbook/1-2-1.pdf

131. Potier, O., Brun, J., Le Masson, P., Weil, B., 2015. How innovative design can contribute to Chemical and Process Engineering development? Opening new innovation paths by applying the C–K method, Chem. Eng. Res. Des. 103, 108-122.

132. Power Sector (PS) at a Glance all INDIA, Electrical energy production comparison on basis of fuel used. https://powermin.nic.in/en/content/power-sector-glance-all-india (Accessed on December, 2018).

133. PROGEPI/SYSMATEC, 2000. Instruction Manual of RTD Analysis Software, DTSPro, V.4.2, Nancy, France.

134. Rahmat, M.F., 1996, Instrumentation of Particle Conveying Using Electrical Charge Tomography. Sheffield Hallam University: Ph.D. Thesis.

135. Ramírez, F.P., Eugenia Cortés, M., 2004. The determination of residence times in a pilot plant, Nucl. Instrum. Methods Phys. Res., Sect. B, 213, 144-148.
136. Rao, J.S., Ramani, N.V.S., Pant, H.J., Reddy, D.N., 2012. Measurement of residence time distributions of coal particles in a pressurized fluidized bed gasifier (PFBG) using radio tracer technique, Indian J. Sci. Technol., 5 (12), 3746-3752.
137. Reungoat, D., Riviere, N., Faure´ J., 2007. 3C PIV and PLIF measurement in turbulent mixing round jet impingement. J Visual. 10 (1), 99–110.
138. Rielly C.D., Britter R.E., 1985. Mixing time for passive tracers in stirred tanks. In: Proceedings of the Fifth European Conference on Mixing, pp. 365–375.
139. Roemer M.H., Durbin L.D., 1987.Transient response and moments analysis of backflow cell model for flow systems with longitudinal mixing, Ind. Eng. Chem. Fund 6(1),120–129.
140. Rousseaux, J., Muhr, H., Plasari, E., 2001. Mixing and micromixing times in the forced vortex region of unbaffled mixing devices. Can. J. Chem. Eng. 79 (5), 697–707.
141. Roy A., Adhikari B., Majumder S. B., Equilibrium, Kinetic, and Thermodynamic Studies of Azo Dye Adsorption from Aqueous Solution by Chemically Modified Lignocellulosic Jute Fiber, Ind. Eng. Chem. Res. 2013, 52, 6502-6512.
142. Roy, S., 2017. Radiotracer and particle tracking methods, modeling and scale-up, AIChE J, 63 (1), 314-326.
143. Samantray J. S., Goswami S., Sharma V. K., Biswal J., Pant H.J., 2014. Leak detection in a high-pressure heat exchanger system in a refinery using radiotracer technique, J. Radioanal. Nucl. Chem. 302, 979–982.

144. Schlieper, G., Huppmann, W.J., Kozuch, A., 1987. Non-destructive determination of sectional densities by the gamma densomatry, Prog. Powder Metall. 43, 351–362.

145. Scott, G.M., 1985. A study of two-phase liquid–liquid flow at variable inclinations. M.S. Thesis, University of Texas at Austin, USA.

146. Sharma V.K., Pant H.J., Kulkarni U.P., Chakraborty K., Mukhopadhyay S., Pendharkar A.S., 2006. Sediment Transport Investigations in Hugli Estuary Using Radiotracer Technique. International Conference on "Application of Radiotracers in Chemical, Environmental and Biological Sciences (ARCEBS-06)" at Saha Institute of Nuclear Physics, Kolkata, India.

147. Sheoran, M., Chandra, A., Bhunia, H., Bajpai, P.K., Pant, H.J., 2018. Residence time distribution studies using radiotracers in chemical industry—A review, Chem. Eng. Commun. 205 (6), 739-758.

148. Sheoran, M., Goswami, S., Pant, H.J., Biswal, J., Sharma, V.K., Chandra, A., Bhunia, H., Bajpai, P.K., Rao, S.M., Dash, A., 2016. Measurement of residence time distribution of liquid phase in an industrial-scale continuous pulp digester using radiotracer technique, Appl. Radiat. Isot. 111, 10-17.

149. Sprowll, R.L., Phillips, W.A., 1980. Modern Physics: The Quantum Physics of Atoms, Solids and Nuclei, third ed. Wiley, New York.

150. Stahl, P., Rohr, P.R.V., 2004. On the accuracy of void fraction measurements by single beam gamma-densitometry for gas–liquid two-phase flows in pipes. Exp. Therm. Fluid Sci. 28, 533–544.

151. Stahl, P., Rohr, P.R.V., 2004. On the accuracy of void fraction measurements by single beam gamma-densitometry for gas–liquid two-phase flows in pipes. Exp. Therm. Fluid Sci. 28, 533–544.

152. Stegowski, Z., 1993. Accuracy of Residence Time Distribution Function Parameters. Nucl. Geophys. 7, 2, 335-341.

153. Stęgowski, Z., Nowak, E., 2007. Radiotracer experiments and CFD simulation for industrial hydrocyclone performance, Nukleonika,52 (3): pp.115-123.

154. Stepien L., Sciazko M., 2015. Fluidization, Department of Energy and Fuels, AGH University, Kraków, Poland.

155. Tan H.T., Dong G.G., Wei Y.D., Shi M.X., 2007. Application of γ-ray attenuation technology in measurement of solid concentration of gas-solid two-phase flow in a FCC riser, The Chin. J. Process. Eng. 7(5), 895-899.

156. Thatte, A.R., Ghadge R.S., Patwardhan A.W., Joshi J. B., Singh G., 2004. Local Gas Holdup Measurement in Sparged and Aerated Tanks by γ-Ray Attenuation Technique, I&EC Research 43 (17), 5389-5399.

157. Thyn, J., 1996. Effect of measured volume size on the homogenization time. The Chem. Eng. J. 12, 211–217.

158. Thýn, J., Žitný, R., 2004. Radiotracer applications for the analysis of complex flow structure in industrial apparatuses, Nucl. Instrum. Methods Phys. Res., Sect. B 213, 339-347.

159. Thyn, J., Zitny, R., Kluson, J., Cechak, T., 2000. Analysis and diagnostics of industrial processes by radiotracers and radioistope sealed sources. Vydavatelstvi CVUT, Praha.

160. Tjugum, S.A., Frieling, J., Johansen, G.A., 2002. A compact low energy multibeam gamma-ray densitometer for pipe-flow measurements. Nucl. Instrum. Methods Phys. Res., B 197, 301–309.

161. Tsamatsoulis, D., Papayannakos, N., 1994. Axial dispersion and holdup in bench-scale trickle bed reactor at operating conditions. Chem. Eng. Sci. 49 (4), 523–529.

162. Upadhyay, R.K., 2010. Investigation of multiphase reactors using radioactive particle tracking, Ph.D. Thesis, Indian Institute of Technology, Delhi, India.

163. Utgikar V.P., Modelling in multiphase reactor design: Solid phase residence time distribution in three phase sparged reactor Ind. Eng. Chem. Res. 48(2009) 7910-7914.

164. Veluswamy G. K., Upadhyay R. K., Utikar R. P., Geoffrey M.E., Tade M. O., Glenny M. E., Roy S., Pareek V. K., 2011. Hydrodynamics of a Fluid Catalytic Cracking Stripper using γ-ray Densitometry, I&EC Research 50 (10), 5933-5941.

165. Vijayaraghavan, K., Padmesh, T.V.N., Palanivelu, K., Velan, M., 2006. Biosorption of nickel(II) ions onto Sargassum wightii: Application of two-parameter and three-parameter isotherm models. J. Hazard. Mater., B133, 304–308.

166. Vusse J., 1955. Mixing by agitation of miscible liquids Part I. Chem. Eng. Sci. 4, 178–200.

167. Wang Z., Shaozeng S., Hao C., Qigang D., Guangbo Z., Shaohua W., 2009. Experimental investigation on flow asymmetry in solid entrance region of a square circulating fluidized bed, Particuology 7(6), 483-490.

168. Wang, R. C., and Y.-C. Han, 1999. Momentum dissipation of jet dispersion in a gas-solid fluidized bed. J. Chin. Inst. Chem. Eng. 30 (3): 263-271.

169. Wilkinson, F. (2004). Scintillators. Emission Tomography, 229–254Alpha Spectra, Inc. Grand Junction, Colorado, Alpha Spectra, Inc. Grand Junction, Colorado.

170. Yates J.G., Cheesman D.J., Lettieri P., Newton D., 2002. X-ray analysis of fluidized beds and other multiphase system, Kona Powder Part J., 20:133–143

171. Zhu, C. S., Wang, L.P., Chen, W.,2009. Removal of Cu(II) from aqueous solution by agricultural by-product: Peanut hull. J. Hazard. Mater. 168, 739–746.

172. Zlokarnik M., 1967. Eignung von Rührern zum Homogenisieren von Flüssig keitsgemischen Chemie-Ingenieur-Technik 39, 539–548.

173. Zlokarnik, M., 1988. Mixing: Ullmann’s Encyclopedia of Industrial Chemistry, 6.Verlag Chemie, Weinheim 25–1.